To the Graduate Council:

I am submitting herewith a dissertation written by Patrick John Murphy entitled "Optical Determination of Mean Particle Size in a Two-Phase Free-Jet". I have examined the final copy of this dissertation for form and content and recommend that it be accepted in partial fulfillment of the requirements for the degree of Doctor of Philosophy, with a major in Engineering Science.

Walter Frost, Major Professor

We have read this dissertation and recommend its acceptance:

B A Mason

C C Limbaugh

W K McGregor

Robert E. Turner

Reinhard Mengel

Accepted for the Council:

Vice Provost and Dean
of the Graduate School

OPTICAL DETERMINATION OF MEAN PARTICLE SIZE IN A TWO-PHASE FREE-JET

A Dissertation

Presented for the

Doctor of Philosophy

Degree

The University of Tennessee, Knoxville

Patrick John Murphy

August 1990

ACKNOWLEDGEMENTS

The author would like to express his sincere appreciation to the many individuals who have supported and encouraged him in this effort throughout the years. In particluar, I would like to extend sincere thanks to my advisor, Dr. Walter Frost, for his guidance and encouragement, and to the other menbers of my faculty committee for their helpful input and suggestions. Dr. Wheeler McGregor has been especially helpful in defining the topic and providing guidance through many of the technical issues. Dr. Arthur Mason, my first graduate school professor, guided me through my Master's degree and has continued to provide valuable academic support in my studies through the years. Through his patient explanations and enthusiasm for the subject, Dr. Chad Limbaugh, has been very helpful in the numerical aspects of this work, and Dr. Robert Turner has provided helpful suggestions on the final manuscript. I would also like to express my sincere gratitude to Dr. Reinhard Menzel for providing both his technical wisdom and friendship throughout our years of acquaintance.

In addition to my faculty committee, many others have helped me through this effort. Dr. Robert Reed provided much insight on the nature of scattering and extinction phenomena, and has greatly enhanced my understanding of this subject. I am also grateful to Mr. H.Thomas Bentley, who has long been a valuable friend and advisor, for his input on many aspects of particle sizing and statistics. My thanks are also extended to Mr. C.R. Darlington and Dr. J.C. Adams, Jr. for their encouragement and administrative support.

The author is extremely grateful for the opportunities provided by the United States Air Force to continue my graduate education while employed at Arnold Engineering Development Center. A special debt of thanks is owed to Dr. Keith

Kushman for reviewing the manuscript, and for taking the time out of his schedule to help me keep mine.

Thanks are also extended to Martha Craddock for her expert preparation of the final manuscript, to Robert Suttles for his artistic support, to Loretta Crowe for assistance in preparing the figures, and to Kelly Sharber for her helpful editorial comments.

Finally, I would like to acknowledge my deepest appreciation to my wife, Jeanne, for her patience and perseverence throughout this long ordeal.

ABSTRACT

Measurements of light scattering and extinction through ensembles of spherical particles can provide valuable particle size information. Most of the associated measurement techniques assume that the local particle size distribution function is independent of position within the ensemble. Physically realistic particle clouds, however, have spatial density variations caused by inertial effects and collision kinetics, which increase the complexity of the problem, and demand a more sophisticated analytical and experimental treatment.

Using the results of Mie scattering theory, this work presents the development of analytical and experimental procedures for determining the average size and spatial distribution of particles in an axisymmetric ensemble. Cylindrically symmetric particulate-laden flow fields are a particularly useful class of spatially nonuniform particle ensembles that yield tractable solutions to the problem of particle size measurement. Basic definitions from the Mie theory that pertain to extinction and scattering from particle ensembles are reviewed, along with elements of fundamental statistics of size distributions. The standard approach for obtaining average particle size from extinction measurements through a uniform slab of particles is extended to the more general case of spatially nonuniform clouds that have radial symmetry. Multiple path extinction measurements are then combined with the analytical techniques of Abel inversions to ascertain the spatial dependence of the mean particle size.

Methods for measuring the mean particle size of an ensemble based on diffraction and backscatter techniques are also developed, and the approach required to obtain information about the distribution of particle sizes using simultaneous extinction and backscatter measurements at several optical wavelengths is reviewed. The

theoretical feasibility of using the proposed concepts for determining the mean particle size of an ensemble is demonstrated with a numerical simulation of scattering and extinction. Finally, the results of a simple multiple-path extinction experiment are described, in which the distributions of mass flux and mean particle size are deduced.

TABLE OF CONTENTS

CHAPTER		PAGE
I.	INTRODUCTION	1
II.	REVIEW OF MIE SCATTERING THEORY	8
III.	PARTICLE SIZE STATISTICS	28
IV.	MEAN PARTICLE SIZE OBTAINED FROM SINGLE-PATH EXTINCTION MEASUREMENTS	43
	Extinction Through A Uniform Spatial Distribution	43
	Multiple Wavelength Extinction Measurements	65
	Extinction Through Spatially Nonuniform Distributions	66
V.	MEAN PARTICLE SIZE DISTRIBUTION FROM MULTI- PATH EXTINCTION MEASUREMENTS	75
VI.	PARTICLE SIZE OBTAINED FROM SCATTERING MEASUREMENTS	86
	Diffraction Measurements of Mean Size	89
	Backscatter Measurements of Mean Size	97
VII.	DETERMINATION OF THE PARTICLE SIZE DISTRIBUTION	107
VIII.	NUMERICAL SIMULATION OF MEAN PARTICLE SIZE MEASUREMENT TECHNIQUES	114
IX.	EXPERIMENTAL RESULTS OF A MULTI-PATH EXTINCTION MEASUREMENT	128
X.	SUMMARY AND CONCLUSIONS	142
	Recommendations for Future Research	145
	BIBLIOGRAPHY	147
	APPENDIX A - Particle Size Distribution Functions	157
	APPENDIX B - Comments on Extinction Measurement Uncertainties	160
	VITA	165

LIST OF FIGURES

FIGURE	TITLE	PAGE
1.1.	Dependence of particle distribution on flowfield location	2
2.1.	Spherical coordinate system for light scattering by a sphere	10
2.2.	Angular scattering function for a 0.01 μm particle	16
2.3.	Angular scattering function for a 0.1 μm particle	17
2.4.	Angular scattering function for a 1.0 μm particle	18
2.5.	Angular scattering function for a 10.0 μm particle	19
2.6.	Scattering cross section as a function of diameter	22
2.7.	Extinction cross section as a function of diameter	23
2.8.	Backscatter cross section as a function of diameter	24
2.9.	Extinction efficiency vs. real refractive index	25
2.10.	Extinction efficiency vs. imaginary refractive index	26
3.1.	Typical particle size distribution functions	30
3.2.	Cumulative probability distribution functions	31
3.3.	Gaussian distribution function and mean diameters	37
3.4.	Log-normal distribution function and mean diameters	38
3.5.	Mean diameters as a function of the distribution mode	40
3.6.	Distribution width as a function of the width parameter	41
4.1.	Light extinction through a homogeneous particle slab	46
4.2.	Mean specific extinction efficiency	50
4.3.	Effect of distribution width on mean specific extinction	51
4.4.	Extinction efficiency as a function of real refractive index	53
4.5.	Extinction efficiency as a function of imaginary refractive index	54
4.6.	Mean extinction efficiency as a function of real refractive index	55

LIST OF FIGURES, continued

FIGURE	TITLE	PAGE
4.7.	Extinction efficiency as a function of imaginary refractive index	56
4.8.	Real refractive index effects on mean specific extinction efficiency of large particles	57
4.9.	Imaginary refractive index effects on mean specific extinction efficiency of large particles	58
4.10.	Effect of distribution type on mean specific extinction efficiency in the large particle limit	59
4.11.	Theoretical optical depth as a function of mean particle diameter for large sizes	61
4.12.	Effect of distribution type on mean specific extinction efficiency in small particle limit	62
4.13.	Theoretical optical depth as a function of mean particle diameter for small sizes	64
4.14.	Dual wavelength extinction as a function of D_{32}	67
4.15.	Light extinction through a radially inhomogeneous particle cloud	69
4.16.	Effects of radial mass distribution on theoretical optical depth	74
5.1.	Abel inversion geometry for an axisymmetric cloud	77
6.1.	Measurement geometry for multiple angle scattering	88
6.2.	Effect of distribution type on angular diffraction profile	93
6.3.	Effects of distribution width on angular diffraction profile	94
6.4.	Normalized angular diffraction profile	96
6.5.	Comparison of backscatter profile predicted from Mie and Fraunhofer theories	98
6.6.	Backscatter efficiency as a function of particle size	99
6.7.	Backscatter measurement geometry	101

LIST OF FIGURES, continued

FIGURE	TITLE	PAGE
6.8.	Mean backscatter efficiency as a function of mean particle diameter	103
6.9.	Mean specific backscatter efficiency as a function of mean particle diameter	105
7.1.	Measurement geometry for combined scattering and extinction	108
8.1.	Measurement geometry for simulated extinction/backscatter/ diffraction experiment	116
8.2.	Theoretical optical depth as a function of D_{32}	118
8.3.	Theoretical normalized diffraction profiles	121
8.4.	Theoretical ensemble backscatter efficiency	125
9.1.	Multiple path extinction measurement geometry	129
9.2.	Nd:YAG laser system schematic diagram	131
9.3.	HeNe laser system schematic diagram	132
9.4.	Inverted experimental attenuation coefficient	134
9.5.	Trial functions for the experimental radial attenuation coefficient	136
9.6.	Calculated distribution of mean particle size based on trial functions	137
9.7.	Optical depth ratios as function of mean particle diameter	139
9.8.	Optical depth for single path, single wavelength measurement	140

LIST OF TABLES

TABLE	TITLE	PAGE
4.1	Weighting Factors for Mass Distribution Functions	72
8.1	Experimental Simulation Parameters	115
8.2	Recovered D_{32} Using Simulated Optical Extinction	119
8.3	Recovered D_{42} From Simulated Diffraction Measurements	122
8.4	Recovery of D_{32} From Simulated Backscatter Measurements	124
8.5	Results of Data Recovery From Combined Measurements	126
9.1	Results of Optical Depth Experimental Measurements	133
9.2	Distribution of Mean Particle Sizes, D_{32}	141

NOMENCLATURE

a_n	Amplitude "a" scattering coefficient
A	Flowfield cross sectional area
b_n	Amplitude "b" scattering coefficient
$\overline{B}$	Magnetic flux density vector
c_m	Mass concentration
c_n	Number concentration
c_v	Volume concentration
C_a	Absorption cross section
C_e	Extinction cross section
C_s	Scattering cross section
D	Particle diameter
$\overline{D}$	Electric displacement vector
D_m	Mode diameter of particle size distribution function
D_{mm}	Mass median diameter of a particle distribution
D_{MN}	Ratio of M and N moments of size distribution
e_j	Flow geometry parameter
$\overline{E}$	Electric field vector
$\overline{E}_i$	Incident electric field vector
$\overline{E}_1$	Internal electric field vector
$\overline{E}_2$	External electric field vector
$f(D)$	Probability density function
$h_n^{(1)}$	Spherical Hankel function of the first kind
$h_n^{(2)}$	Spherical Hankel function of the second kind
$\overline{H}$	Magnetic field intensity vector

$\overline{H}_s$	Scattered magnetic field intensity vector
i_1	Perpendicular intensity function
i_2	Parallel intensity function
I_1	Perpendicular component of scattered light intensity
I_2	Parallel component of scattered light intensity
$j_n(p)$	Spherical Bessel function of the first kind
$\overline{J}$	Electric current density vector
$J_{n+1/2}$	Bessel function of the first kind
k	Wave propagation vector
L	Optical path length through particle cloud
$\dot{m}$	Mass flow rate
$\dot{m}_T$	Total mass flow rate
m	Complex refractive index
m_i	Imaginary part of refractive index
m_r	Real part of refractive index
$\overline{M}$	Vector harmonic solution to the vector wave equation
$n(D)$	Particle size distribution function
$\overline{N}$	Vector harmonic obtained from $\overline{M}$
N_o	Total number of particles
$N(D)$	Number of particles per micron
$P(D)$	Cumulative probability distribution
P_n^l	Associated Legendre functions
Q_a	Absorption efficiency
Q_b	Backscatter efficiency
Q_e	Extinction efficiency
Q_s	Scattering efficiency

r	Radial coordinate in axisymmetric flowfield
$\bar{r}$	Position vector of observer relative to particle
S_1	Amplitude scattering function (perpendicular)
S_2	Amplitude scattering function (parallel)
T	Fraction of transmitted intensity
U	Uncertainty
v	Particle velocity
V	Volume containing particles
W	Beam width
W_d	Distribution width parameter
$y_n(p)$	Spherical Bessel function of the second kind
$Y_{n+1/2}$	Bessel function of the second kind
z	Axial coordinate in axisymmetric flowfield
$z_n(p)$	Generalized spherical Bessel function
α	Mie size parameter
ϵ	Electric permittivity
κ	Bulk attenuation coefficient
λ	Wavelength of light
μ	Magnetic Permeability
ν	Variance of a size distribution function
ω	Angular frequency
Φ_e	Even azimuthal solution to the scalar wave equation
Φ_o	Odd azimuthal solution to the scalar wave equation
π_n	Angular scattering function
$\psi_n(p)$	Ricatti-Bessel function of the first kind
$\psi(r,\theta,\Phi)$	General solution to homogeneous scalar wave equation

ρ	Particle material density
ρ_e	Electric charge density
σ	Standard deviation of a distribution
$\sigma(R)$	Mass flow rate per unit area
τ	Optical depth
τ_n	Angular scattering function
Θ_h	Divergence half-angle
$\xi_n(p)$	Ricatti-Bessel function of the second kind

CHAPTER I

INTRODUCTION

This work describes the results of an investigation of the application of light scattering and extinction techniques to the measurement of mean particle sizes both in homogeneous particle ensembles, and in axisymmetric ensembles that have spatially nonuniform mass distributions. Optical techniques for particle sizing were studied because of the interest in developing nonintrusive measurement capability. Axisymmetric particle distributions were of interest because they form an important class of real-life measurement problems comprised of spray nozzle calibrations[1-2], smoke particulate monitoring[3-4], and combustion diagnostics[5-6]. In these applications, the particle size distribution function may vary in number density depending on the flowfield characteristics of the experiment. In spatially large scale particle fields, the mean sizes often depend on location within the particle field, as depicted in Figure 1.1, with larger particles concentrated toward the center and smaller particles near the edge.

Particle size measurement is a well-studied and often controversial field. Sizing techniques have been based on both direct particle sampling and optical measurements, the results of which are sometimes dependent on the chosen method. Direct sampling techniques, in which particles are withdrawn from the particle cloud and subsequently examined by optical or scanning electron microscope, well serve low density, low velocity measurements. Intrusive sampling probes, however, may bias the collected sample by causing particle breakup or agglomeration. The desire for remote measurements of particle flows, therefore, has motivated the development of non-intrusive optically based sizing techniques.

Optical methods for particle size determination are based on either imaging,

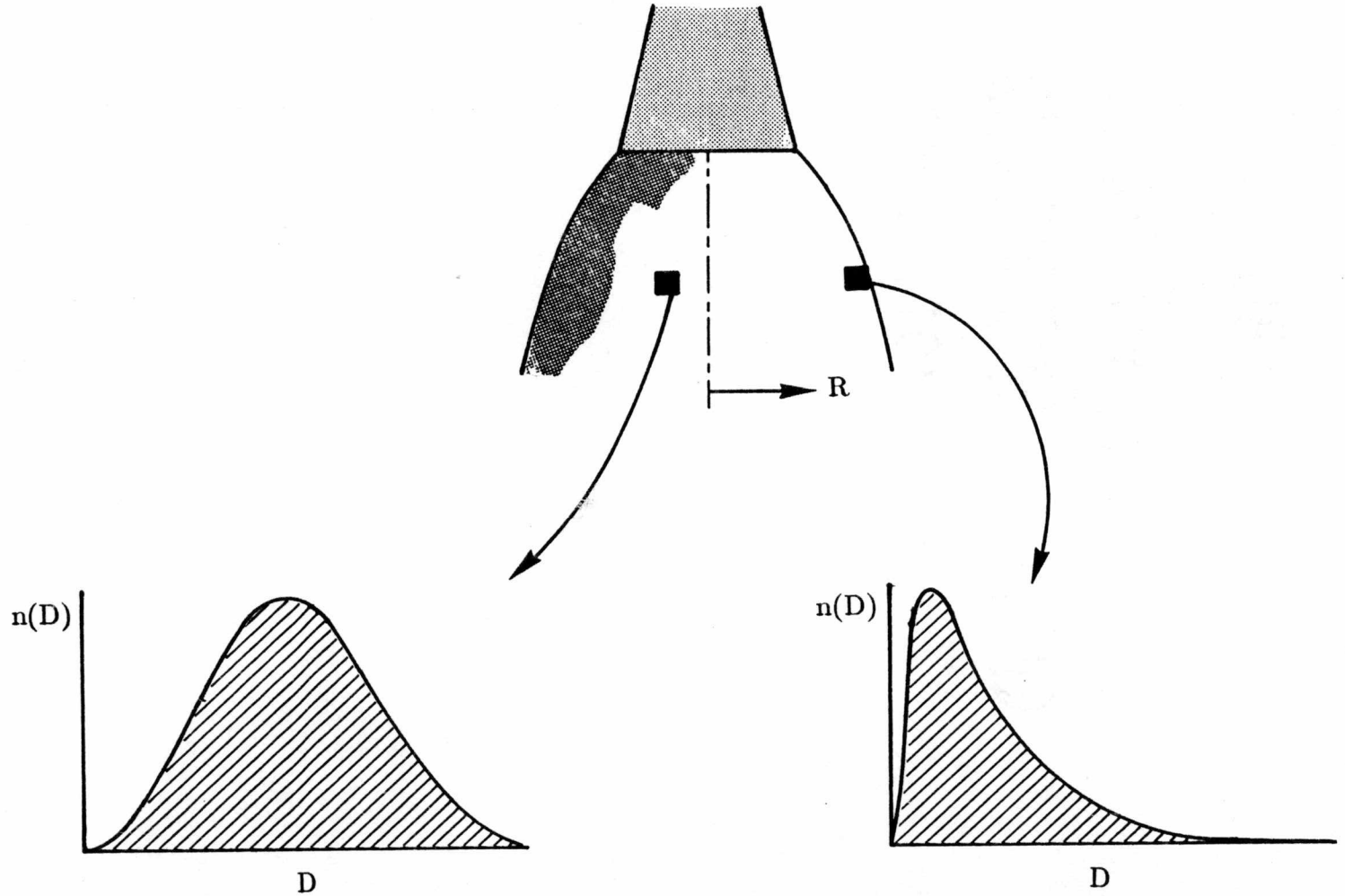


Figure 1.1. Dependence of particle distribution on flowfield location.

scattering, or extinction measurements. Optical imaging techniques, which include photography[7-8], holography[9-13], and optical array probes[14-16], have been successfully used to provide reliable size and shape information on individual particles moving at relatively low velocities. Imaging techniques, however, are impractical for high number density clouds. The particle size range for imaging techniques is determined by the resolution of the optical system, and is limited practically to particles greater than approximately 10 microns in diameter.

Light scattering techniques have been applied to both single particle[17-22] and particle ensemble measurements[23-24], and are particularly useful for diameters less than 10 microns. Scattering instrumentation developed for particle velocity measurements have also been applied to the determination of particle size[25-31]. Most of the reported light scattering techniques have been applied to low density clouds with small sampling volumes, in which single particle scattering is valid and the geometry of the experiment is well defined. Particle ensembles, which generally include a range of particle sizes, are often examined with techniques that provide the average sizes of the distribution. For large, spatially nonuniform particle clouds, an extension of existing light scattering techniques is required to provide the spatial distribution of particle size within the cloud.

The measurement technique chosen for a particular experiment depends largely on the geometry of the experiment, the optical properties of the particles, and the spatial density profiles of the size distribution. Typical particle size distribution functions (PSDF) may vary both in number density and mass concentration, depending on the flowfield characteristics of the particulate generator. Optical properties affect the recovery of particle size information through the calculation of the Mie scattering coefficients. Although scattering methods offer the best solution to the problem of size measurements in large scale flows, potential limitations in

existing techniques must be overcome. Some of these limitations are:

1. Small volumes are usually required, so that the scattering angles will be the same for all particles in the sample.
2. Scattering techniques are difficult to interpret in high density ensembles, because of the combined effects of extinction and multiple scattering.
3. The results of scattering measurements are acutely dependent on refractive index, which may be unknown for some applications, and require the assumption of spherical particles and known chemical composition.

Techniques are sought, therefore, which are relatively robust against uncertainties in particle shape and optical properties.

Scattering measurements based on the Mie theory[32] require spherical particles of known refractive index. Nonspherical particle scattering is orientation dependent and demands cumbersome numerical scattering calculations which make the inverse problem (i.e., determining the particle size and shape from the scattering signature) virtually intractable. Because the scattering coefficients are functions of the complex refractive index, temperature variations in the real and imaginary parts of the refractive index can lead to measurement errors, especially in conditions of two-phase flow. Multiple scattering of light by optically dense particle ensembles also can cause misinterpretation of data unless appropriate precautions are observed. In many particle measurement applications, however, particle characteristics are either known or their influence on the results can be minimized by the appropriate choice of experimental technique. Subsequent chapters address these issues in more detail.

Estimates of the mean size and the particle size distribution function in some cases may be determined from a combination of transmittance and scattering measurements at several wavelengths[33–34]. Transmittance measurements provide an

estimate of the mean particle diameter of a particle field by measuring the net extinction of a beam of light traversing the field. This technique provides a path length integrated average measurement through the entire plume or particle field, and is relatively insensitive to the shape of the PSDF, or to uncertainties in the refractive index[35]. Transmission measurements, however, fail to provide any information about the details of the particle distribution in either size or shape unless the spatial distribution is homogeneous.

Angular scattering measurements can, in principle, provide information about the particle size distribution function, as well as the ratios of the moments of diameter, if adequate angular scattering information is acquired[36-38]. This technique is often applied to measurements of particles within a small volume element, in which the PSDF is assumed to be independent of position within the particle ensemble. Scattering measurements are inherently sensitive to particle size distribution, particle shape, and refractive index. This is particularly true of backscatter measurements, as will be demonstrated in later chapters.

An approach under development for several years at the Arnold Engineering Development Center (AEDC) attempts to measure the spatial distribution of average size in dense particle fields of large spatial extent where single particle measurements are not possible. To improve performance predictions for flow characterization, techniques are needed that measure both the size and spatial distributions of particles in these types of processes. This work specifically examines particle sizing techniques for use in homogeneous particle clouds, and in axisymmetric particle flowfields with spatially varying mass density profile, such as encountered in a two-phase free-jet. The chief objective is to obtain as much information as possible about particle size, with the least amount of information about the particle optical characteristics or distribution.

Reported here are the results of recent investigations by the author of extinction and scattering measurement techniques that potentially may reveal particle field characteristics in axisymmetric flow conditions. Methods were developed for providing estimates of the mean size and spatial distribution of particles using several simultaneous measurements. This work builds upon well-known extinction techniques for measurement of spatially homogeneous particle distributions and extends these processes to determine particle size information for large scale, spatially nonuniform particle flows. Two new scattering techniques are also introduced for determining mean particle sizes. The particle sizes of experimental interest in this research are less than about 10 microns, although the approach presented is valid for larger particles if the appropriate wavelengths are chosen.

Chapter II reviews the fundamental definitions of the Mie scattering theory. Scattering from randomly oriented nonspherical particles is beyond the scope of this effort. The concepts of scattering cross-sections and efficiencies are introduced. These quantities depend strongly on the particle shape, complex refractive index, particle size, and the illumination wavelength. The intensity of the scattered light is dependent on the polarization of the incident electric field and the angle from which the particle is observed. A brief discussion of the small and large particle approximations, described by Rayleigh scattering and Fraunhofer diffraction, respectively, also is included.

The light scattered from an ensemble of particles consists of a superposition of the scattered intensities from each particle in the distribution. Therefore, Chapter III presents the basic elements of particle distribution statistics, with emphasis on the aspects used to retrieve size content from scattering and extinction measurements. Also discussed are the concepts of the distribution function, probability density function, and moments of the distribution. This information is then applied

in Chapter IV to the measurement of the extinction of a beam of light through a uniform slab of spherical particles. The extinction is shown to be a function of the average size of the distribution, as defined by various ratios of moments of the distribution.

These concepts are extended in Chapter V to the problem of extinction through a spatially nonuniform, axisymmetric particle distribution having radial mass density dependence. Single wavelength transmission measurements at several paths through the particle cloud yield the spatial distribution of average particle sizes. Scattering measurements, in limited circumstances, may provide additional information on mean particle sizes, as discussed in Chapter VI. Both backscatter and forward scatter techniques are developed that offer insight into the size characteristics of a particle ensemble.

While average particle size is an important parameter, there is no substitute for having the entire particle size distribution function. This is a singularly difficult task to accomplish, however. Chapter VII reviews measurement requirements that have been presented in the literature for inverting multiple wavelength scattering and extinction data to obtain the complete size spectrum.

A numerical simulation of the scattering and extinction methods developed in this work is described in Chapter VIII. Specifically, the simulation examines the ability to retrieve mean size information using multiple wavelength extinction, backscatter, and diffractively scattered light from a homogeneous slab of particles. Chapter IX then describes experimental measurements on particles in a large-scale, two-phase free-jet. The mean particle size and mass flow distribution of the particles were analyzed using the above procedures.

The concluding chapter contains a summary of this effort and recommendations for future work in this area.

CHAPTER II

REVIEW OF MIE SCATTERING THEORY

The application of scattering and extinction measurements to particle sizing requires several assumptions about the nature and distribution of the particles. The characteristics of the scattered lightwave rely on the properties of both the scattering particle and the surrounding medium including such important parameters as particle size, refractive index, and wavelength of the illumination. Conversely, information about these quantities can in principle be obtained from the inverse problem – i.e., measuring the scattered intensities at several angles and wavelengths, and back-calculating the desired parameter. Normally, this is a difficult procedure.

Solutions for nonspherical particles, particularly ellisoidal and cylindrically shaped particles, have been sought by many investigators[39-43], since particle shape impacts the design and interpretation of optical sizing measurements. Scattering is complicated and strongly polarization dependent for nonspherical particles. General solutions to the scattering problem are not analytically possible for arbitrarily shaped particles, but they may be determined numerically by applying the basic theory of dipole scattering to small elements from which the larger particles are constructed. This approach, for example, is used in the Purcell-Pennypacker model[44]. Treatment of nonspherical particles is beyond the scope of this effort, although Mie theory provides a good first-order description of scattering from nonspherical particles. Slight deviations from spherical particle scattering are statistically insignificant when considering the overall random nature of particle ensembles.

Known refractive indices, both the real and imaginary components, must be specified in any Mie theoretical calculations of scattering or extinction efficiencies. The complex refractive index can be written as $m = m_r + im_i$, where m_r is the

real part, and m_i is the imaginary part of m corresponding to the absorption of the material. It is assumed that the particles have a uniform phase, or state, so that the refractive index is homogeneous within an individual particle, since optical properties are typically temperature and wavelength dependent and may change significantly during a phase transition between solid and liquid. Measurement applications in which two-phase particle flow exists would require knowledge of the relative mass fractions of solid and liquid particles. For this reason, measurement techniques are sought that are essentially insensitive to uncertainties in the refractive index.

An additional requirement is that of single particle scattering, which implies that the particle cloud must be optically thin; i.e., it must have low attenuation per unit length. For single scattering produced within low optical density clouds of spherical particles, the initial polarization of the illuminating beam is preserved[45]. Multiple scattering in high density particle clouds, however, generally leads to depolarization[45]. Linear birefringence can also be produced either by physically elongated or nonspherical particles, by spherical particles that have natural birefringence, or possibly by spherical particles that have nonhomogeneous refractive indices[45], such as might be found in a material undergoing a phase change. Higher density clouds can still be measured if care is taken to restrict the angular fields of view of the detection optics.

To provide an overview of the fundamental theory and terminology associated with light scattering, an outline is presented here of the Mie theory, which describes the scattering of a monochromatic plane polarized electromagnetic wave by an isotropic, homogeneous sphere of arbitrary size. Rigorous discussions of this material are available in several sources[45–49]. The geometry associated with the scattering of a plane wave from a spherical particle is depicted in Figure 2.1. The

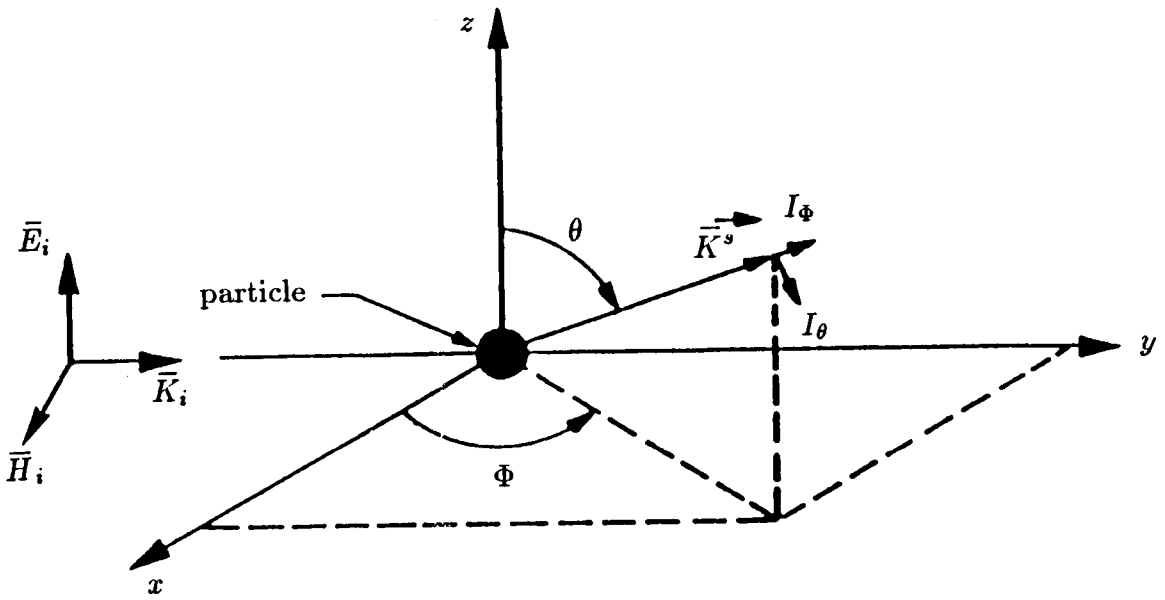


Figure 2.1. Spherical coordinate system for light scattering by a sphere.

electric field, $\overline{E}_i$, incident on a particle with diameter, D, is assumed to be linearly polarized and monochromatic and propagates through a homogeneous, isotropic medium of refractive index m_1. An electric field, $\overline{E}_1$, is produced inside the particle, while the resulting external field in the vicinity of the particle is $\overline{E}_2$. This field is the vector sum of the incident and scattered waves. The fields in all regions of space that surround the particle must satisfy both Maxwell's equations and the appropriate boundary conditions corresponding to the discontinuous change in the electric permittivity ϵ and the magnetic permeability μ at the particle/medium interface. Maxwell's equations are[50]

$$\begin{aligned} \nabla \cdot \overline{D} &= 4\pi\rho_e \qquad \nabla \times \overline{E} = -\frac{d\overline{B}}{dt} \\ \nabla \cdot \overline{B} &= 0 \qquad\qquad \nabla \times \overline{H} = \overline{J} + \frac{d\overline{D}}{dt} \end{aligned} \tag{2.1}$$

where $\overline{D}$ represents the electric displacement, $\overline{B}$ is the magnetic flux density vector, $\overline{H}$ is the magnetic intensity, $\overline{J}$ is the current density, and ρ_e is the electric charge density.

Boundary conditions require the tangential components of the electric and magnetic fields, $\overline{E}$ and $\overline{H}$, to be continuous across the interface. Taking the curl of each of the above equations, it is found that both $\overline{E}$ and $\overline{H}$ must satisfy the vector wave equation[50]

$$\begin{aligned} \nabla^2\overline{E} + k^2\overline{E} &= 0 \\ \nabla^2\overline{H} + k^2\overline{H} &= 0 \end{aligned} \tag{2.2}$$

where k is the wave propagation constant equal to $2\pi/\lambda$.

With the approach offered by Bohren and Huffman[47], the solution to the vector wave equation in spherical polar coordinates is simplified by introducing a vector, $\overline{M}$, defined as

$$\overline{M} = \nabla \times (\overline{r}\,\psi) \tag{2.3}$$

which is a solution of the vector wave equation in spherical polar coordinates if $\overline{r}$ is chosen to be the position vector of the observer relative to a coordinate system centered on the spherical particle, and if ψ is a general solution of the homogeneous scalar wave equation. Another vector is constructed from the vector $\overline{M}$ in the form

$$\overline{N} = \nabla \times \overline{M} \; / \; k \tag{2.4}$$

where $\overline{N}$ has zero divergence ($\nabla \cdot \overline{N} = 0$) and also is a solution of the vector wave equation. $\overline{M}$ and $\overline{N}$ are known as the vector harmonics.

If the function ψ satisfies the scalar wave equation in spherical polar coordinates, then the vectors $\overline{M}$ and $\overline{N}$ are solutions of the vector wave equation in spherical polar coordinates.

The scalar wave equation in spherical polar coordinates is[47]

$$\frac{1}{r^2} \; \frac{\partial}{\partial r} \left(r^2 \frac{\partial \psi}{\partial r} \right) + \frac{1}{r^2 \; sin\theta} \; \frac{\partial}{\partial \theta} \left(sin\theta \; \frac{\partial \psi}{\partial \theta} \right) + \frac{1}{r^2 \; sin\theta} \; \frac{\partial^2 \psi}{\partial \phi^2} + k^2 \psi = 0 \tag{2.5}$$

where θ represents the colatitude and ϕ represents the azimuthal angle.

Solutions to this equation are found in any standard text on electromagnetic theory or modern physics[47,50-51]. To find the solution, ψ, of the scalar wave equation in spherical polar coordinates, the technique of separation of variables is applied using

$$\psi(r, \theta, \Phi) = R(r) \; \Theta(\theta) \; \Phi(\phi) \tag{2.6}$$

The even and odd azimuthal solutions are, respectively[47],

$$\Phi_e = cos \; l\phi, \qquad \Phi_o = sin \; l\phi \tag{2.7}$$

where l is an integer. The θ solutions are the associated Legendre functions of the first kind

$$\Theta = P_n^l \; (cos \; \theta) \tag{2.8}$$

The solutions to the radial equation are the spherical Bessel functions of the first and second kind, defined by[47]

$$j_n(p) = \sqrt{\pi/2p}\; J_{n+1/2}\;(p), \qquad y_n(p) = \sqrt{\pi/2p}\; Y_{n+1/2}\;(p) \tag{2.9}$$

where $p = kr$. $J_{n+1/2}(p)$ and $Y_{n+1/2}(p)$ are known as the Bessel functions of the first and second kind, respectively. Linear combinations of j_n and y_n also are acceptable solutions to the wave equation. It is common, therefore, to employ a particular type of linear combination of these functions defined as the spherical Hankel functions of the first and second kind

$$h_n^{(1)} = j_n + iy_n, \qquad h_n^{(2)} = j_n - iy_n \tag{2.10}$$

The complete even solution to the scalar wave equation is

$$\psi_{eln} = cos\; l\phi\; P_n^l\;(cos\;\theta)\; z_n(kr) \tag{2.11}$$

with a similar form for the odd solution. The function $z_n(kr)$ represents any of the spherical Bessel functions that satisfy the appropriate boundary conditions. Using the scalar solutions, the vector harmonics $\overline{M}$ and $\overline{N}$ for the even solutions may now be determined from[47]

$$\begin{aligned} \overline{M}_{eln} &= \nabla \times (r\psi_{eln}) \\ \overline{N}_{eln} &= \nabla \times \overline{M}_{eln}/k \end{aligned} \tag{2.12}$$

with similar forms for the odd solutions. Because the vector harmonic solutions are linear combinations of orthogonal functions, it is possible to describe any wave disturbance as a linear combination of the vector harmonics. The incident and scattered wave fields, therefore, can be expanded in the vector spherical harmonics

$$\begin{aligned} E_s &= \Sigma\; E_n\;(i\; a_n N - b_n M) \\ H_s &= \frac{k}{\omega cos\theta}\;\Sigma\; E_n\;(i\; b_n N + a_n M) \end{aligned} \tag{2.13}$$

where a_n and b_n are defined as the scattering coefficients, ω is the angular frequency of the electromagnetic wave, and $i = \sqrt{-1}$.

At this point, further simplification occurs by introducing the angular functions

$$\pi_n(\theta) = P_n^l \; / \; sin\theta$$
$$\tau_n(\theta) = dP_n^l \; / \; d\theta \tag{2.14}$$

The field equations are solved for the scattering coefficients after the additional simplification afforded by the Ricatti-Bessel functions is evoked:

$$\psi_n(p) = p \; j_n(p)$$
$$\xi_n(p) = p \; h_n^{(1)}(p) \tag{2.15}$$

Computation of the intensity scattering functions for a sphere consists of a two step procedure in which, first, the scattering coefficients a_n and b_n are evaluated from the Ricatti-Bessel functions; and, second, the scattering amplitude functions are then formed by combining the scattering coefficients with appropriate Legendre functions. The scattering coefficients then are solved and written as functions of the Ricatti-Bessel functions[46-47]

$$a_n = \frac{m\psi_n\,(m\alpha)\;\;\psi_n'\,(\alpha) \;-\; \psi_n\,(\alpha)\;\;\psi_n'\,(m\alpha)}{m\psi_n\,(m\alpha)\;\;\xi_n'\,(\alpha) \;-\; \xi_n\,(\alpha)\;\;\psi_n'\,(m\alpha)}$$
$$b_n = \frac{\psi_n\,(m\alpha)\;\;\psi_n'\,(\alpha) \;-\; m\psi_n\,(\alpha)\;\;\psi_n'\,(m\alpha)}{\psi_n\,(m\alpha)\;\;\xi_n'\,(\alpha) \;-\; m\xi_n\,(\alpha)\;\;\psi_n'\,(m\alpha)} \tag{2.16}$$

where $\alpha = \pi D \; / \; \lambda$ is defined as the Mie parameter, or size parameter, which presents the results of Mie calculations in a generalized, nondimensional form.

From the a_n and b_n scattering coefficients, the amplitude scattering functions are defined by [47]

$$S_1 = \sum_{n=1}^{\infty} \frac{2n+1}{n(n+1)} \; [a_n\pi_n + b_n\tau_n]$$
$$S_2 = \sum_{n=1}^{\infty} \frac{2n+1}{n(n+1)} \; [a_n\tau_n + b_n\pi_n] \tag{2.17}$$

The functions S_1 and S_2 calculated from the Mie theory represent the amplitude components of the scattered lightwave perpendicular and parallel respectively, to the scattering plane.

The intensity of the scattered wave is proportional to the square of the amplitude function and is described by[45-47]

$$I_1 = \frac{k^2}{r^2} |S_1|^2 \, sin^2\phi = \frac{k^2}{r^2} \, i_1 \, sin^2\phi$$
$$I_2 = \frac{k^2}{r^2} |S_2|^2 \, cos^2\phi = \frac{k^2}{r^2} \, i_2 \, cos^2\phi \tag{2.18}$$

where i_1, and i_2 are the intensity functions. I_1 and I_2 represent the intensities of the perpendicular and parallel components of the lightwave relative to the scattering plane. Examples of the scattered intensity functions for particles with diameters of 0.01, 0.1, 1.0, and 10.0 microns are shown in Figures 2.2 through 2.5, respectively for light which is polarized perpendicular to the plane of incidence. These functions were generated from the Mie scattering code presented in Bohren and Huffman[47]. The scattering profiles shown in these figures are characteristic of light scattering from particles with diameters smaller than, on the order of, and greater than the wavelength of the illumination, respectively and are included to illustrate the complex nature of particle scattering.

If the particles are spherical in shape and the incident beam is polarized perpendicular to the scattering plane, the scattered light is also perpendicularly polarized and has intensity i_1. It is noteworthy that both the magnitude and angular distribution of scattered light vary with size and optical properties of the particle, as illustrated in Figures 2.2 through 2.5.

Particles small in contrast to the wavelength of the incident illumination are described by an approximation to the Mie theory known as Rayleigh scattering. This type of scattering is basically the result of dipole scattering. The intensity of

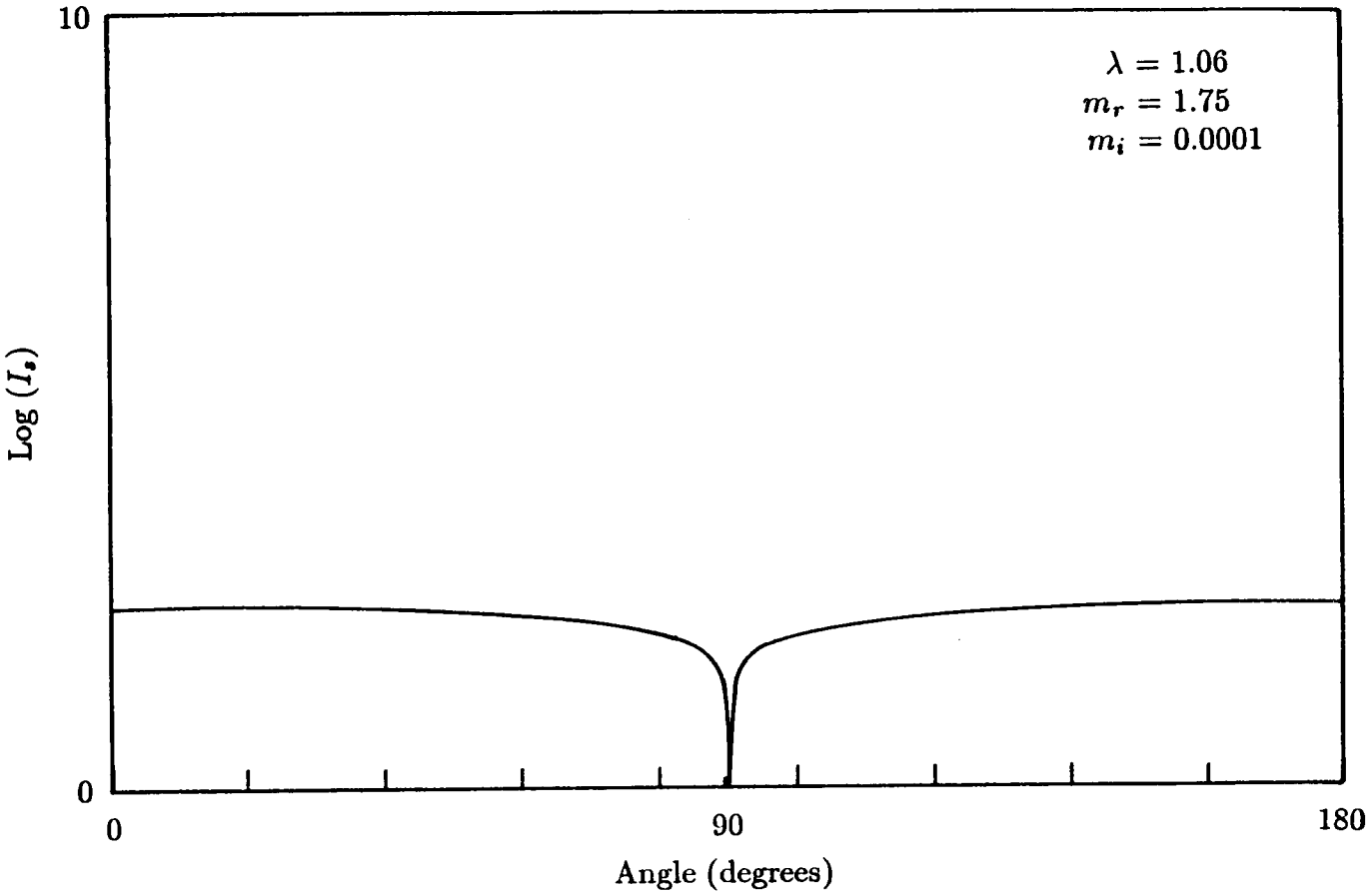


Figure 2.2. Angular scattering function for a 0.01 μm particle.

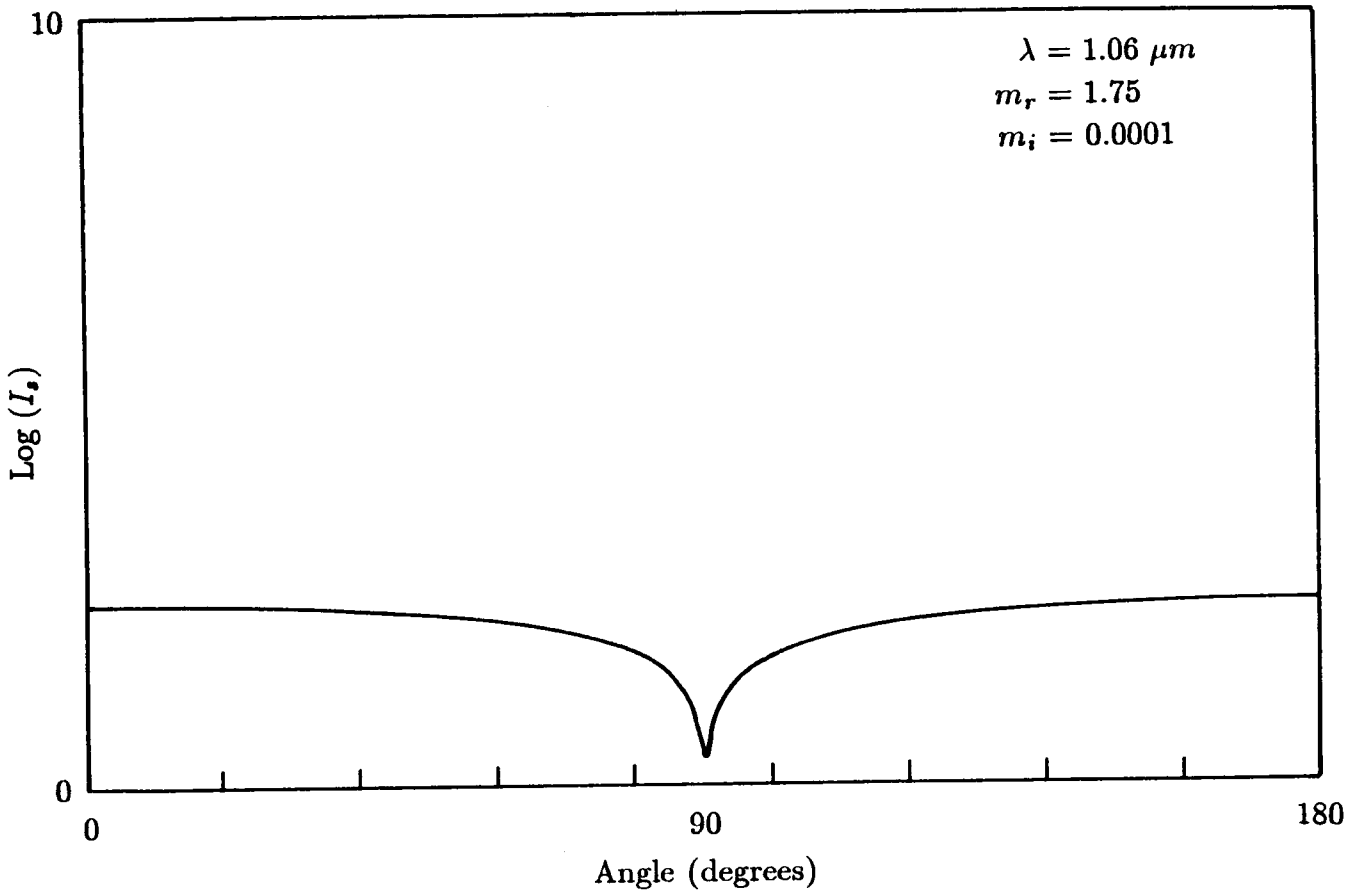


Figure 2.3. Angular scattering function for a $0.1\mu m$ particle.

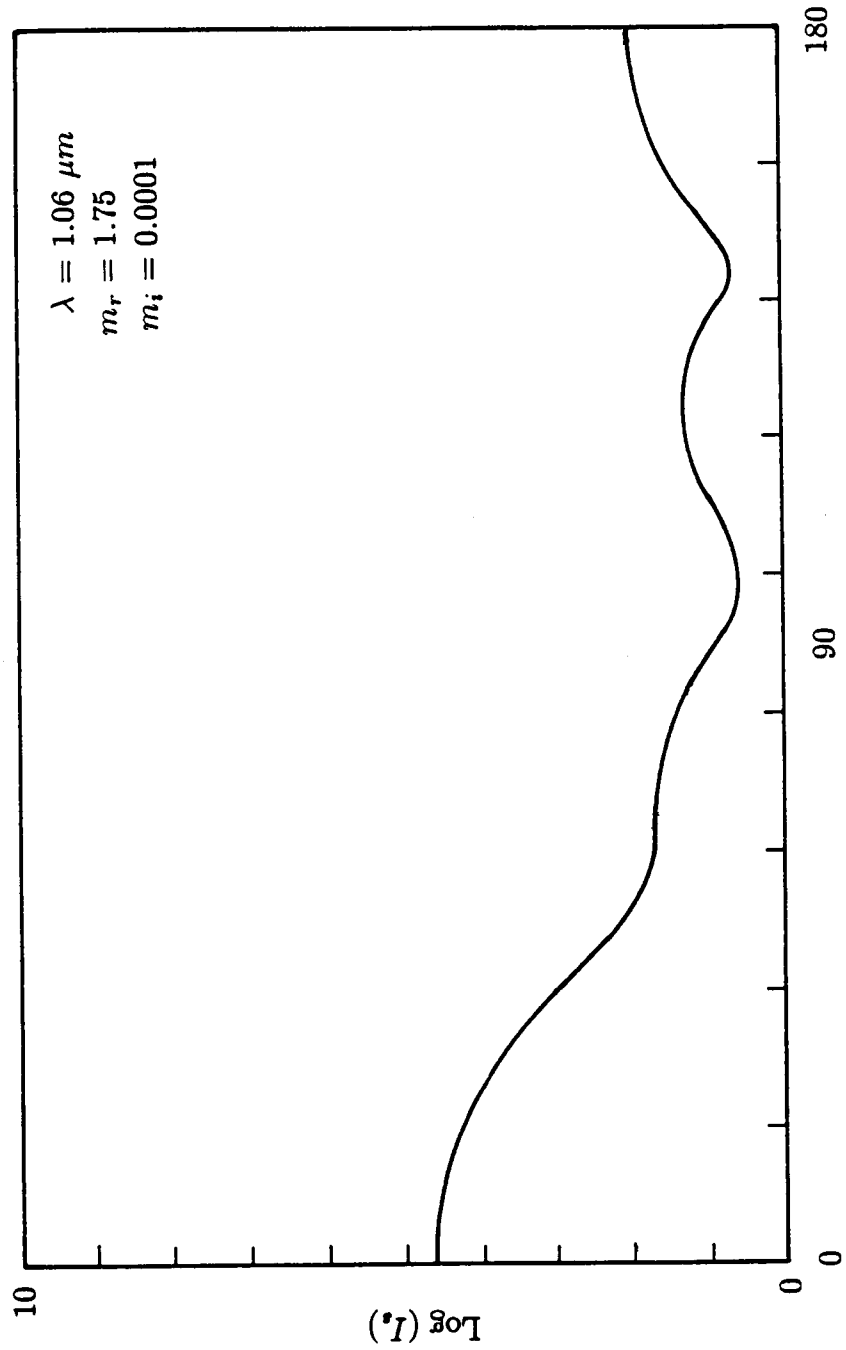


Figure 2.4. Angular scattering function for a $1.0 \mu m$ particle.

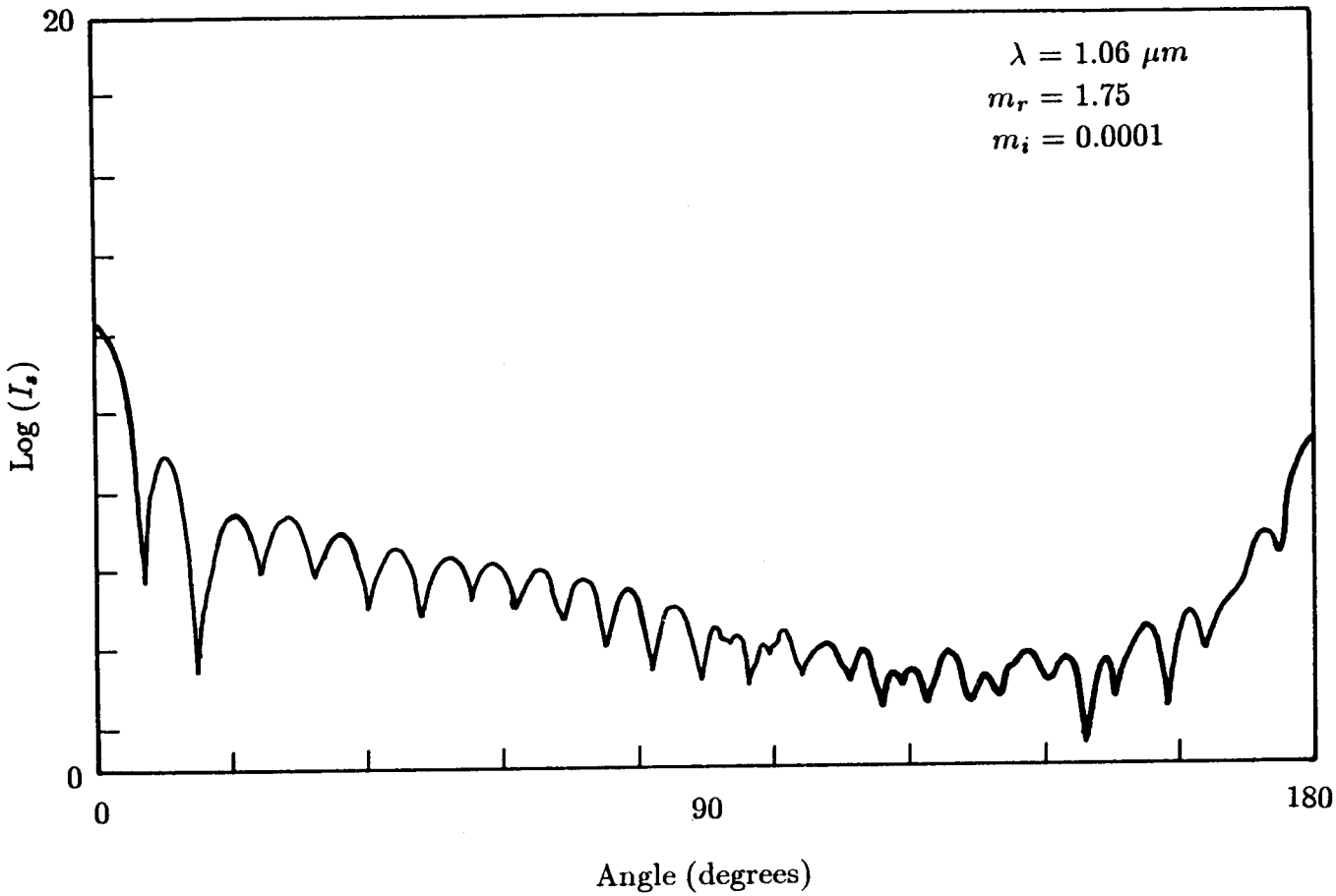


Figure 2.5. Angular scattering function for a $10.0\mu m$ particle.

Rayleigh scattered light, I_R, for unpolarized incident illumination is given by[46]

$$I_R = \frac{I_1 + I_2}{2} = \frac{D^6}{128\ k^4 r^2} \left| \frac{m^2 - 1}{m^2 + 1} \right|^2 (1 + cos^2\theta) \tag{2.19}$$

The condition for Rayleigh scattering is that the size of the particle must be much smaller than the wavelength, or, more specifically,[45]

$$D \ll \lambda \ / \ 2\pi \tag{2.20}$$

The full theory generally is used to calculate scattering for particles with diameters on the order of the wavelength of light. The exact solution for plane wave scattering from a spherical particle is obtained directly from the Mie theory. However, for very large particles, the Fraunhofer diffraction theory is used to describe the bending of the lightwaves in and around the particle. The normalized angular intensity of the light diffracted by a spherical particle is given by[46]

$$I = 4\ I_o\ [J_1(\alpha\ sin\theta)\ /\ (\alpha\ sin\theta)]^2 \tag{2.21}$$

where I_o is the intensity of the incident unpolarized light.

The scattering cross section is defined by the total energy removed from the incident beam of uniform intensity which is equal to the amount of energy incident on a cross sectional area, C_s. Similar definitions apply to the extinction and absorption cross sections, C_e and C_a, respectively. The sum of the scattering and absorption cross sections is equal to the extinction cross section[45],

$$C_e = C_s + C_a \tag{2.22}$$

Dimensionless cross sections, or efficiency factors, are defined for extinction, scattering, and absorption as the cross section per geometrical cross sectional area

of the particle[45], or

$$Q_e = 4\ C_e\ /\ (\pi\ D^2)$$
$$Q_s = 4\ C_s\ /\ (\pi\ D^2) \tag{2.23}$$
$$Q_a = 4\ C_a\ /\ (\pi\ D^2)$$

Similar to the extinction cross section, the extinction efficiency is related to the scattering and absorption efficiencies by[45]

$$Q_e = Q_s + Q_a \tag{2.24}$$

The cross sections and corresponding efficiencies are calculated from the Mie theory using the scattering coefficients. The extinction and scattering cross sections, for example, are defined by[47]

$$C_e = \frac{\lambda^2}{2\pi} \sum_{n=1}^{\infty} (2n+1)\ \{Re(a_n + b_n)\}$$
$$C_s = \frac{\lambda^2}{2\pi} \sum_{n=1}^{\infty} (2n+1)\ \{\ |a_n|^2 + |b_n|^2\ \} \tag{2.25}$$

where $Re(a_n + b_n)$ indicates the real part of the complex quantity $(a_n + b_n)$. The extinction cross section of a large particle is approximately equal to twice the geometric cross section.

Figures 2.6 and 2.7 present examples of the scattering cross section and the extinction cross section, respectively. Figure 2.8 illustrates the backscatter efficiency, Q_b, which is the scattering efficiency, sometimes denoted $Q_s\ (180^o)$, relative to the incident illumination, for several wavelengths. The extinction and backscatter efficiencies in particular will be used to estimate mean particle sizes in later chapters. The dependence of the extinction efficiency on the real and imaginary parts of the refractive index is demonstrated in Figures 2.9 and 2.10, respectively.

The extinction cross section is useful for determining the attenuation of a beam of light transmitted through a cloud of particles. The Lambert-Beer law[35,45] states

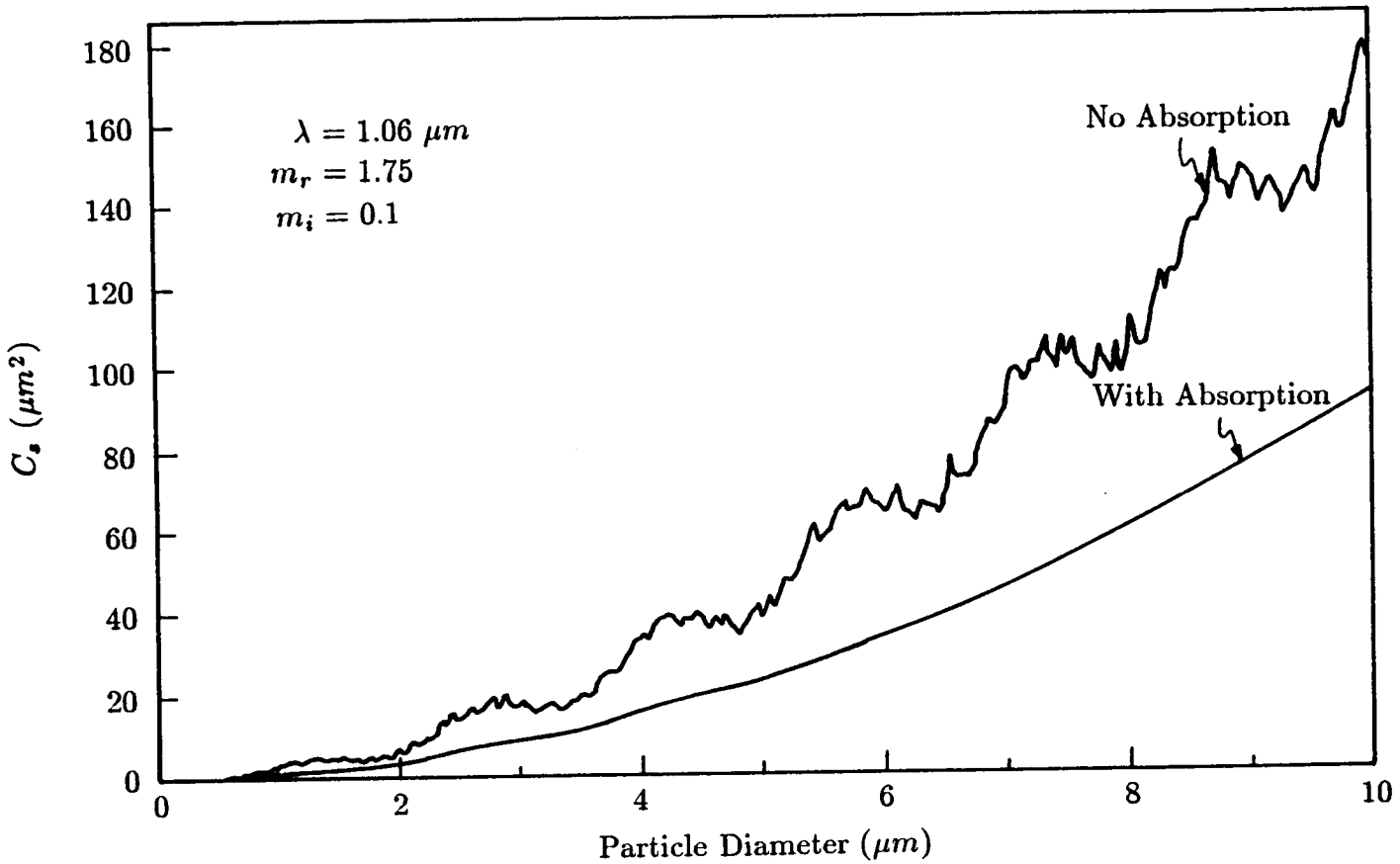


Figure 2.6. Scattering cross section as a function of diameter.

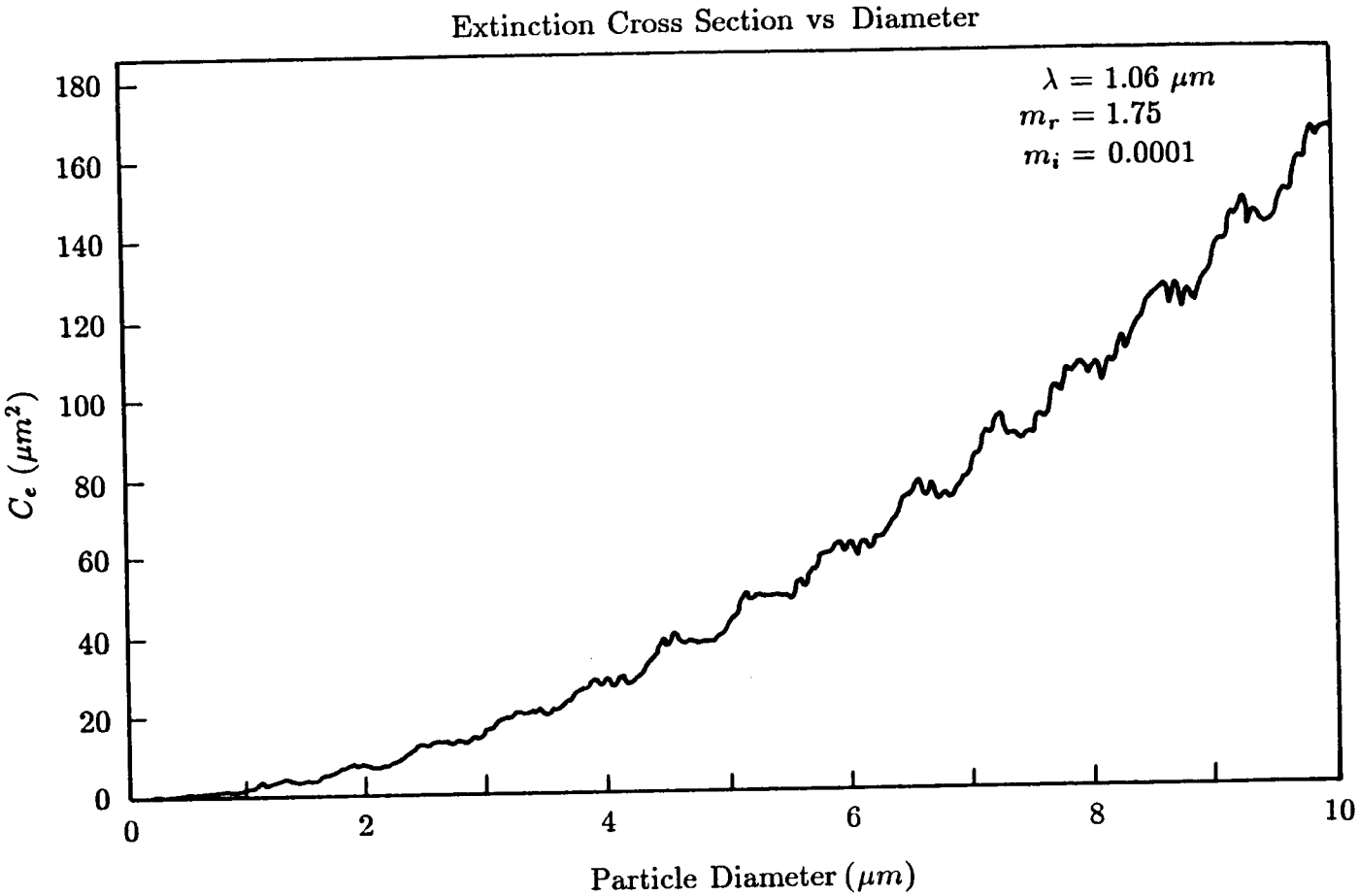


Figure 2.7. Extinction cross section as a function of diameter.

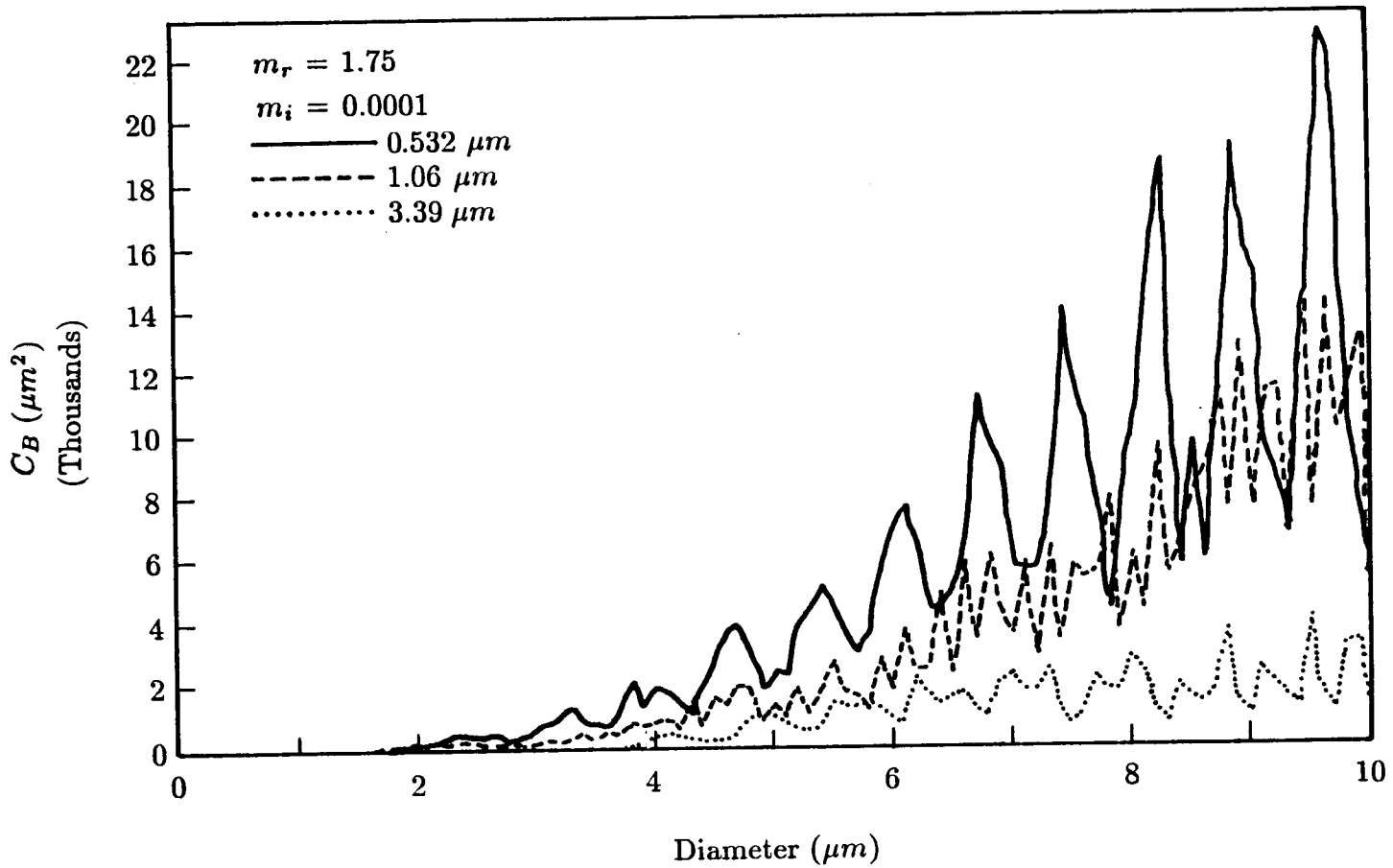


Figure 2.8. Backscatter cross section as a function of diameter.

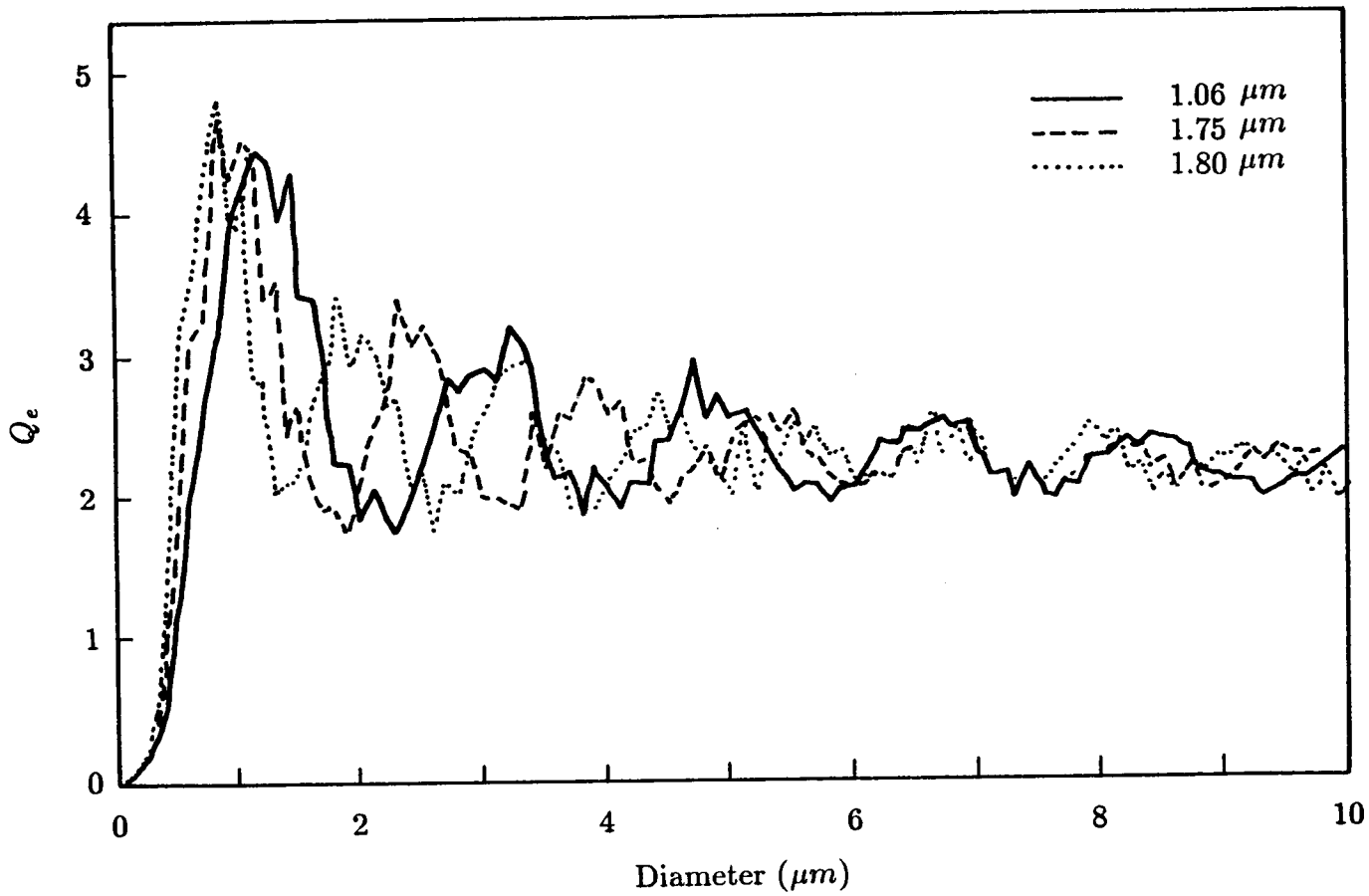


Figure 2.9. Extinction efficiency vs. real refractive index.

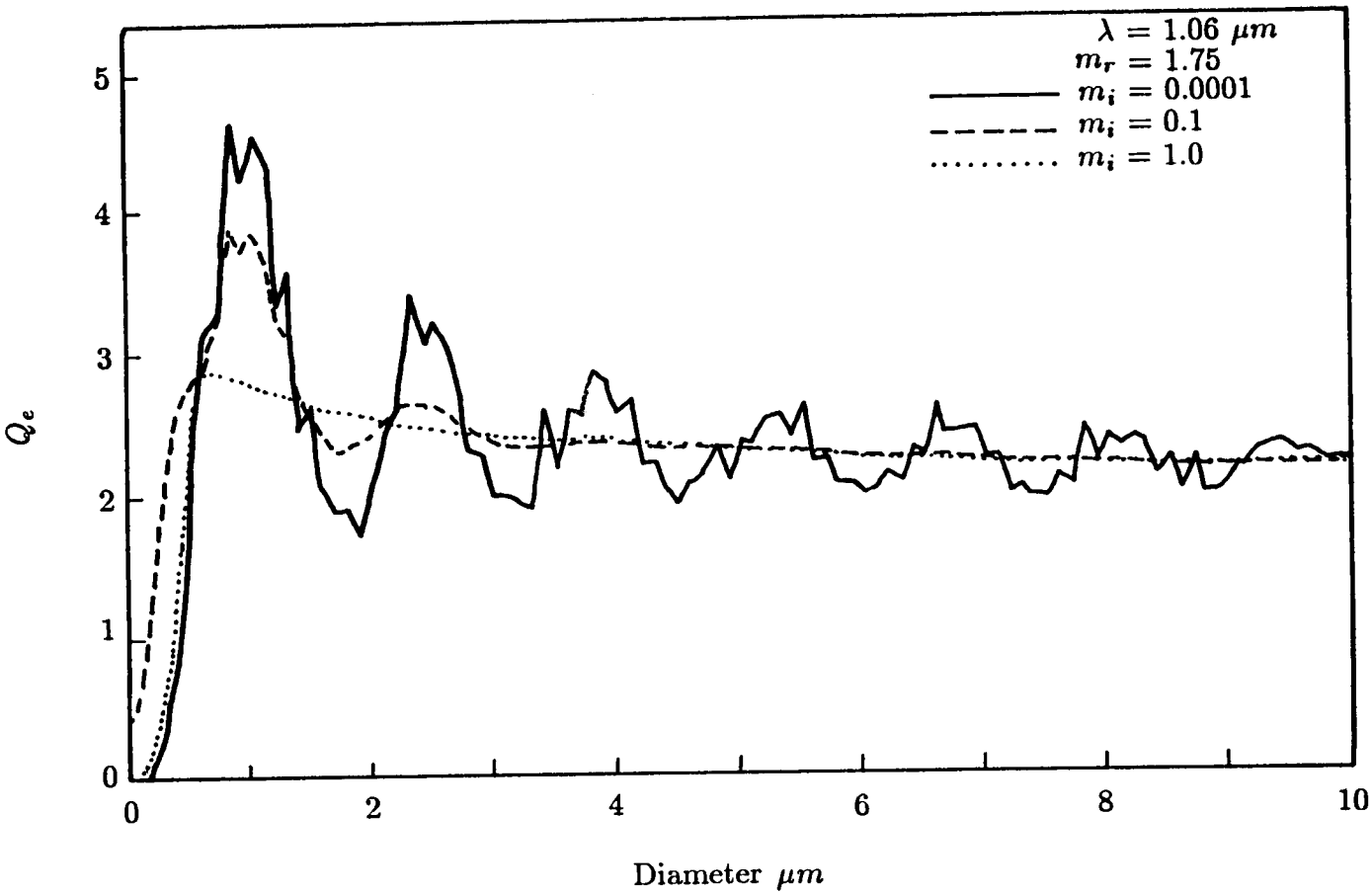


Figure 2.10. Extinction efficiency vs. imaginary refractive index.

that

$$T = exp\ (-\kappa x) \tag{2.26}$$

where κ is the attenuation coefficient and x is the path length through the cloud. The attenuation coefficient is interpreted as the total extinction cross section per cubic centimeter[45], or

$$\kappa = \int C_e(D)\ n(D)\ dD \tag{2.27}$$

where $n(D)$ is the particle number density distribution that describes the number of particles per unit volume with diameter D. Extinction measurements are generally applicable to large number density particle ensembles and, therefore, are significant for particle size measurements.

CHAPTER III

PARTICLE SIZE STATISTICS

The size of an individual spherical particle is determined in principle by measuring the scattered or attenuated light intensity and then relating the measurement to the particle size through the Mie scattering function for that particle. The angular scattering function for a particle with a specific size and refractive index is unique and, therefore, yields a direct measurement of particle size.

For ensembles of particles, the total intensity scattered into any angle is the sum of the contributions of the light scattered by each individual particle. The angular scattering function for a cloud of particles with a specific refractive index, but with a range of sizes, is no longer unique. Similarly, the light attenuated through an ensemble of particles is caused by the combined extinction and absorption cross-sections of every particle. The interference effects, manifested by the existence of angular intensity variations for single particle scattering, generally average out when large numbers of particles are observed simultaneously. To characterize the scattering properties of particle ensembles, an understanding of the definitions and statistics of particle size distributions is essential.

The size spectrum of a polydisperse collection of particles located within a volume element is characterized by the cumulative probability distribution function, or simply the probability distribution, $P(D)$, which represents the net probability of finding a particle in the size range 0 to D,[52] or

$$P(D) = P\{0 < \text{size} < \text{D}\} \tag{3.1}$$

where D is the particle diameter. The probability, as expressed here, is a fraction and therefore dimensionless.

Particle size distributions also are represented mathematically through a probability density function, $f(D)$, defined as the probability per unit size that a particle within the prescribed volume will have diameter D. The probability density function is related to the cumulative probability distribution by

$$f(D) = \frac{d}{dD} P(D) \tag{3.2}$$

The probability of finding a specific particle that has a diameter in the range $D_1 < D < D_2$ is stated mathematically by the expression[53]

$$\begin{aligned} P\{D_1 < D < D_2\} &= P(D_2) - P(D_1) \\ &= \int_{D_1}^{D_2} f(D)\, dD \end{aligned} \tag{3.3}$$

Integrating the probability density function over the entire range of possible particle sizes must yield a total probability equal to 1. The specific mathematical function utilized for the probability density must be normalized, therefore, according to

$$\int_o^\infty f(D)\, dD = 1 \tag{3.4}$$

Although the limits of integration range from zero to infinity, the upper integration limit may be replaced by the largest expected particle size, D_{max}.

Commonly used algebraic forms of the probability density functions for describing particle size distributions include the normal, or Gaussian, the log-normal, the beta, the gamma, and the rectangular distributions. Several of these functions are shown in Figure 3.1. A more complete discussion of the pertinent features of several of the distribution functions, which will be used periodically in this effort, are included for reference in Appendix A. Figure 3.2 illustrates the probability distributions corresponding to each of the density functions shown in Figure 3.1.

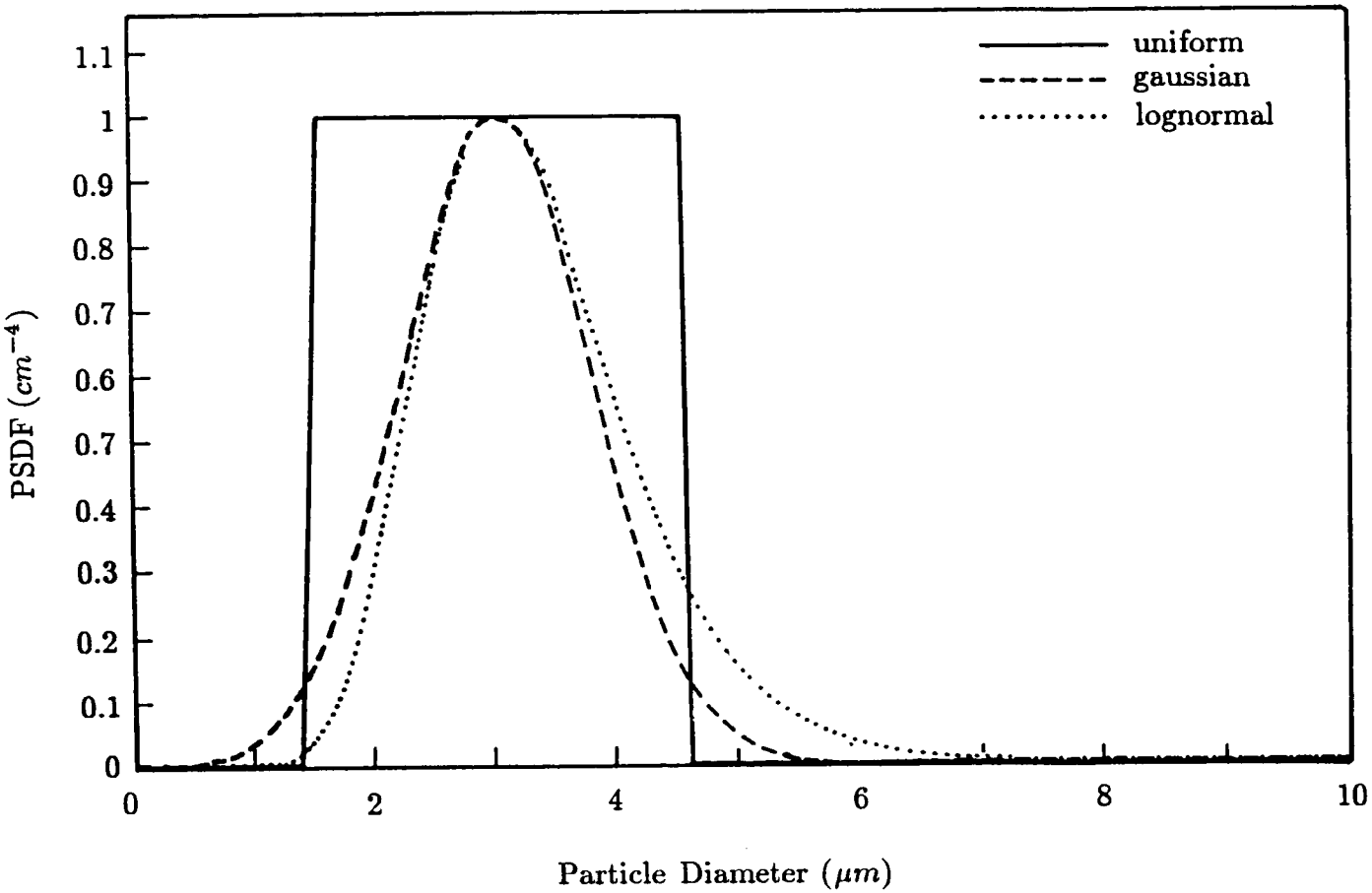


Figure 3.1. Typical particle size distribution functions.

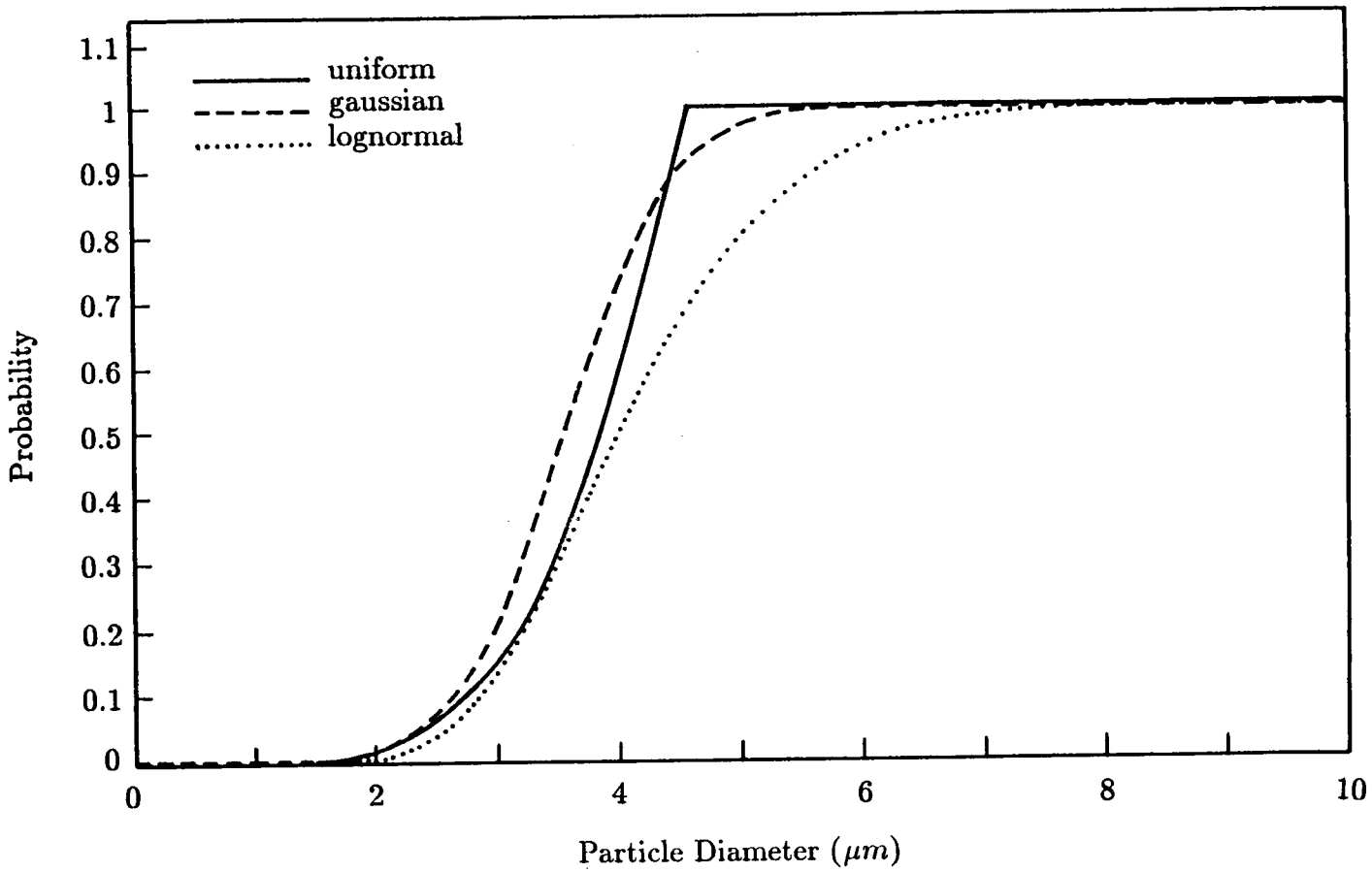


Figure 3.2. Cumulative probability distribution functions.

Most naturally occurring particle distributions are skewed in shape, and are best described with functions such as the log-normal, beta, or gamma distributions. The log-normal function will be used throughout this work to represent natural, skewed distributions because of its relatively simple form. Results of calculations made using the log-normal distribution will also be compared with those obtained using uniform and Gaussian distribution functions, which are symmetric. The reason for considering these physically unrealistic distribution functions, in addition to the skewed functions, will become apparent in the next chapter, where it is demonstrated that average particle size determination is relatively insensitive to the shape of the distribution function under certain circumstances.

Consider a volume element in space that contains a discrete number of particles of varying size. If D_i represents a given diameter, then $N(D_i)$ is the total number of particles per unit size of diameter $D_i \pm dD/2$ within the volume element. If N_o is the total number of particles of all sizes contained in the sample, then

$$N_o = \int_o^\infty N(D)\, dD \tag{3.5}$$

and the expression

$$\begin{aligned} N\{D_1 < D < D_2\} &= N_o \int_{D_1}^{D_2} f(D)\, dD \\ &= \int_{D_1}^{D_2} N(D)\, dD \end{aligned} \tag{3.6}$$

represents the actual number of particles having diameters in the range $D_1 < D < D_2$. The quantity $N(D)$, which represents the particle number distribution, has units of cm^{-1}.

For numerical use, the probability density can also be represented in incremen-

tal form as a function of the particle number distribution as[53]

$$\begin{aligned} f(D) &= \frac{1}{N_o}\,\frac{dN(D)}{dD} \\ &= \frac{1}{N_o}\,\frac{\Delta N(D)}{\Delta D} \end{aligned} \tag{3.7}$$

More frequently, it is useful to consider the particle number concentration, c_n, which is defined as the total number of particles per unit volume of space and has units of cm^{-3}. If the total number concentration is c_n, then the number concentration of particles having diameters in the range $D_1 < D < D_2$ is

$$c_n\{D_1 < D < D_2\} = c_n \int_{D_1}^{D_2} f(D)\, dD \tag{3.8}$$

which, in other words, is simply the total number concentration times the fraction of particles that have diameters ranging between D_1 and D_2.

Number concentration also is related to a probability density function called the particle number density distribution, $n(D)$, which has units of cm^{-4}. With this definition, the number concentration of particles having diameters in the range $D_1 < D < D_2$ is

$$c_n\{D_1 < D < D_2\} = \int_{D_1}^{D_2} n(D)\, dD \tag{3.9}$$

where $n(D) = c_n\, f(D)$. The number density distribution is the preferred treatment of particle ensembles, and is normally referred to as the particle size distribution function, or PSDF.

Several other pertinent quantities can be introduced at this time. The particle volume concentration, c_v, defined as the total volume of all the individual particles per unit volume of space, is given by

$$\begin{aligned} c_v &= c_n\,\frac{\pi}{6}\int_o^\infty D^3\, f(D)\, dD \\ &= \frac{\pi}{6} \int_o^\infty D^3\, n(D)\, dD \end{aligned} \tag{3.10}$$

A related quantity is the mass concentration, c_m, which is defined as the mass of all the particles within the volume per unit volume, and is related simply to the volume concentration by

$$\begin{aligned} c_m &= \rho\ c_v \\ &= \rho\ \frac{\pi}{6}\ \int_o^\infty\ D^3\ n(D)\ dD \end{aligned} \tag{3.11}$$

where ρ is the density of the particle material.

Now that the particle size distribution has been presented, it is useful to define and examine the salient features of distribution functions. The mode, D_m, of the PSDF is defined as the value of D that occurs with highest frequency, or the diameter corresponding to the maximum value of the probability density function, and represents the size range that contains the greatest number of particles.

Average sizes of the distributions are defined by various diameter-weighted moments of the distribution. The mean, or expectation value, of the diameter is defined as

$$< D > = \int_o^\infty\ D\ n(D)\ dD \tag{3.12}$$

for any particle size distribution function. This definition is generalized to include any weighting function of the particle diameter where, for example, the expected value of a function $g(D)$ is

$$< g(D) > = \int_o^\infty\ g(D)\ n(D)\ dD \tag{3.13}$$

For the particular case where $g(D) = D^P, P = 1, 2, 3, ...$, the expected value of the distribution is referred to as a moment, or central moment of the distribution. The mean square diameter, for example, takes the form

$$< D^2 > = \int_o^\infty\ D^2\ n(D)\ dD \tag{3.14}$$

The median particle diameter, D_{med}, is that value of D for which half of the distribution is contained in the diameter range $0 < D < D_{med}$. Mathematically, this is expressed in the form

$$\int_o^{D_{med}} n(D)\, dD = \frac{1}{2}\int_o^{\infty} n(D)\, dD \tag{3.15}$$

Similarly, the mass median diameter, D_{mm}, is that value of D for which half of the mass of the distribution is contained in the diameter range $0 < D < D_{mm}$,

$$\int_o^{D_{mm}} D^3\, n(D)\, dD = \frac{1}{2}\int_o^{\infty} D^3\, n(D)\, dD \tag{3.16}$$

A measure of the spread, width, or precision of the distribution of diameters about the mean value is the variance, which is defined as the mean square deviation of D about the mean diameter. Mathematically, for a continuous distribution of random variables, this is written as[52]

$$\begin{aligned} \nu &= \int_o^{\infty} (D - < D >)^2\, n(D)\, dD \\ &= < D^2 > - < D >^2 \end{aligned} \tag{3.17}$$

The square root of the variance is the standard deviation, σ, of the distribution.

Ratios of the moments of diameter provide statistical mean diameters that are useful in relating the characteristics of the size distribution to certain physical processes. For example, it is shown in Chapter IV that measurement of light extinction through a cloud of particles yields the ratio of $< D^3 > / < D^2 >$, which is commonly called the Sauter mean diameter, D_{32}. This quantity represents a mean volume to surface area ratio and is useful for determining the surface area of a known mass of particulate material. Explicitly, the Sauter mean diameter is written in the form[53]

$$D_{32} = \frac{< D^3 >}{< D^2 >} = \frac{\int D^3\, n(D)\, dD}{\int D^2\, n(D)\, dD} \tag{3.18}$$

In general, the average diameter that results from a ratio of two moments of particle diameter, $< D_M >$ and $< D_N >$, is defined according to the expression[53]

$$D_{MN} = \left[\frac{< D^M >}{< D^N >}\right]^{\frac{1}{(M-N)}} \tag{3.19}$$

In this notation, $< D >$ can also be expressed as D_{10}, and D_{20} is equivalent to $< D^2 >^{\frac{1}{2}}$, representing a root-mean-square diameter. Unfortunately, not every D_{MN} has such simple interpretation; they should, therefore, be regarded only as weighted mean values of the distribution.

Figure 3.3 shows plots of a typical symmetric (Gaussian) distribution, including the positions of the various moments of diameter for these distributions. Figure 3.4 illustrates similar details for a skewed (log-normal) distribution. For a broad size distribution, the mass median diameter will be larger than, for example, both D_{43} and D_{32}. The Sauter mean diameter typically is the smaller of these three quantities. Furthermore, the moment ratios of the distribution functions generally are greater than or equal to the mode diameter, and generally it is true that $D_{IJ} > D_{KL}$ if $I > K$ or $J > L$.

One reason for considering moment ratios is that knowledge of any two of these quantities, in principle, uniquely specifies the probability density function for a given type of two parameter distribution[54]. This is illustrated using a log-normal distribution function for which closed form analytical solutions are written. Consider a log-normal function with mode D_m and width σ,

$$n(D) = \frac{1}{\sqrt{2\pi}\ D\ ln(\sigma)}\ exp\left[-\frac{1}{2}\left(ln(D/D_m)\ /\ ln(\sigma)\right)^2\right] \tag{3.20}$$

The mean diameter, D_{PQ}, for the log-normal distribution is related to the mode diameter in the form

$$D_{PQ} = D_m\ exp\left[\left[ln(\sigma)\right]^2\ (P+Q)\ /\ 2\right] \tag{3.21}$$

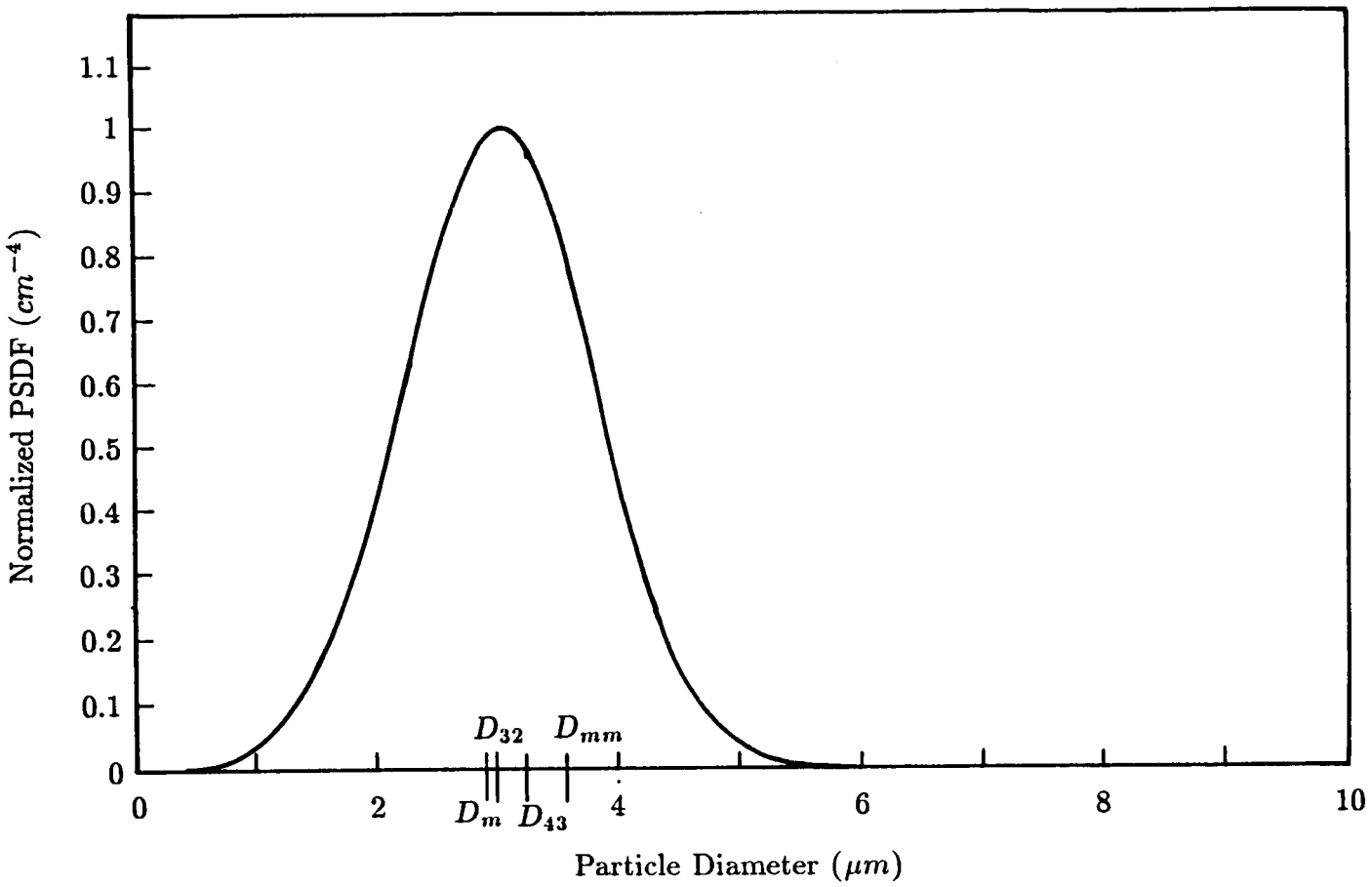


Figure 3.3. Gaussian distribution function and mean diameters.

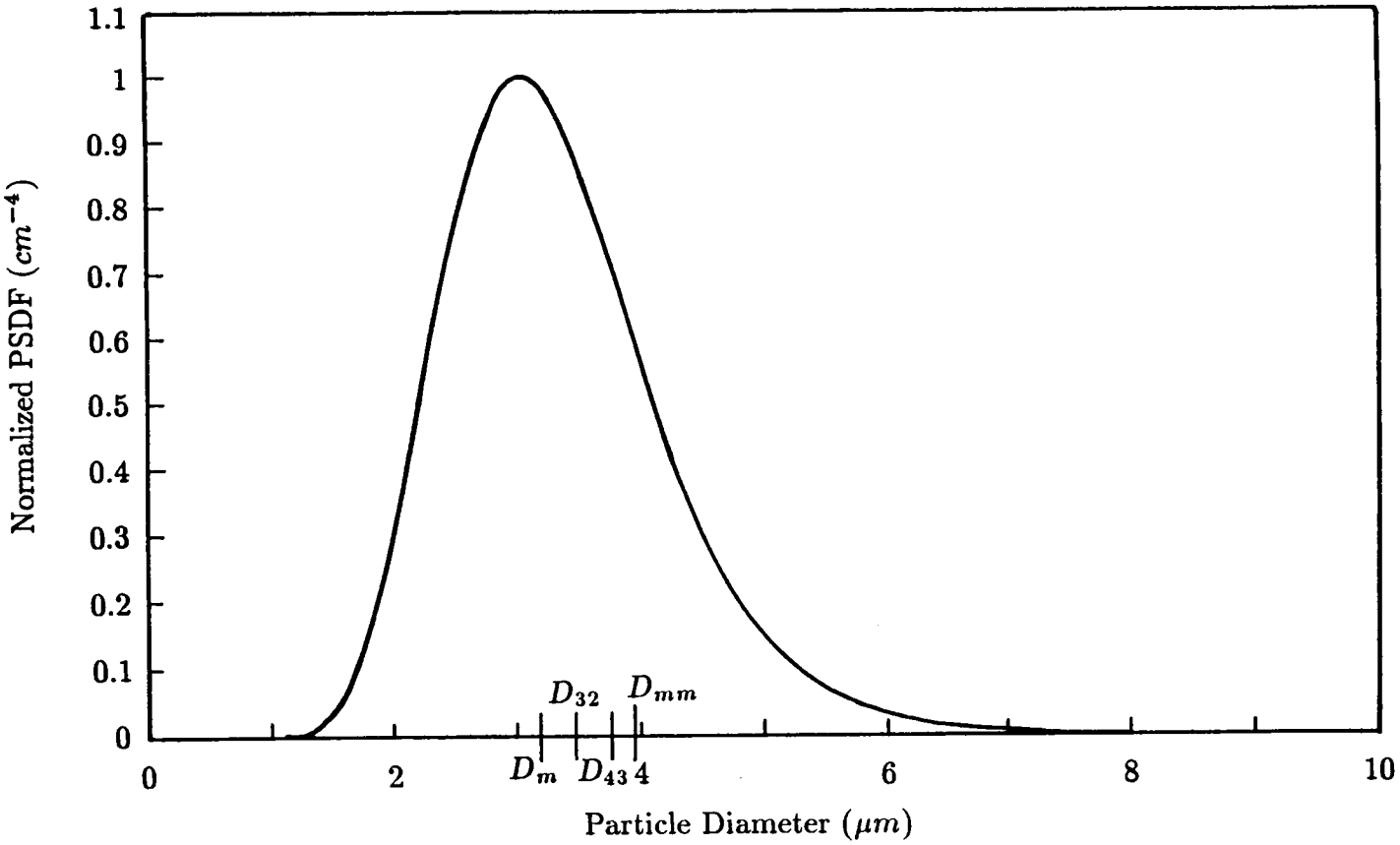


Figure 3.4. Log-normal distribution function and mean diameters.

where the argument of the exponential is a constant for given values of P, Q, and σ. Figure 3.5 shows the mean sizes D_{32} and D_{43} as linear functions of the distribution width with the slope equal to the exponential in the previous equation.

Consider another mean diameter, D_{ST}, having the same form as D_{PQ}

$$D_{ST} = D_m \; exp\Big[ln(\sigma)^2 \; (S+T) \; / \; 2\Big] \tag{3.22}$$

If both of these mean diameters are known from measurements, the last two equations can be solved for D_m and σ. In general, for a log-normal distribution, the distribution width is

$$\sigma = exp\big[2 \; ln(D_{PQ}/D_{ST})/(P+Q-S-T)\big] \tag{3.23}$$

which depends only on the ratios D_{PQ} and D_{ST}. The mode diameter has the closed form solution

$$D_m = D_{PQ} \; exp\Big[-\big\{ln(D_{PQ}/D_{ST})\big\} \;\; \big\{(P+Q)/(P+Q-S-T)\big\}\Big] \tag{3.24}$$

for the log-normal function. Closed form solutions were not investigated for other types of distributions and, indeed, may not exist. However, an alternate, semi-empirical way of visualizing the solution for σ for a general PSDF is through the introduction of a distribution width parameter, W_d, defined as

$$W_d = (D_{PQ} - D_{ST}) \; / \; (D_{PQ} + D_{ST}) \tag{3.25}$$

which is constant for a given value of σ, and type of distribution function.

For a log-normal function having diameters D_{32} and D_{43}, for example, the width σ is plotted in Figure 3.6 as a function of the width parameter. Measurement of D_{PQ} and D_{ST} produces a unique value of W_α, from which the value of σ is determined. Knowing σ, the value of D_m can be obtained graphically from Figure 3.5. The distribution function then is completely specified.

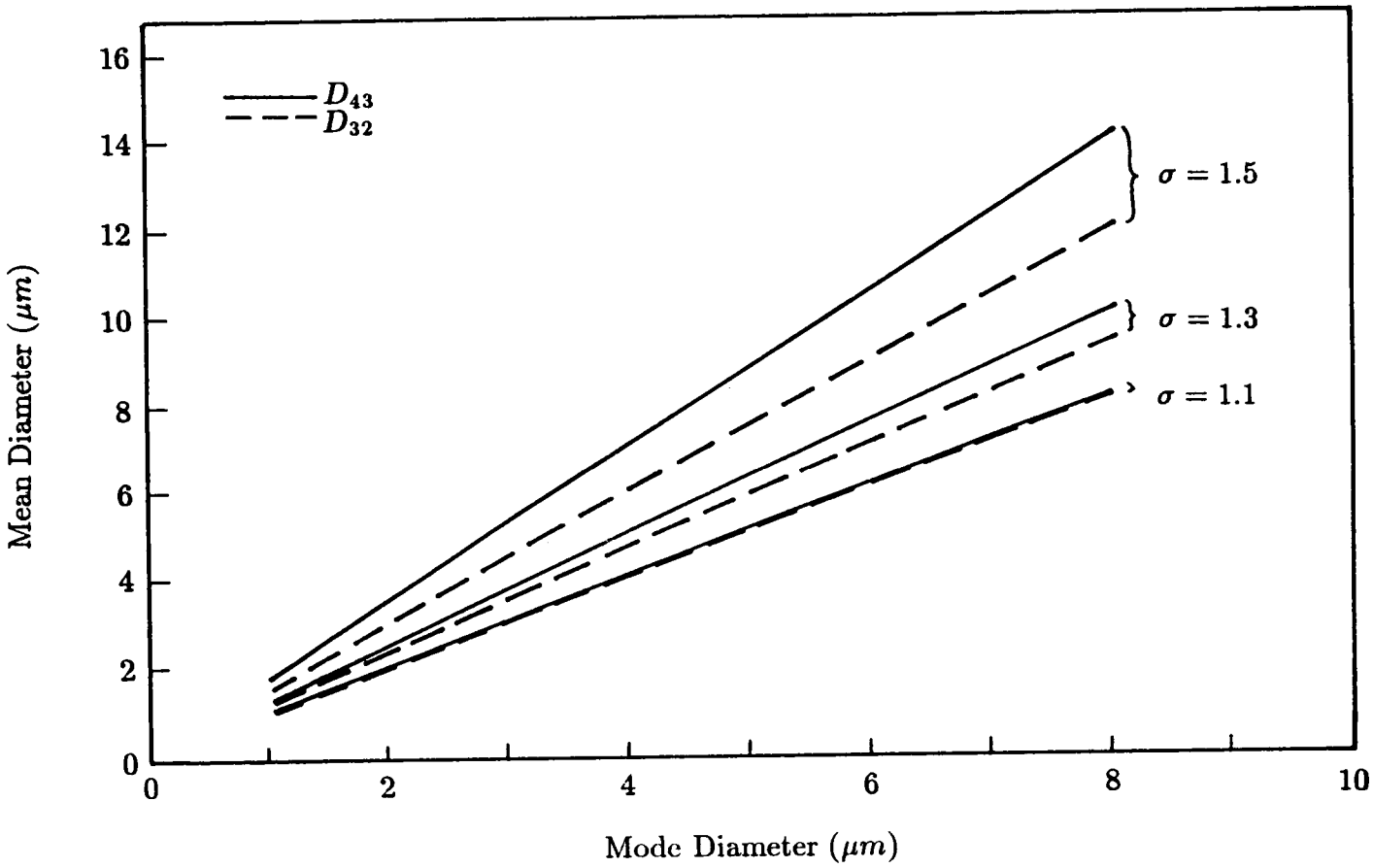


Figure 3.5. Mean diameters as a function of the distribution mode.

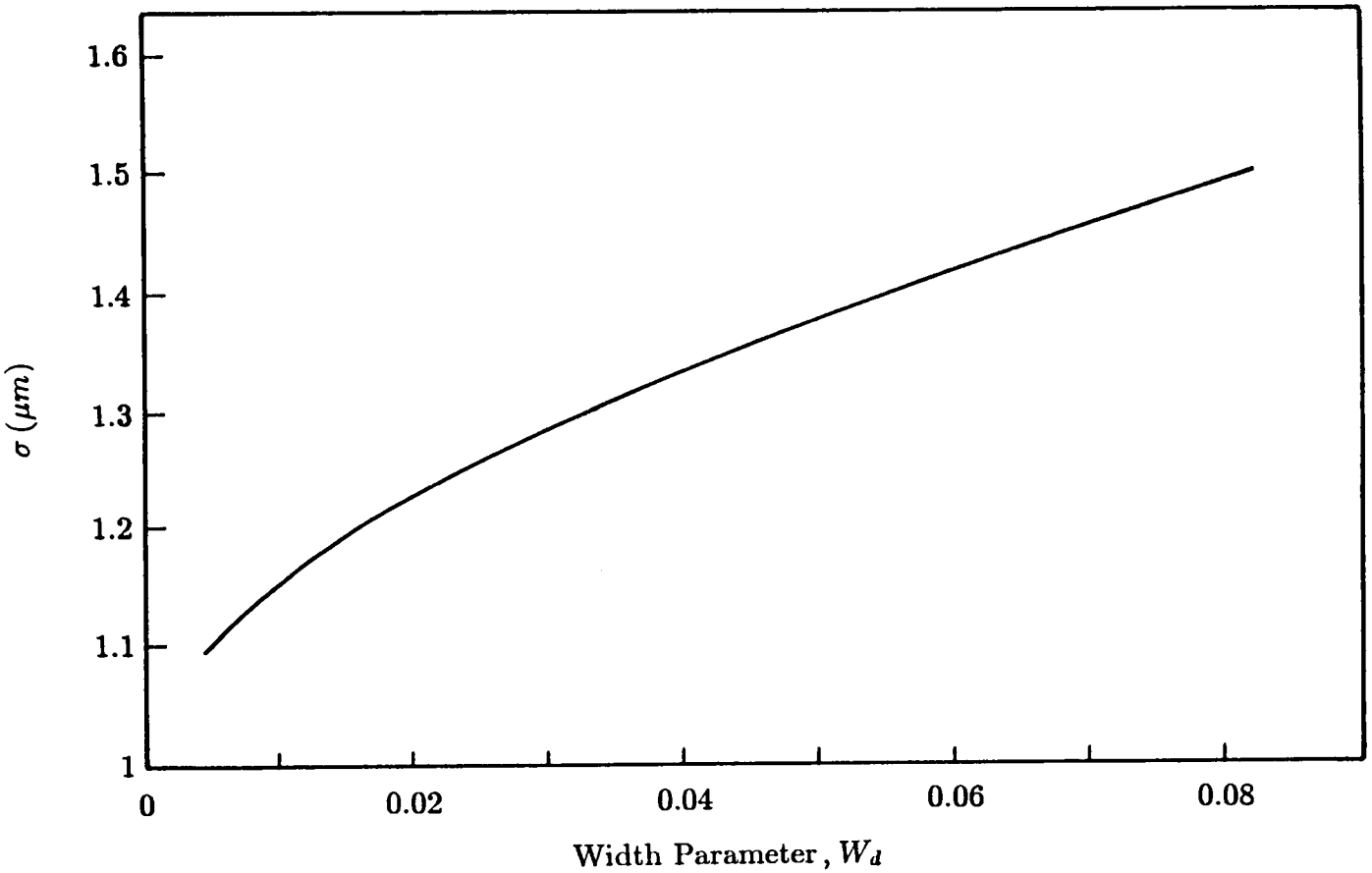


Figure 3.6. Distribution width as a function of the width parameter.

Uncertainty in the measurement of D_{PQ} and D_{ST} results in an error in the recovered values of D_m and σ. For example, the uncertainty ΔD_m is, to a linear approximation,

$$\Delta D_m = \frac{\partial\, D_m}{\partial\, D_{PQ}}\ \Delta D_{PQ} + \frac{\partial\, D_m}{\partial\, D_{ST}}\ \Delta D_{ST} \tag{3.26}$$

To illustrate, given $D_{32} = 12\ \mu m$ and $D_{43} = 14.25\ \mu m$, with an uncertainty of 10% on each measurement and assuming a log-normal PSDF, the recovered mode diameter is approximately $D_m = 8 \pm 2.9\ \mu m$ with a width $\sigma = 1.4 \pm 0.4$, corresponding to 37 and 30 percent errors, respectively. This technique is sensitive to small errors in the mean diameters used to calculate D_m and ∂, and is therefore primarily useful for obtaining estimates of the actual distribution function.

The approach outlined above identifies a closed form solution for simple determination of the particle size distribution function from two measured mean diameters for a specific type of PSDF. This approach does not apply to a bimodal distribution, for example, because it generally would require 3 or more parameters to uniquely specify the distribution. In principle, however, a 3-parameter distribution might be uniquely determined by three ratios of mean sizes if these were experimentally available. This effort is directed at identifying measurement techniques that have the potential to provide various mean diameters which are needed to specify the size distribution. The following chapter addresses the methods for determining average particle sizes of particle clouds using light extinction measurement techniques.

CHAPTER IV

MEAN PARTICLE SIZE OBTAINED FROM SINGLE-PATH EXTINCTION MEASUREMENTS

Extinction Through a Uniform Spatial Distribution

Transmission measurement techniques are reported in the literature as a means of determining the average particle size or mass concentration of a distribution of particles[55–57]. These measurements are especially useful in densely laden particle flows, in which multiple scattered light becomes significant and may adversely influence the results of a light scattering experiment. Transmittance measurements are less sensitive to error due to multiple scattering than are scattering measurements[55].

This chapter reviews the application of extinction measurements to average particle size determination in spatially uniform particle flowfields. These techniques then are extended to the more complicated problem of spatially nonuniform distributions.

Complete determination of the particle size distribution function, or PSDF, for spatially uniform size distributions requires transmittance measurements at several wavelengths. Spatially nonuniform distributions, on the other hand, require transmittance measurements through several paths. Solutions to these problems are discussed in later sections.

Dobbins[35] investigated single wavelength extinction through a homogeneous particle distribution in order to estimate the mean particle size in small rocket motors. He found that the resulting transmission of a beam of light through a polydisperse particle distribution is relatively independent of the shape of the size distribution and complex refractive index, and relatively easy to implement experimentally. Holve and Self[58] applied extinction measurement techniques to the de-

termination of mean particle sizes of ash particulates from the exhaust of coal-fired magnetohydrodynamic (MHD) generators. Using a similar approach, Cashdollar[59] used a three wavelength transmissometer to obtain both the mean size and concentration of smoke particulates. Gougeon[60], in describing a visible/infrared double extinction technique through a uniform slab of particles, emphasized the need for careful selection of wavelengths to optimize the sensitivity of the experiment.

Particle size distributions using multiple wavelength measurements were obtained by Uthe[61], who used 14 wavelengths and assumed a spatially uniform particle distribution. Despite the vast effort that has been devoted to the extraction of particle size information from extinction measurements, scant emphasis has been placed on techniques other than extinction, or on applying these techniques to spatially nonuniform particle fields – such as might be expected, for example, from a spray nozzle or two-phase free-jet. The remainder of this work seeks to determine the requirements and conditions for making particle size measurements in spatially uniform and nonuniform flows, and introduces several alternative methods for obtaining size information.

Laser extinction, or transmission, measurement techniques are used to determine the average particle size in a distribution of particles if the optical properties and mass concentrations are known. The traditional approach taken to relate a single wavelength extinction measurement to particle size assumes that the particles are uniformly distributed in the measurement volume. The medium is assumed to be homogeneous and transparent, the particle density is low enough that multiple scattering can be neglected, and the particles are randomly distributed so that the scattered fields add incoherently.

The extinction of a monochromatic beam of light through a spatially homogeneous monodisperse slab of particles is described by the Lambert-Beer law in the

form[55]

$$\begin{aligned} T &= exp\,(-\kappa\, L) \\ &= exp\,(-c_n\, \frac{\pi\, D^2}{4}\, Q_e\, L) \end{aligned} \tag{4.1}$$

where the transmittance, T, describes the fraction of light transmitted through a scattering and absorbing medium, κ is the bulk attenuation coefficient, Q_e is the particle extinction efficiency obtained from the Mie theory, c_n is the particle number concentration, $\frac{\pi\, D^2}{4}$ is the geometrical cross section of the particle, and L is the optical path length through the particle ensemble. The geometry for this problem is illustrated in Figure 4.1. The attenuation coefficient, κ, which also is referred to as the extinction coefficient or the turbidity[45], is independent of the state of polarization of the incident lightwave and has dimensions of inverse length. Generally, the Lambert-Beer law is invalid for high number densities where multiple scattering exists, i.e., when the particles are so closely spaced (less than a few particle diameters from each other) that they interact electromagnetically[62]. Only single scattering phenomena are included in this analysis.

Attenuation is caused by a combination of both scattering and absorption, and so the attenuation coefficient is related to the various cross-sections by

$$\kappa = c_n\, C_e = c_n\, C_s + c_n\, C_a \tag{4.2}$$

Furthermore, a quantity called the optical depth, τ, is related to the transmittance by

$$\tau = -ln\,(T) \tag{4.3}$$

Physically, the optical depth represents the attenuation per unit length through the scattering and absorbing medium. This definition is useful in that the optical depth is linearly dependent on the number density, extinction cross-section, and the path integration length.

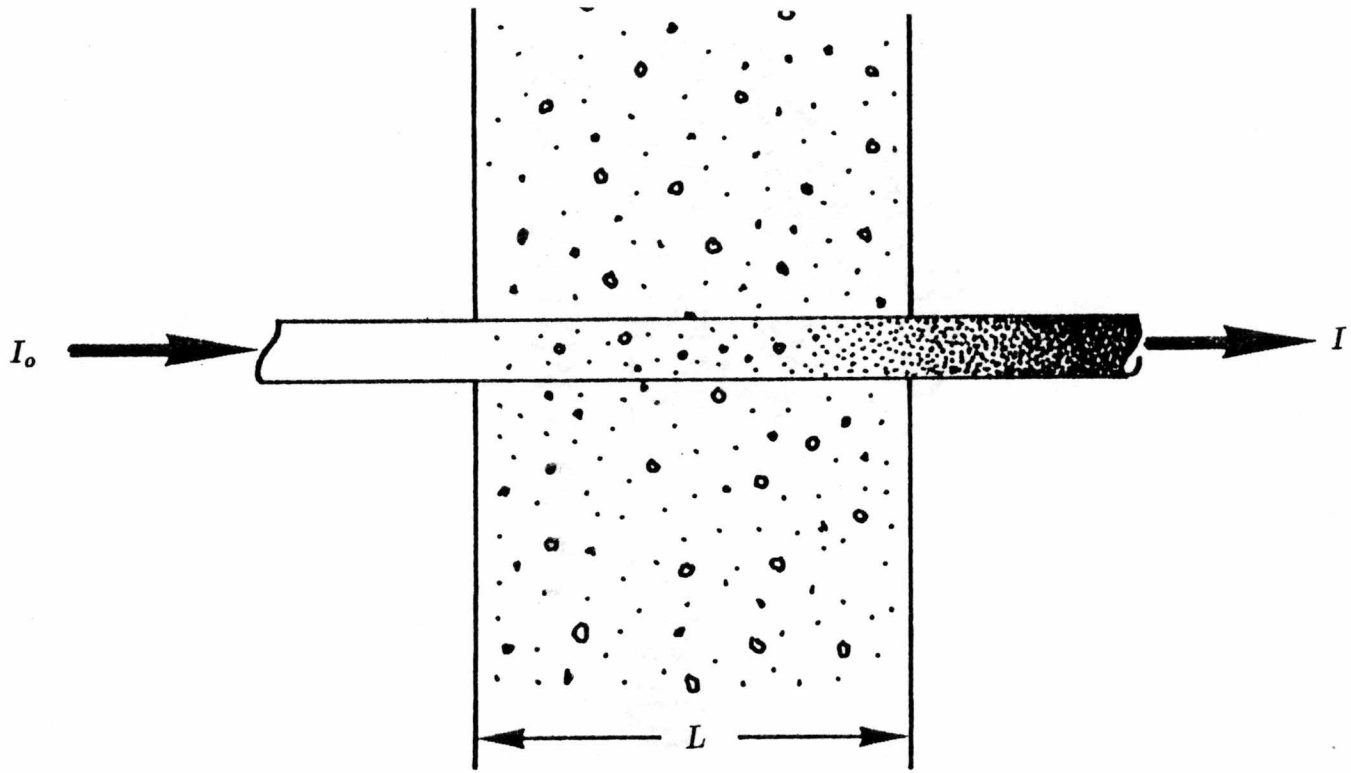


Figure 4.1. Light extinction through a homogeneous particle slab.

For a polydisperse particle size distribution that is uniformly spatially distributed, the extinction efficiency is a function of particle size and must be integrated over the PSDF. The attenuation coefficient can then be interpreted as the total extinction cross-section per cubic centimeter, and is related to the particle size distribution by[55]

$$\kappa = \frac{\pi}{4} \int Q_e(D)\, D^2\, n(D)\, dD \tag{4.4}$$

where the extinction efficiency is an explicit function of the particle diameter, D. The optical depth then takes the form

$$\tau = L\, \frac{\pi}{4} \int Q_e(D)\, D^2\, n(D)\, dD \tag{4.5}$$

Chapter II illustrated that the extinction efficiency is a function of particle properties including size, shape, and refractive index. Particle ensembles will generally contain a distribution of sizes, and, hence, a range of extinction efficiencies. The variations in the size dependent extinction efficiency caused by interference phenomena are smoothed out by the combined interference effects due to all of the particles in the polydispersion. To discern the effect of the size distribution on the transmission of light through the particle ensemble, it is useful to introduce a mean extinction efficiency, $< Q_e >$, defined as[55]

$$< Q_e > = \frac{\int Q_e(D)\, D^2\, n(D)\, dD}{\int D^2\, n(D)\, dD} \tag{4.6}$$

With this definition, the expression for optical depth becomes

$$\tau = L\ < Q_e >\ \frac{\pi}{4} \int D^2\, n(D)\, dD \tag{4.7}$$

Substituting the Sauter mean diameter from Equation (3.18), in addition to the definitions of the mass and volume concentrations from Equation (3.11), the

optical depth takes the form[55]

$$\begin{aligned} \tau &= 3\, c_m\ <Q_e>\ L\ /\ 2\ \rho\ D_{32} \\ &= 3\, c_v\ <Q_e>\ L\ /\ 2\ D_{32} \end{aligned} \tag{4.8}$$

This equation can be generalized to the case of a moving flow of particles, such as might occur in spray nozzles, rocket exhausts, or free-jets, through the equation of continuity, which relates the mass flow rate to the mass concentration

$$\dot{m} = c_m\ A\ v \tag{4.9}$$

where $\dot{m}$ is the mass flow rate, v is the particle flow velocity, and $A = \frac{\pi L^2}{4}$ is the flow cross-sectional area of a cylindrical flowfield with the transmission measurement obtained across the diameter. The optical depth is then expressed in terms of the mass flow rate, the measurement geometry, the average particle diameter, and the average Mie extinction efficiency, as

$$\tau = \frac{6\ \dot{m}\ <Q_e>}{\pi \rho L v D_{32}} \tag{4.10}$$

The mean specific extinction efficiency can be defined as[35,55]

$$\overline{Q}_e = <Q_e>\ /\ D_{32} \tag{4.11}$$

Then, Equation (4.10) can be written

$$\tau = \frac{6\ \dot{m}\ \overline{Q}_e}{\pi\ \rho\ L\ v} \tag{4.12}$$

which implies that the mean specific extinction efficiency can be determined by an attenuation measurement if the mass concentration, density, and geometry are known.

Particle size is determined in practice by measuring the transmittance of a beam of light through the particle ensemble and calculating the optical depth from

Equation (4.3). The particle size may be determined by plotting the theoretical optical depth from Equation (4.12) as a function of D_{32} and comparing the measured optical depth as shown in Figure 4.2. In general, multiple values of particle size are possible solutions, so measurements at additional wavelengths are normally required to eliminate this ambiguity.

Examining the behavior of the mean specific extinction efficiency for different PSDF's furnishes insight into the effect that an unknown PSDF might have on determining an average size from a cloud of particles. For the general case of intermediate size particles, on the order of the illumination wavelength, Q_e oscillates between typical values of 0 to 4 depending on the size parameter, α. The average extinction efficiency, however, is somewhat better behaved for polydisperse size distributions. Figure 4.3 shows the mean specific extinction efficiency as a function of D_{32} for several example particle size distributions, including rectangular, Gaussian, and log-normal, that have the same widths. The variation in $\overline{Q}_e$ for these different types of distributions is quite small, and agrees to within a few percent for each of these over the entire range of particle sizes. Calculations of $\overline{Q}_e$ have also been made for several log-normal functions that have different mean sizes and standard deviations. Here, too, the maximum variation was found to be small, which further illustrates the lack of sensitivity of the mean specific extinction efficiency on the particular nature of the PSDF. The significance of the insensitivity of $< Q_e >$ or $\overline{Q}_e$ to the distribution shape is that this technique may be applied with confidence to any particle ensemble, even if the form of the distribution function $n(D)$ is unknown.

Near the extinction resonance region, in which the particle diameter is approximately equal to the illumination wavelength, interference within the particle enhances the attenuation. Here, the functional variation in $< Q_e >$ is greatest, and the results depend more keenly on the accuracy to which the extinction efficiencies

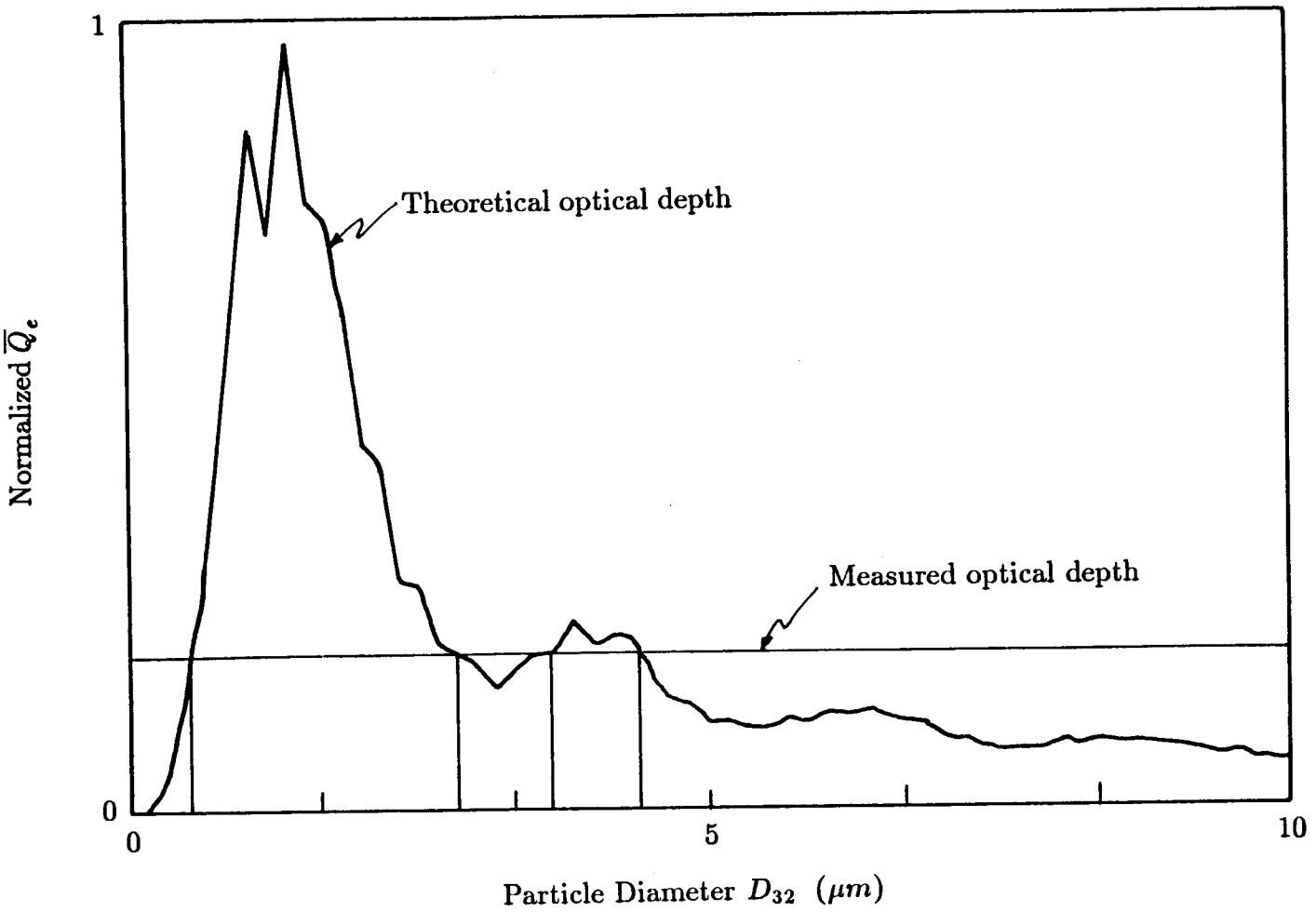


Figure 4.2. Mean specific extinction efficiency.

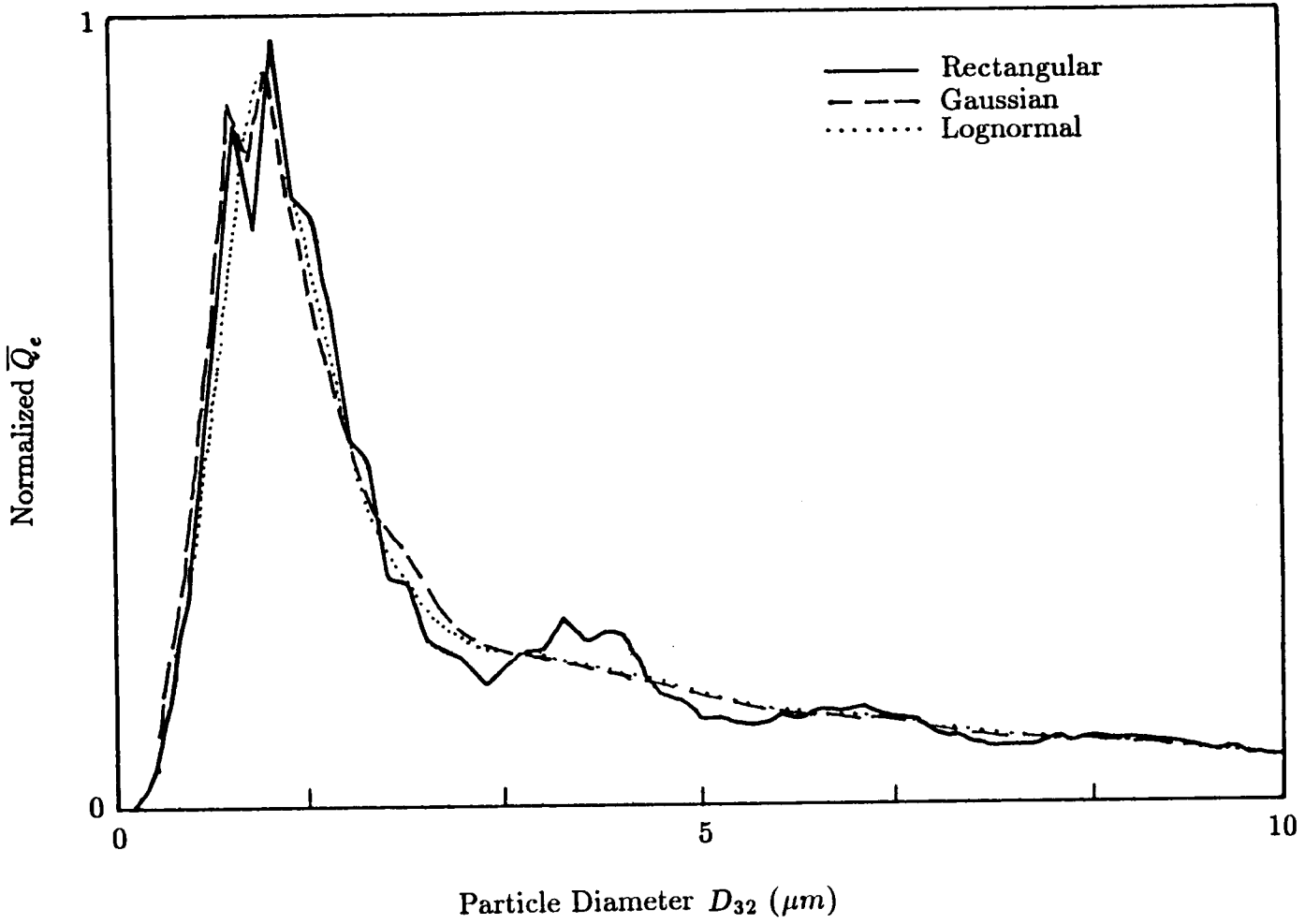


Figure 4.3. Effect of distribution width on mean specific extinction.

are calculable. For distributions that have mean sizes near the resonant region, the measurements are more heavily dependent on effects such as particle shape and refractive index. Calculations of $Q_e(D)$ are represented in Figure 4.4 and 4.5 over a range of real and imaginary refractive indices, respectively, for a wavelength of 1.06 μm. Note that the location and amplitude of the resonant region vary with real refractive index, and that increasing the imaginary index diminishes the oscillatory behavior of the function. For particle ensembles containing a range of diameters, the oscillatory behavior is averaged out. Figures 4.6 and 4.7 demonstrate the refractive index dependence of the mean extinction efficiency, $< Q_e >$, a quantity that represents the ensemble extinction. In this example, using a log-normal distribution, an 8.6% uncertainty in the real refractive index contributes approximately a 33% worst case uncertainty in $< Q_e >$ for particle diameters on the order of the wavelength of light; for larger diameters, or D greater than approximately 2λ, the uncertainty is negligible. Knowledge of the imaginary refractive index is less critical, because a four order of magnitude change in absorption ($0.0001 < M_i < 1.0$) leads to maximum uncertainties of approximately 20% for small particles.

Mean specific extinction efficiencies for large sizes are presented in Figures 4.8 and 4.9 showing the effects of real and imaginary refractive index, respectively. For particles large relative to the wavelength of light, $Q_e(D)$ approaches 2, as does $< Q_e >$. The mean specific extinction efficiency therefore goes as $2/D_{32}$. In this case, the result is virtually independent of the details of the size distribution. Figure 4.10 illustrates the mean specific extinction efficiency in the large particle limit for rectangular, Gaussian, and log-normal distributions. Only a small variation in the values of $< Q_e > /D_{32}$ is seen between these example functions.

In the large particle limit, the mean particle diameter is related to the optical depth by

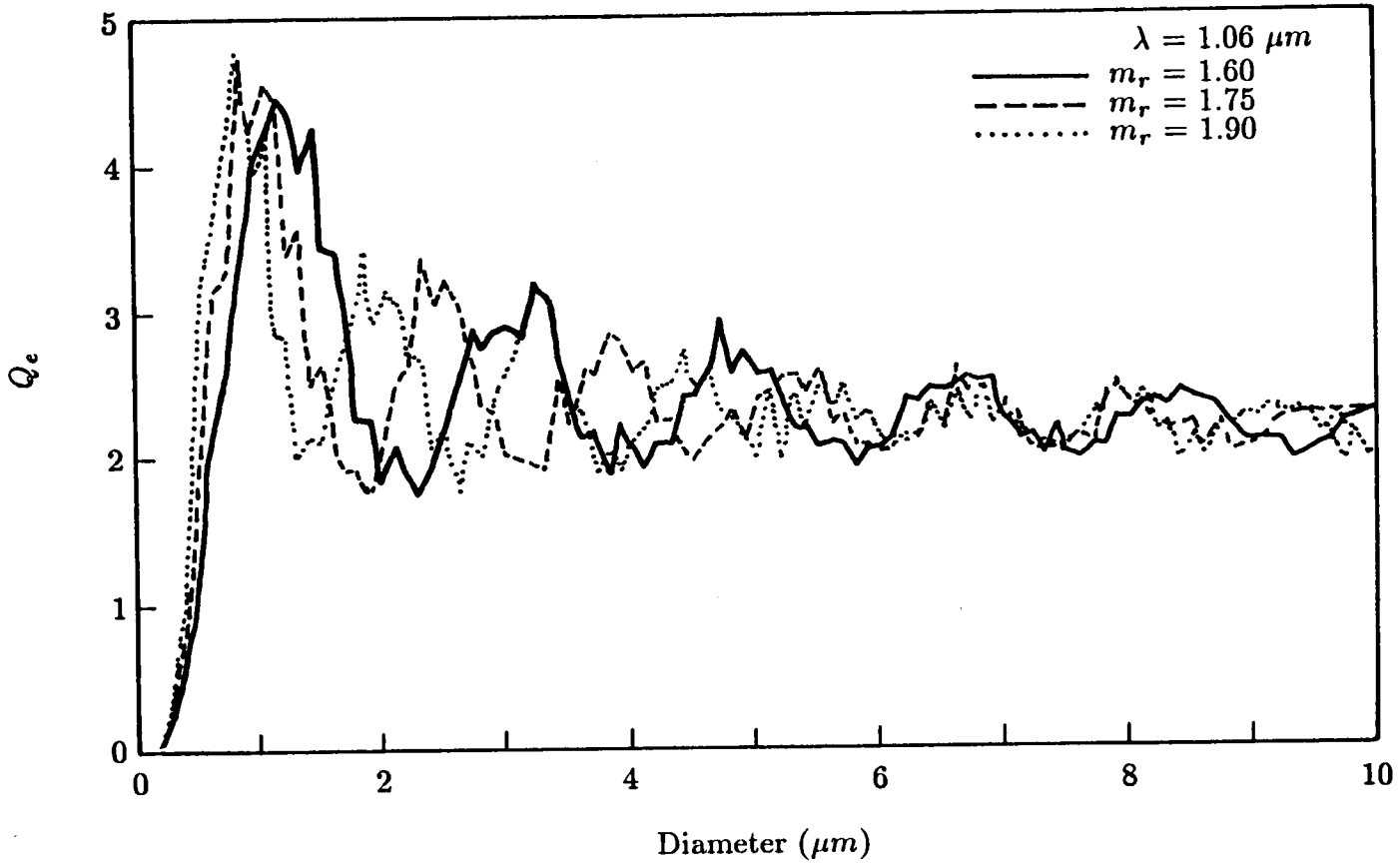


Figure 4.4. Extinction efficiency as a function of real refractive index.

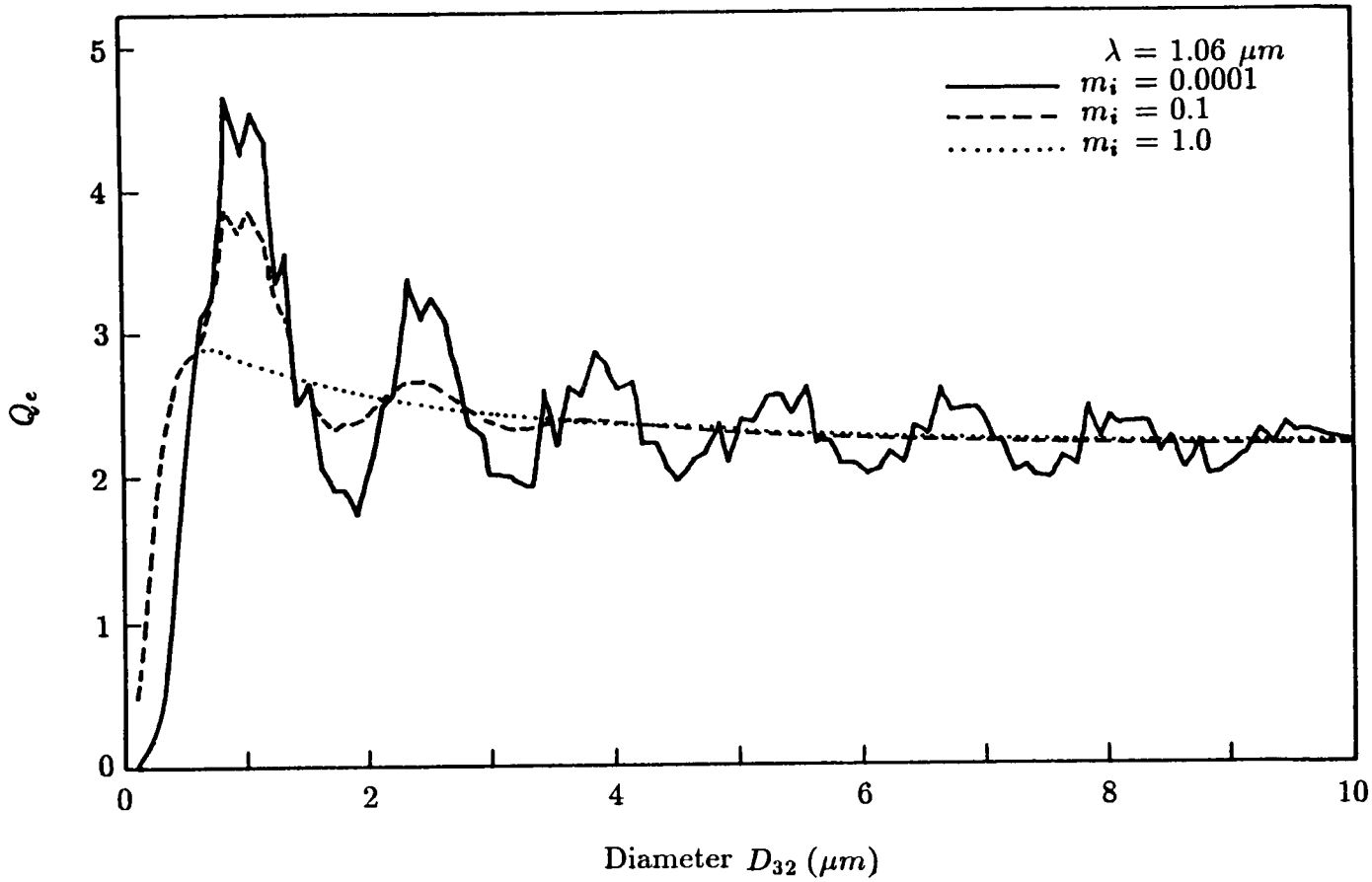


Figure 4.5. Extinction efficiency as a function of imaginary refractive index.

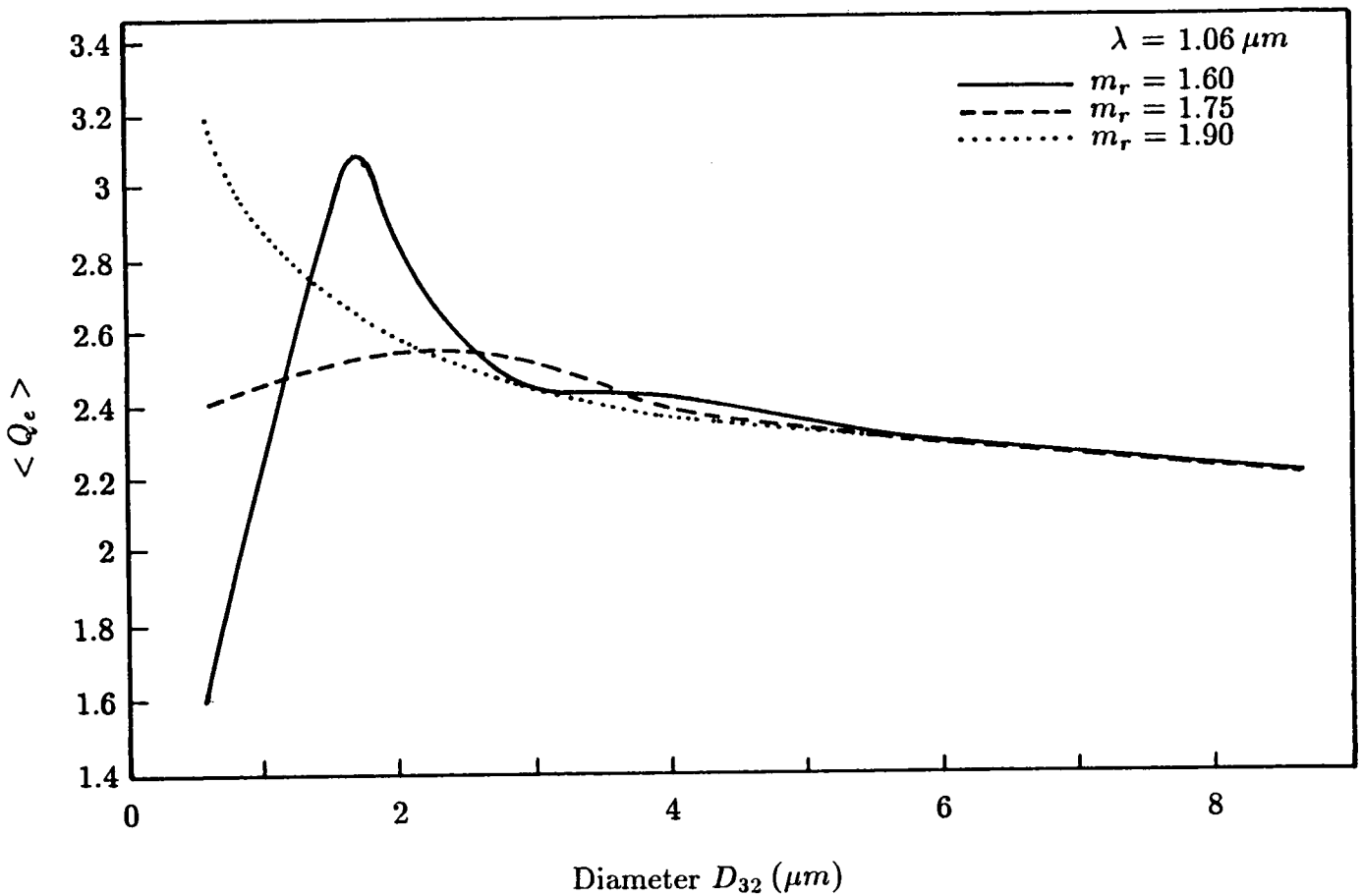


Figure 4.6. Mean extinction efficiency as a function of real refractive index.

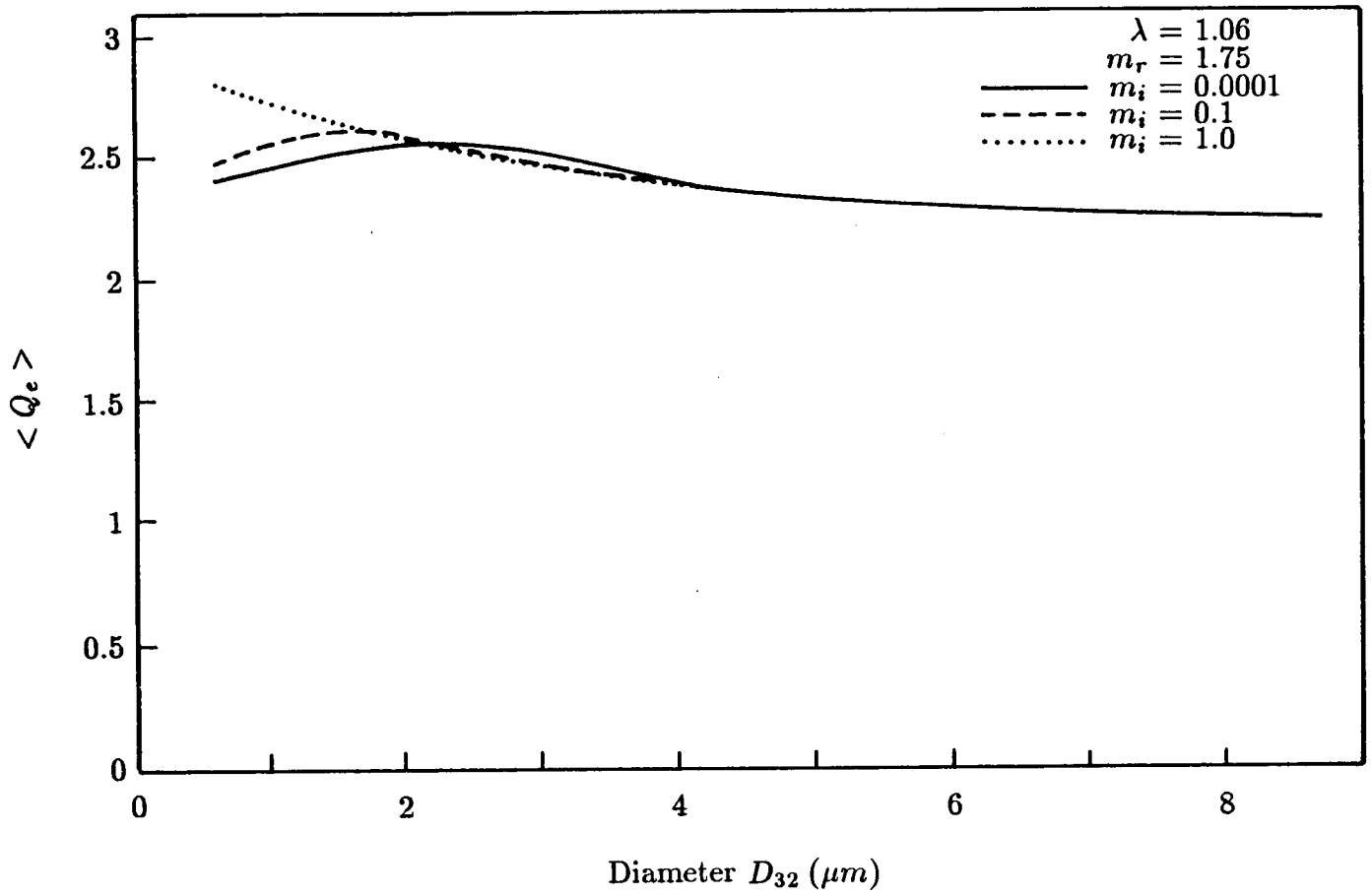


Figure 4.7. Mean extinction efficiency as a function of imaginary refractive index.

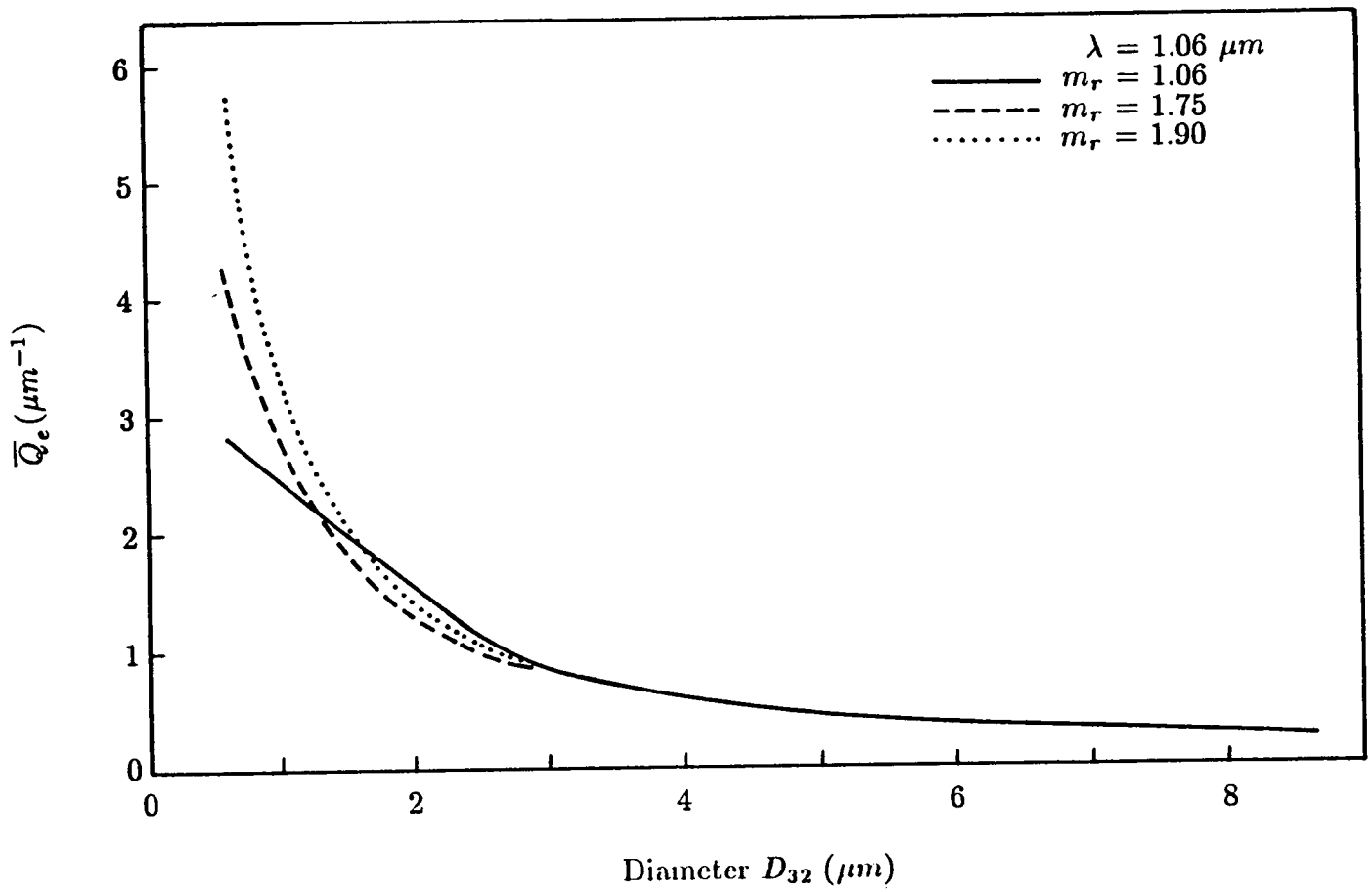


Figure 4.8. Real refractive index effects on mean specific extinction efficiency of large particles.

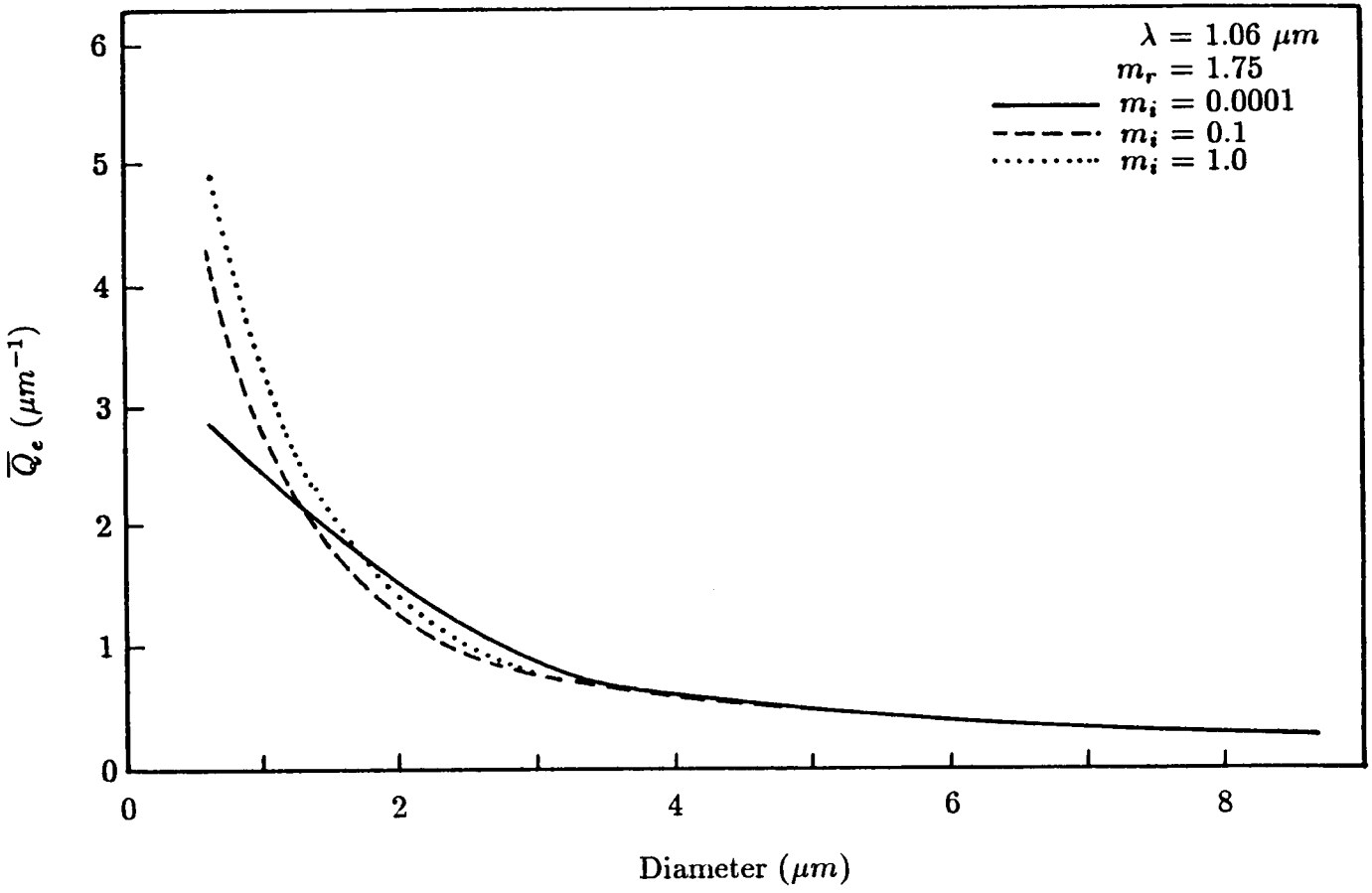


Figure 4.9. Imaginary refractive index effects on mean specific extinction efficiency of large particles.

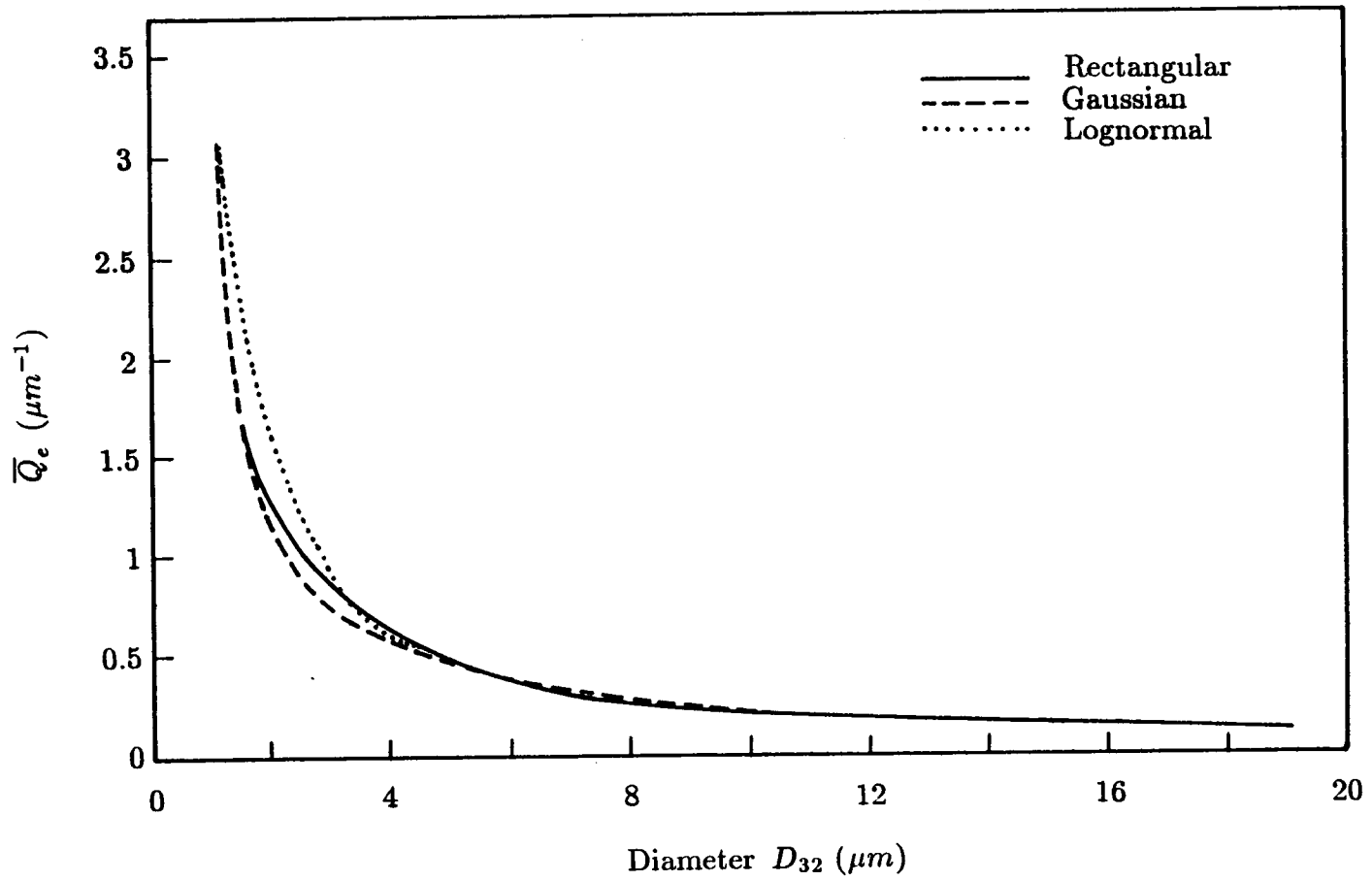


Figure 4.10. Effect of distribution type on mean specific extinction efficiency in the large particle limit.

$$\tau = \frac{12\ \dot{m}}{\pi \rho L v D_{32}} \tag{4.13}$$

and, therefore, a single transmission measurement provides D_{32} if the mass concentration or mass flow rate is known, regardless of the details of the size distribution. Figure 4.11 plots the theoretical optical depth as a function of mean particle diameter for large particles, using the values $\dot{m} = 15\ kg/sec$, $v = 2500\ m/sec$, $\rho = 3000\ kg/m^3$, and $L = 1\ m$. Note that because Q_e is approximately constant for large particle sizes (size parameters), Figures 4.10 and 4.11 reveal a similar $1/D_{32}$ dependence.

Accurate particle sizing is limited to diameters less than approximately $8-10\ \lambda$ because the slope of the optical depth curve is small beyond this region. In fact, the uncertainty in particle size, ΔD, is approximately

$$\Delta D = \Delta\tau\ |\frac{\pi \rho L v D_{32}^2}{12\ \dot{m}}| \tag{4.14}$$

where $\Delta\tau$ is the experimental uncertainty in the measured optical depth.

In the small particle limit, the extinction cross section for non-absorbing Rayleigh scatterers is[46]

$$C_e = \frac{\pi\ \kappa^4\ D^6}{24} \left|\frac{m^2 - 1}{m^2 + 2}\right|^2 \tag{4.15}$$

where m is the complex refractive index of the particle material. In the Rayleigh scattering approximation, Q_e is therefore proportional to D^4, so that $< Q_e >$ looks like D_{63}^3. Kerker[46] refers to the quantity, D_{63}, as the turbidity average. In this case, the relevant mean size measurement related to the particle flowfield parameters is D_{63}, where

$$\tau = \frac{\kappa^4\ \dot{m}}{\pi\ \rho\ L\ v} \left|\frac{m^2 - 1}{m^2 + 1}\right|^2\ D_{63}^3 \propto \frac{6\ \dot{m}\ D_{63}^3}{\pi\ \rho\ L\ v} \tag{4.16}$$

Mean specific extinction efficiency versus particle size is plotted in Figure 4.12 in the small particle limit for rectangular, Gaussian, and log-normal distributions.

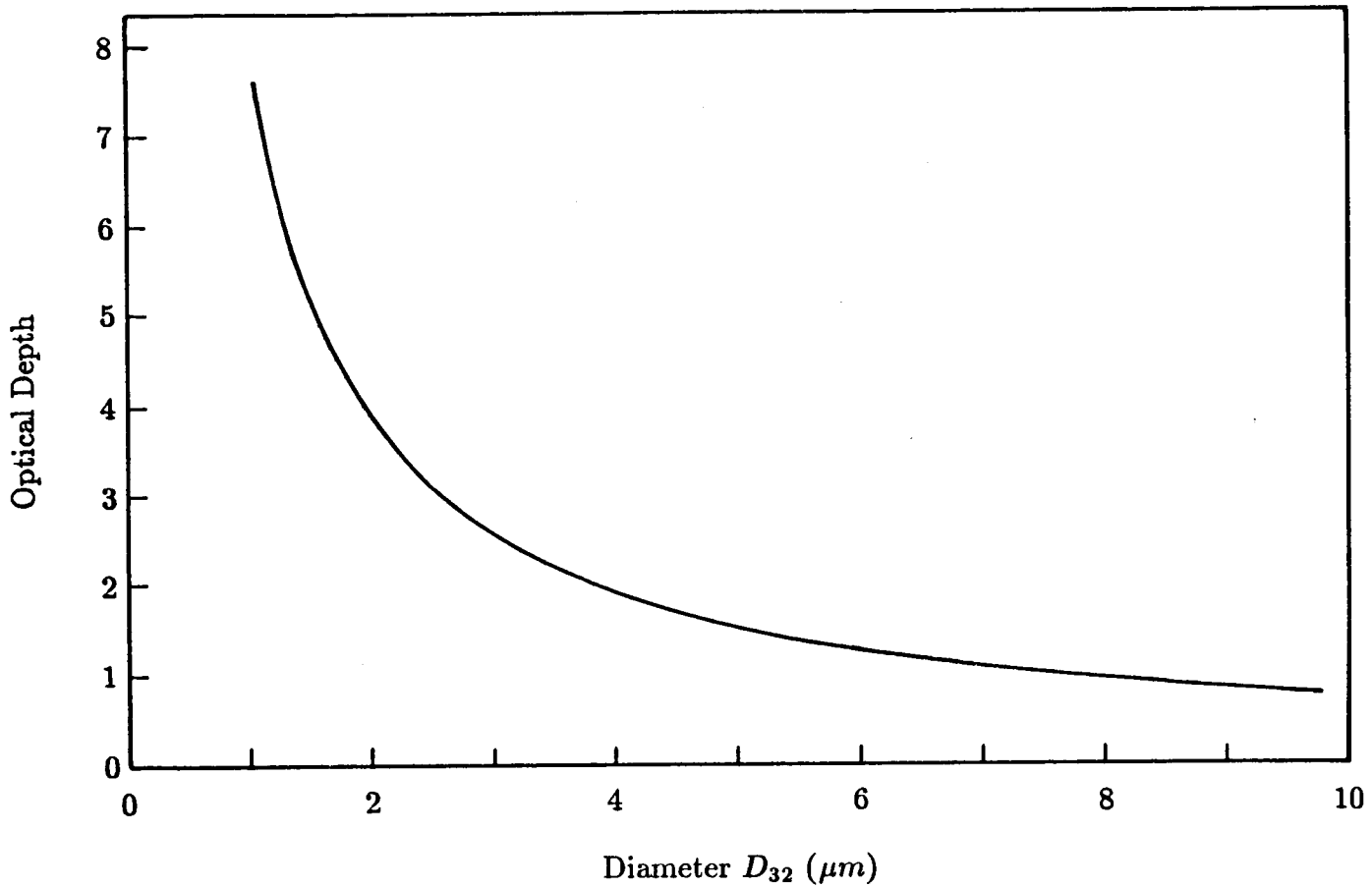


Figure 4.11. Theoretical optical depth as a function of mean particle diameter for large sizes.

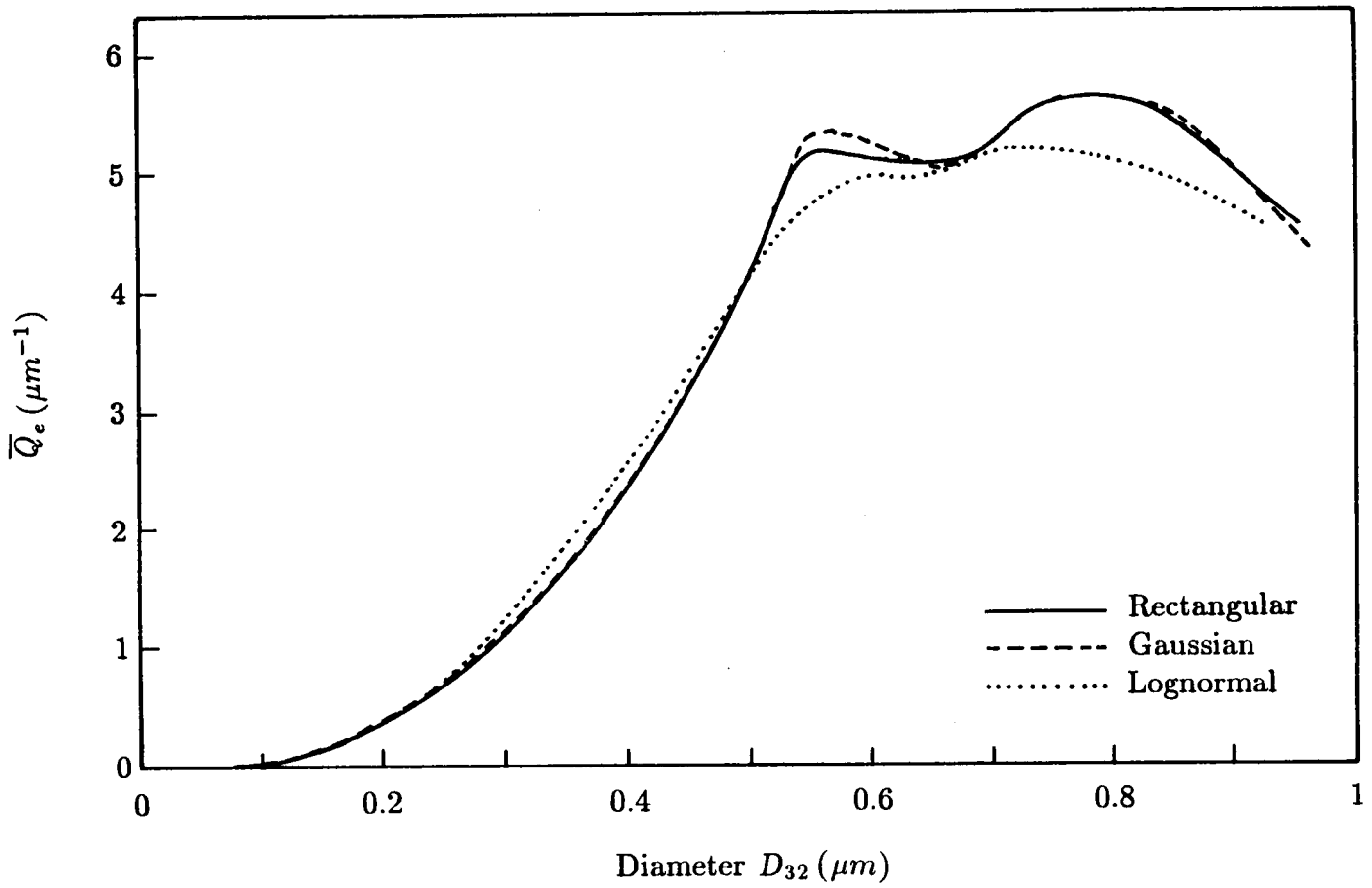


Figure 4.12. Effect of distribution type on mean specific extinction efficiency in small particle limit.

In the size regime below the extinction resonance there is negligible variation in the mean specific extinction efficiency for different types of distribution functions.

Figure 4.13 shows the theoretical optical depth as a function of particle diameter for small particles. In this size region, a single transmission measurement provides unambiguous determination of the mean particle size. The magnitude of the particle size uncertainty is itself size dependent according to

$$\Delta D \propto \Delta \tau \, | \frac{\pi \, \rho \, L \, v}{18 \, \dot{m} \, D^2} | \tag{4.17}$$

and therefore becomes large for extremely small particles. This limits the size resolution attainable in the small particle limit. Additional discussion of the effects of uncertainties in obtaining mean particle from extinction measurements is included for reference in Appendix B.

Up to this point, the theoretical procedure for obtaining the Sauter mean diameter of an ensemble of large particles, and the method of determining D_{63} of an ensemble of small particles using extinction measurement techniques have been reviewed. These techniques are potentially very useful in determining the mean diameters of particle clouds in which the properties of the particle distribution are unknown or poorly known. Experimental uncertainties associated with the extinction measurement technique become unacceptably large in both the large and the small particle limits where the theoretical optical depth becomes insensitive to particle diameter. It is, therefore, important to carefully choose the illumination wavelength so that the expected range of particle sizes fall within approximately 2-10 λ for large particles, and approximately 0.2-0.8 λ for small particles.

Successful extinction measurements also require careful design of the light collection system. The measured bulk attenuation coefficient depends on the reception cone angle of the optical instrument. For large particles, the diffracted light from

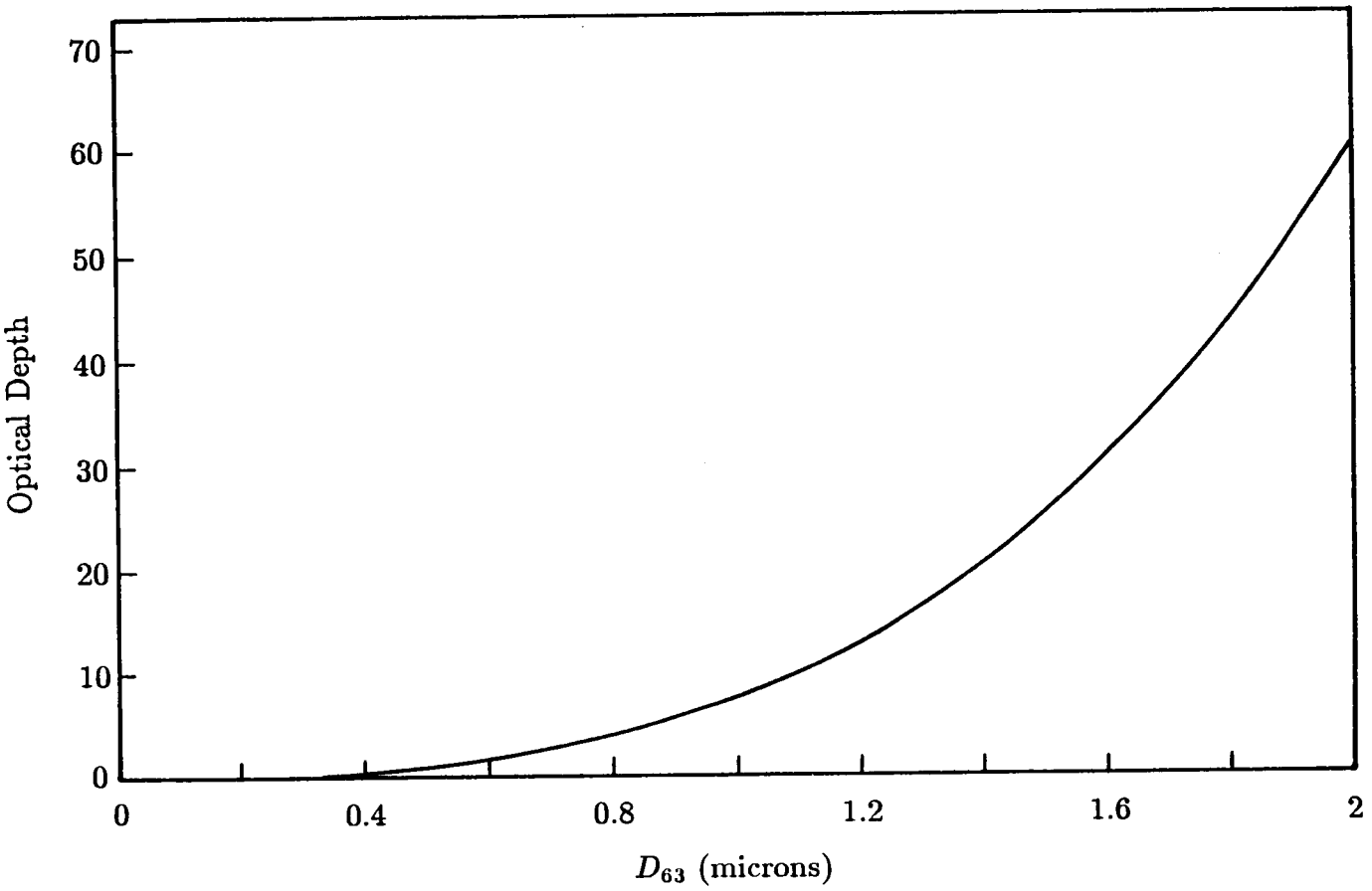


Figure 4.13. Theoretical optical depth as a function of mean particle diameter for small sizes.

the particle is strongly concentrated in the forward direction. The most important consideration in performing a transmission measurement of this type is to discriminate between direct and forward scattered light by keeping the detector acceptance angle sufficiently small[63]. Although single scattering is assumed in this analysis, the Lambert-Beer transmission law is expected to apply in the multiple scattering regime for large particle number densities, as long as the detection field of view is smaller than the divergence angle of the Fraunhofer diffraction pattern of an aperture (represented in this case by a particle) of diameter D. Gougeon[60] states that "the collection angle should be less than 10% of the angular extension of the principle lobe of the Fraunhofer diffraction". In other words[59],

$$\theta_h < \frac{\lambda}{7D} \tag{4.18}$$

where θ_h is the divergence half-angle of the receiving optics measured in degrees, and λ is the wavelength of light. For optically thick plumes, the forward scattered light is spread over a larger angle, but the direct beam is strongly attenuated. The field of view requirements are more restrictive in this case, but the following rule-of-thumb applies[64]

$$\theta_h \ll \lambda \sqrt{\tau\, e^{-\tau}} \,/\, D \tag{4.19}$$

For particle diameters on the order of 5 μm, for example, acceptable half-angles range from approximately 0.5 degrees for the near ultraviolet wavelengths, up to 15 degrees for a wavelength of 10 μm.

Multiple Wavelength Extinction Measurements

Single path extinction methods for particle size determination typically call for measurements at two or more wavelengths to eliminate the ambiguity shown in Figure 4.2 that results from the multi-valued nature of the Mie scattering functions[59].

Ideally, for maximum sensitivity, at least one wavelength shorter than the expected particle diameter, and one wavelength longer, should be used[60]. This effectively yields one measurement in the large particle limit and one in the small particle limit, respectively.

Consider the ratio of the optical depths τ_1/τ_2 obtained from transmittance measurements through the same sample at two wavelengths, λ_1 and λ_2, respectively. This ratio is written as[59]

$$\tau_1/\tau_2 = \tau_{12} = < Q_{e1} > / < Q_{e2} > \tag{4.20}$$

If the particle size is much greater than the wavelength, λ_2, but on the order of λ_1, then $< Q_{e_2} >$ approaches 2, and

$$\tau_{12} = < Q_{e1} > / 2 \tag{4.21}$$

This ratio is dependent on D_{32} for particle diameters on the order of the shorter wavelength, because each mean extinction coefficient is also a function of D_{32}. Figure 4.14 shows a graph of τ_1/τ_2 versus D_{32}. For particles much larger than either wavelength, this ratio approaches a constant value of 1 because the mean extinction coefficient approaches 2 in the limit of large size parameter. Multiple wavelength measurements are advantageous because a known path length and particle number density are not required. Practical multiwavelength extinction measurements are possible because of the variety of compact, high power, commercially available lasers ranging in wavelength from the UV to the IR. Optimum sensitivity is illustrated in Figure 4.14 when the particle diameter in microns is less than the ratio of λ_1/λ_2.

Extinction Through Spatially Nonuniform Distributions

The preceding discussion aids in determining the average particle size of a uniform spatial distribution of particles that have a given size spectrum, especially if

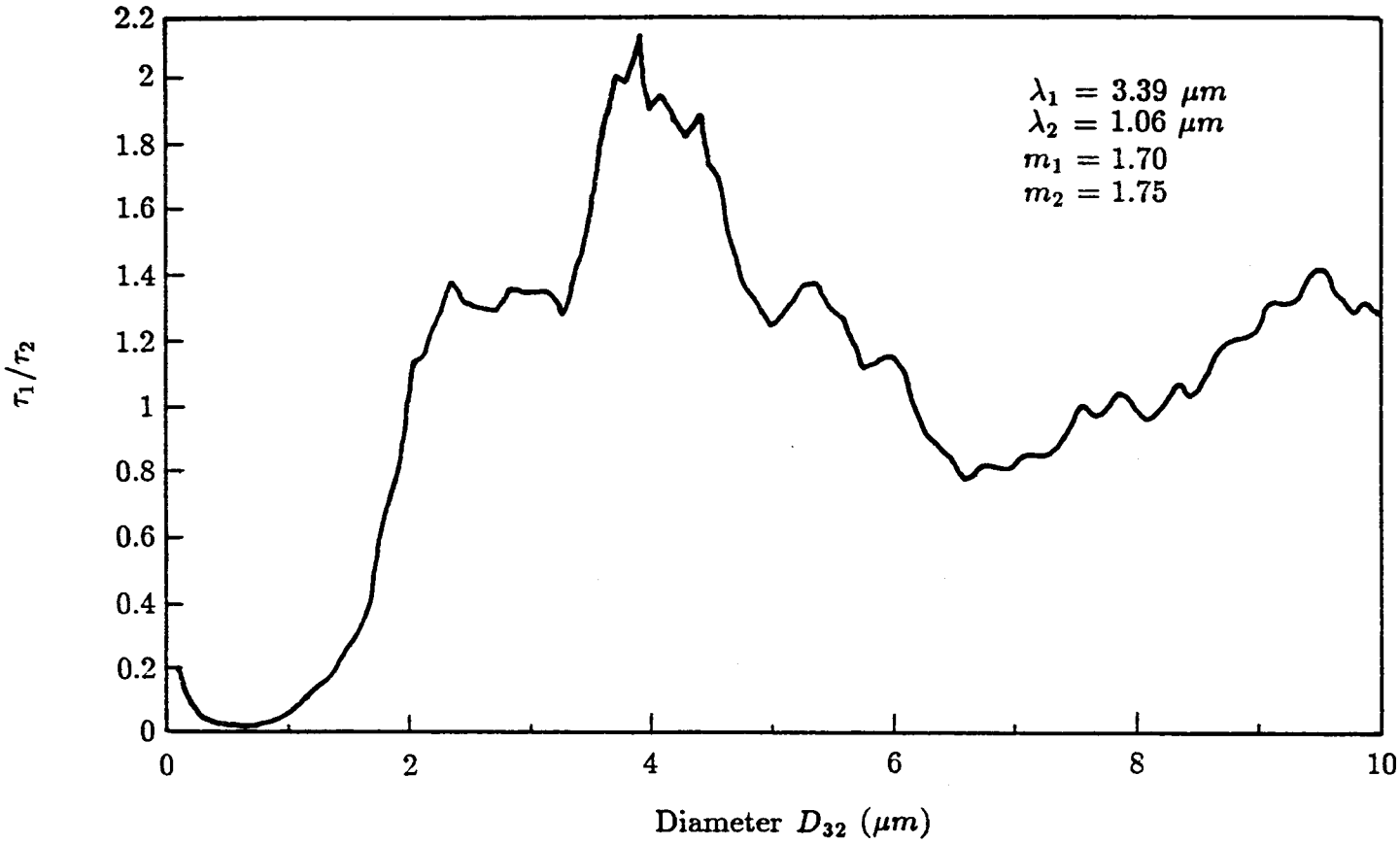


Figure 4.14. Dual wavelength extinction as a function of D_{32}.

information about the PSDF of the particle ensemble is unimportant for a particular experiment. This approach is limited because no spatially dependent size information can be retrieved for spatially nonuniform clouds of particles. An analysis of particle size effects on real flows, however, typically requires the complete particle size and spatial distribution. In general, the particle field is not homogeneous, so the size distribution and the mass density vary according to location within the particle field. In a cylindrically symmetrical plume flowfield, these parameters are assumed to be functions of the plume radius, R. An error in the calculated value of D_{32} from an extinction measurement will occur because of the variation in mass flux density along the beam path. The analytical approach presented in the previous sections must be modified to reflect this new geometry.

For a nonuniform axisymmetric particle distribution, the Lambert-Beer law must be written in terms of the spatially dependent attenuation coefficient, $\kappa(r)$

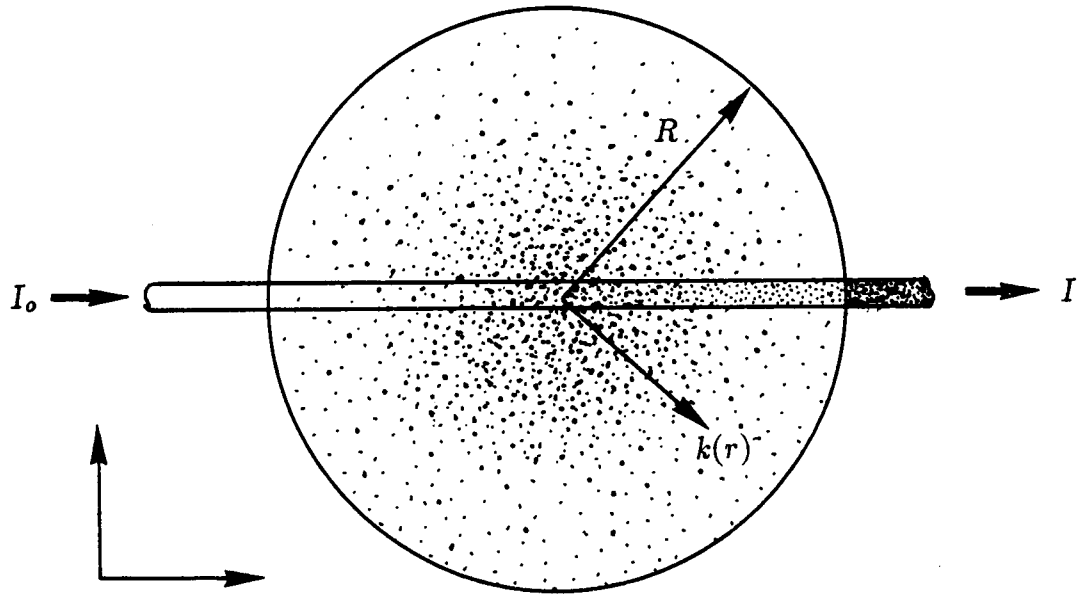
$$T = exp\left(-\int \kappa(r)\, dx\right) \tag{4.22}$$

where x is the coordinate of the optical path length through the plume, and r denotes the radial position within the plume. This geometry is illustrated in Figure 4.15.

A more descriptive form of the attenuation equation includes the extinction efficiency of each particle and the particle size distribution function

$$T = exp\left(-\frac{\pi}{4}\int D^2 Q_e(D)\, n(D,r)\, dD\, dx\right) \tag{4.23}$$

where Q_e is the extinction efficiency calculated by the results of Mie theory, and $n(D,r)$ is the spatially varying particle size distribution function (PSDF). Note that the PSDF is a function of both the size of the particles and the location within the particle cloud. Failure to account for this will result in errors in the particle size estimate.



$$T = \frac{I}{I_o} = e^{-\int k(r)dx}$$

Figure 4.15. Light extinction through a radially inhomogeneous particle cloud.

To illustrate the effects that a nonuniform spatial distribution may have on the determination of average particle size, consider a cylindrical flow of particulates moving with velocity v where the size distribution is the same thoughout. The cross sectional area of the flowfield is $A = \pi R^2$, where R is the flowfield radius, and the particles travel a distance $z = vdt$ along the axis in time dt. As demonstrated earlier, for spatially homogeneous particle flows, a measurement of optical density provides an estimate of D_{32} from

$$D_{32} = \frac{6\ \dot{m}\ < Q_e >}{\pi\ \rho\ L\ v\ \tau} \tag{4.24}$$

where, in the present case, $L = 2R$ is the plume diameter.

The calculated mean particle size is directly proportional to the mass flow through the illuminating beam. For a fixed total mass flow rate in the overall cylindrical flow, the mass flow rate through the illuminating beam depends on how the mass is radially distributed.

The total mass flow rate through a cross section of the cylindrical flowfield, assuming that all the particles have the same velocity, is

$$\dot{m}_T = c_m\ A\ v \tag{4.25}$$

In expanding or contracting conically shaped flowfields, the velocity will generally vary with radial position in the flow and introduce an uncertainty in the measured value of the mean particle size. Particles near the flow boundary in high speed flows, for example, will approach the velocity of the medium external to the flowfield. In most cases, the total mass of particles in the boundary region will be small and will have negligible contribution to the overall extinction. In any case, only the special case of cylindrical flowfields will be considered in this work.

For a uniform flowfield, $c_m = c_{mo}$ = constant, and so

$$\dot{m}_T = v\ c_{mo} \int dA = c_{mo}\ A\ v \tag{4.26}$$

If the flowfield is assumed to have cylindrical symmetry, then $c_m = c_m(r) = \sigma(r)/z$, and

$$\dot{m}_T = v \int c_m(r)\, dA = 2\pi v z \int r\, \sigma(r)\, dr \tag{4.27}$$

where $\sigma(r)$ is the mass flux density, or mass flow rate per unit cross sectional area of the particle cloud, and z is the axial dimension (i.e., the diameter) of the light beam traversing the particle cloud. The appropriate mass flux density function must be normalized to the total mass flow rate.

As an example of the effects of the spatial distribution on the mass flow, $\dot{m}$, through the beam, and the resulting influence on the predicted particle size, suppose that the total mass flow rate $\dot{m}_T$ is known a priori but the radial distribution of mass flux is unknown. Let c_{mo} be the average density of the flowfield (total mass divided by the volume of a cylindrical slice of the flowfield with thickness, z) if the mass flow were uniformly distributed. The total mass flow rate through a beam of width z is obtained from Equation (4.26) and has the form

$$\dot{m} = 2\, zRvc_{mo} \tag{4.28}$$

If, on the other hand, the particle density profile were actually described by the quadratic function

$$\sigma(r) = 2\, \sigma_o(1 - r^2/R^2) \tag{4.29}$$

the total mass flow rate would be the same as if it were caused by a uniform distribution, i.e., $\dot{m}_T = c_{mo}\, Av$. For the quadratic profile, however, the normalized mass flow rate through the beam is calculated from Equation (4.27) to be

$$\dot{m} = \frac{8}{3}\, zRvc_{mo} \tag{4.30}$$

which is $\frac{4}{3}$ times the value obtained assuming a uniform distribution. Since the mean particle size obtained with a single transmission measurement is proportional

to the mass flow rate through the light beam, as described in Equation (4.24), the calculated value of D_{32} will depend on the actual mass distribution within the flowfield.

In general, for any radially symmetric mass distribution, the mass flow rate through the light beam can be written

$$\dot{m} = g' \, zRvc_{mo} \tag{4.31}$$

where the weighting factor g' is determined by evaluating the mass flow integral in Equation (4.27) above. A list of hypothetical spatial mass distributions and their associated weighting factors is shown in Table 4.1.

TABLE 4.1

WEIGHTING FACTORS FOR MASS DISTRIBUTION FUNCTIONS

DISTRIBUTION		g'	RELATIVE WEIGHT, g
Uniform	$\sigma(r) \propto 1$	2	1
Quadratic	$\sigma(r) \propto 1 - r^2$	2.67	1.33
Cosine	$\sigma(r) \propto cos(ar)$	2.75	1.38
Linear	$\sigma(r) \propto 1 - r$	3	1.5

To account for the radially symmetric mass distribution in the determination of particle size, the relative weight, g, defined as the ratio of the radial function weight to the uniform function weight, must be included so that Equation (4.24) becomes

$$D_{32} = \frac{6 \, g \, \dot{m} \, < Q_e >}{\pi \, \rho \, L \, v \, \tau} \tag{4.32}$$

Figure 4.16 demonstrates the effect of the weighting factor in the determination of particle size. The general trend is that a given transmission measurement, τ, will underpredict D_{32} if the erroneously assumed uniform mass flow distribution actually has some radial profile. Also, a similar effect will occur if a radial dependence in the mean size exists. The magnitude of the error in D_{32} depends on D_{32} itself, i.e., on the location of the resonance peak relative to the average particle size as noted earlier. For large particle sizes, the approximate uncertainty in D_{32} is, to first order from Equation (4.14)

$$\Delta D = \Delta\tau \mid \frac{\pi \rho L v D_{32}^2}{12 \dot{m}} \mid g \tag{4.33}$$

Figure 4.16 illustrates that the sensitivity of the optical depth to the mass distribution is dependent on the mean particle size, and therefore emphasizes the need for accurate knowledge of the distribution of mass flow in the particle field. When this knowledge is unavailable, spatially dependent measurements are required to obtain this information. This procedure is discussed in the next chapter.

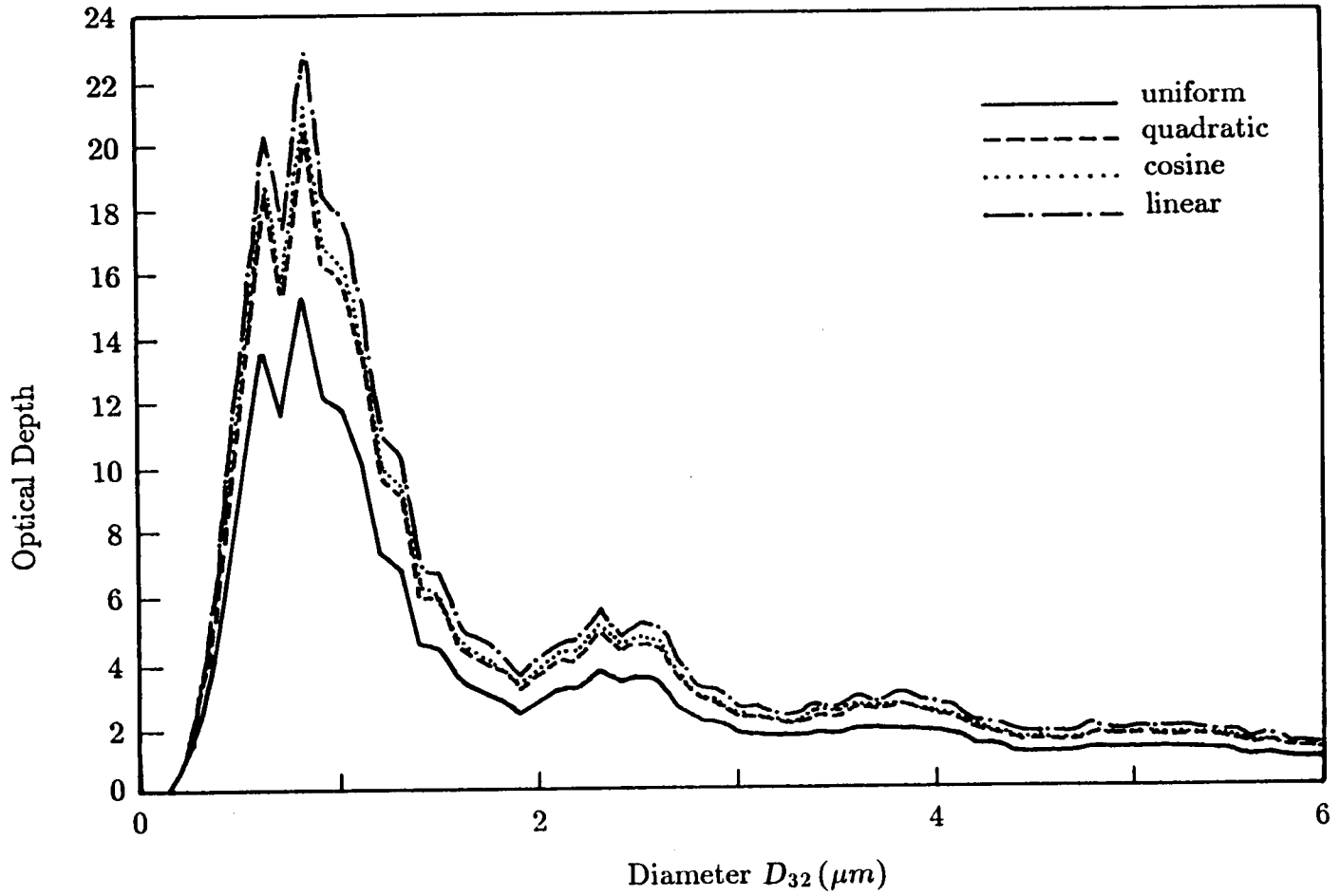


Figure 4.16. Effects of radial mass distribution on theoretical optical depth.

CHAPTER V

MEAN PARTICLE SIZE DISTRIBUTION FROM MULTI-PATH EXTINCTION MEASUREMENTS

Single path light transmission measurements through axisymmetric clouds that have radially dependent mass flow distributions have been shown to yield the average particle size along the integrated beam path. Additional measurements are needed, however, to obtain information about the spatial distribution of particle sizes. Using a set of multiple path extinction measurements in conjunction with a simplified Abel inversion algorithm called an "onion-peel" inversion[65], an approach for determining the average particle size as a function of radial position within the axisymmetric cloud is developed in this section. The technique employed requires a transmission profile across the plume and a knowledge of the plume cross sectional geometry.

For an axisymmetric spatial distribution of particles, the Lambert-Beer extinction law was shown in Equation (4.22) to have the general form

$$T = exp\left(-\int \kappa(r)\, dx\right) \tag{5.1}$$

where the generalized attenuation coefficient, $\kappa(r)$, is a function of particle size and radial position within the cloud, and is integrated over the beam path dx. The attenuation coefficient is obtained by integrating the product of the extinction cross section and the local number density distribution over the range of particle sizes,

$$\kappa(r) = \frac{\pi}{4}\int Q_e(D)\, D^2\, n(D,r)\, dD \tag{5.2}$$

The number density distribution also is dependent on the location within the particle ensemble.

In a region of spatially uniform particle mass distribution, the mean particle

diameter is related to the optical depth through the expression

$$D_{32} = \frac{6\,\dot{m}\ <Q_e>}{\pi\,\rho\,L\,v\,\tau} \tag{5.3}$$

Note that the relative weight, g, is equal to 1 in this case.

Estimates of the distribution of average particle size in an axisymmetric particle cloud are made by obtaining measurements over several paths, each of which consists of discrete regions that have uniform distribution. Determination of the radial average particle size distribution begins by considering the geometry shown in Figure 5.1. An axisymmetric particle cloud is divided into N annular regions, each of which is assumed to have a uniform, homogeneous mass distribution of particles having a specific PSDF, $n_j(D)$, where $j = 1$ to N. This dictates that the bulk attenuation coefficient, κ_j is uniform in each region. Extinction measurements are made for each of N parallel coplanar paths through the particle cloud, as shown in Figure 5.1, with the number of measurement paths equal to the number of annular regions. Knowledge of the radial positions are required for each line-of-sight through the particle ensemble. Data need only be acquired over half of the circular cloud due to symmetry.

Consider an axisymmetric particle ensemble moving with known axial velocity, v. The total mass flow rate, $\dot{m}_T$, is either assumed to be known *a priori* or must be determined experimentally. Again, in the general case of axisymmetric flow, the particle velocity will vary radially within the flowfield, in which case the flow velocity must then be known for each annular region of the flow. In this analysis the flowfield is assumed to be cylindrical. The local mass flow rate, $\dot{m}_j$ varies radially within the ensemble. Defining the local mass flow rate per unit area, σ_j, as

$$\sigma_j = d\dot{m}_j/dA \tag{5.4}$$

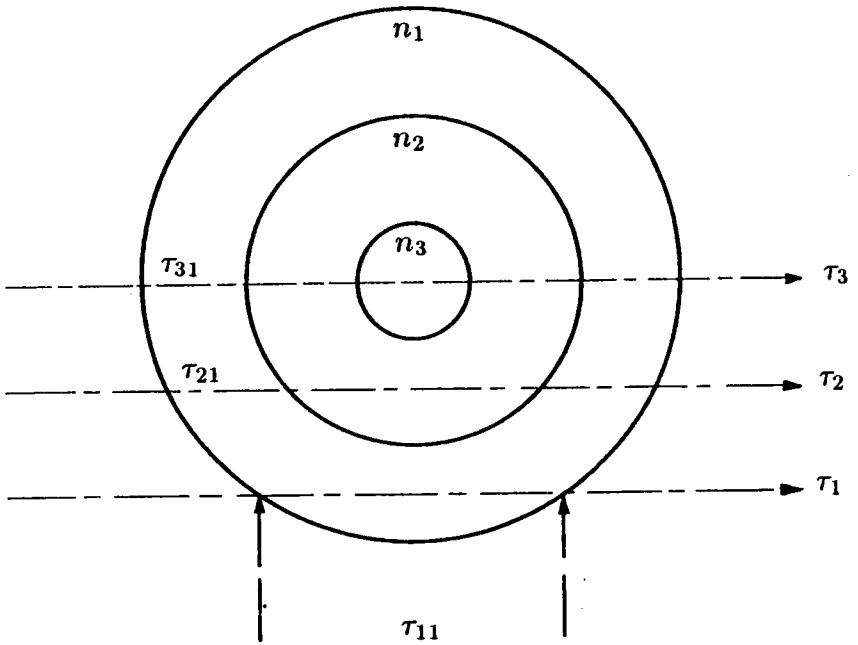
Inversion for Axisymmetric Cloud

Optical Depth

$\tau_i = \sum_{j=i}^{N} \tau_{ij}$

$i \longrightarrow$ path

$j \longrightarrow$ ring



Therefore,

$\tau_1 = \tau_{11}$ ⟶ yields D_{32} in region 1

$\tau_2 = \tau_{21} + \tau_{22}$ ⟶ yeilds D_{32} in region 2

$\tau_3 = \tau_{31} + \tau_{32} + \tau_{33}$ ⟶ yields D_{32} in region 3

Figure 5.1. Abel inversion geometry for an axisymmetric cloud.

where dA is an element of cross sectional area within the particle cloud, the mass flow rate contained in the annular region $r_2 < r_j < r_1$ is obtained from

$$\dot{m}_j = \int_{r_2}^{r_1} 2\pi r\ \sigma(r)\ dr \tag{5.5}$$

The function $\sigma(r)$ is normalized such that

$$\dot{m}_T = \int_o^R 2\pi r\ \sigma(r)\ dr \tag{5.6}$$

where R is the particle cloud radius.

The total mass flow rate in each annular region can be obtained only if the functional form of $\sigma(r)$ is known. Although this is generally not the case, it will be shown in Chapter IX that $\sigma(r)$ may be semi-empirically determined along with the distribution of average particle sizes.

Dividing the particle cloud into N annular regions, $\sigma(r)$ is approximated by N discrete regions, each described by σ_i. Then

$$\sigma_i = \dot{m}_i / A_i \tag{5.7}$$

and

$$\dot{m}_T = \sum_{i=1}^{N} \dot{m}_i = \sum_{i=1}^{N} \sigma_i\ A_i \tag{5.8}$$

The total optical depth, τ_i, of an arbitrary beam traversing several different annular regions is simply the sum of the optical depths in each region, or

$$\tau_i = \sum_{j=1}^{N} \tau_{ij} \tag{5.9}$$

for the i^{th} light path. τ_{ij} is the optical depth of the i^{th} beam through the j^{th} annular region. In general, the optical depth for a given region is wavelength dependent through the Mie extinction efficiency, so

$$\tau_i(\lambda) = \sum_{j=1}^{N} \tau_{ij}(\lambda) \tag{5.10}$$

For an N-path extinction measurement, then,

$$\begin{aligned}
\tau_1(\lambda) &= \tau_{11}(\lambda) \\
\tau_2(\lambda) &= \tau_{21}(\lambda) + \tau_{22}(\lambda) \\
&\vdots \\
\tau_N(\lambda) &= \tau_{N1}(\lambda) + \tau_{N2}(\lambda) + \tau_{N3}(\lambda) + \ldots \tau_{NN}(\lambda)
\end{aligned} \tag{5.11}$$

An empirical fit of the radial profile of the bulk attenuation coefficient is obtained from several extinction measurements at a single wavelength. The attenuation coefficient does not provide direct information about the nature or details of the size distribution, or of the spatial distribution of the particles. It does, however, reveal an important relationship that, when combined with flowfield parameters and extinction coefficients, provides the necessary information to deduce the distribution of average particle sizes.

Because each of the annular regions is assumed to have a uniform distribution of mass, the attenuation coefficient is approximately constant in each region, and for a given wavelength

$$\tau_{ij} = \kappa_j \; x_{ij} \tag{5.12}$$

where x_{ij} is the path length of the i^{th} beam through the j^{th} region. A set of N measurements results in the linear system of equations

$$\begin{aligned}
\tau_1 &= \kappa_1 \; x_{11} \\
\tau_2 &= \kappa_1 \; x_{21} + \kappa_2 \; x_{22} \\
\tau_3 &= \kappa_1 \; x_{31} + \kappa_2 \; x_{32} + \kappa_3 \; x_{33} \\
&\vdots \\
\tau_N &= \kappa_1 \; x_{N1} + \kappa_2 \; x_{N2} + \kappa_3 \; x_{N3} + \; \ldots \; + \kappa_N \; x_{NN} \\
&= \sum_{j=1}^{N} \kappa_j \; x_{Nj}
\end{aligned} \tag{5.13}$$

The above system of equations also may be represented using the matrix notation

$$\overline{\tau} = \overline{\overline{x}}\ \overline{\kappa} \tag{5.14}$$

where the optical path matrix, $\overline{\overline{x}}$, has the form of a lower triangular matrix.

The inversion begins with the outermost layer, $j = 1$, which corresponds with the first beam path, $i = 1$, and proceeds inward through the plume. The particle size distribution is assumed to be spatially uniform within each annular region. Absorbing elements within each path, contributing to the extinction, are bounded by the radial arcs defining each layer and the horizontal beam paths. A characteristic path length, x_{ij}, for each beam is calculated based on an equivalent area between the actual element and a rectangular element having the same thickness; for large clouds this is approximately equal to the intersection length of the light beam and the cloud.

Because there is only one uniform region in the path, the above equation solves easily for the attenuation coefficient, κ_1, as shown below:

$$\kappa_1 = \tau_{11}/x_{11} = \tau_1/x_{11} \tag{5.15}$$

Each successive slice introduces a new onion peel layer into the equation that has the same index as the layer. Attenuation coefficients are known for all outer layers from preceding calculations, and path lengths are calculated from geometry. Therefore, the new κ_i are calculated using the equation:

$$\kappa_i = \left[\tau_i - \sum_{j=1}^{N} \kappa_j\ x_{ij}\right]\ /\ (x_{ii}) \tag{5.16}$$

The error incurred in determining the attenuation coefficients in the outer region can be estimated using a linear, first-order approximation where $d\kappa/\kappa, d\tau/\tau$, and dx/x represent the relative error, respectively, for the quantities κ, τ, and x.

The worst case uncertainity, U_1, in the outermost annular region is calculated as a root-sum-square (RSS) error

$$U_1 = \left(|\frac{d\kappa_1}{\kappa_1}|^2 \right)^{\frac{1}{2}} = \left(|\frac{d\tau_1}{\tau_1}|^2 + |\frac{dx_{11}}{x_{11}}|^2 \right)^{\frac{1}{2}} \tag{5.17}$$

The propagation of errors toward the inner regions consists of accumulated uncertainty from the outer regions. For example, the worst case uncertainty in region 2 is

$$U_2 = \left\{ \left(\frac{\tau_2}{\kappa_2 x_{22}} \right)^2 |\frac{d\tau_2}{\tau_2}|^2 + \left(\frac{\kappa_1 x_{21}}{\kappa_2 x_{22}} \right)^2 |\frac{d\kappa_1}{\kappa_1}|^2 + \left(\frac{\kappa_1 x_{21}}{\kappa_2 x_{22}} \right)^2 |\frac{dx_{21}}{x_{21}}|^2 \right\}^{\frac{1}{2}} \tag{5.18}$$

assuming that the measurement geometry in the inner regions is precisely defined. Typical uncertainties in the measurement of the attenuation coefficient are on the order of a few percent. The dominant terms will typically be the relative uncertainty in the measured optical depth.

The number of annular regions chosen for a particular experiment is dictated by the number of light paths over which the extinction measurements are made. In practice, this number is constrained by the available instrumentation; i.e., the optics, light sources, and detection electronics. Preferably, one would like to use the largest number of light paths possible, in order to maximize the spatial resolution of the measurements.

It should be noted that some flexibility exists in defining the geometry used in the inversion procedure. In particular, the choice of radii used to define the annular regions is somewhat arbitrary. In this work, the annular regions were chosen in such a way that each light path was tangent to the midpoint radius for that region. Defining the radii differently would simply result in a set of mean particle diameters averaged over a different population.

This completes the "onion-peel" inversion procedure for the radial attenuation coefficient. Knowledge of κ_i provides an estimate of $\kappa(r)$, which in turn is related to

the mass density distribution and D_{32}. Multiple path, single wavelength measurements, however, can only be used to obtain average size distributions if the mass flow profile is known. If this is not known, then multiple wavelength measurements are required. An empirical approach for determining the mass flow profile is to calculate the distribution of mean particle sizes for a variety of different trial functions for $\sigma(r)$. The dual-wavelength method described earlier can then be applied in the outermost annular region of the cloud, thereby establishing the mean size in this region fairly precisely. Any trial function that produces a similar mean diameter in the outer region becomes a possible solution for $\sigma(r)$.

The mass flow rate is related to the attenuation coefficient for a uniform spatial distribution of particles through the Lambert-Beer law,

$$\tau = \kappa L = L \ < Q_e > \ \frac{\pi}{4} \int D^2 \ n(D) \ dD \tag{5.19}$$

Through the measurement region, the mass flow rate of particles is

$$\dot{m} = c_v \ \rho \ A \ v = \rho \ A \ v \ D_{32} \ \frac{\pi}{6} \int D^2 \ n(D) \ dD \tag{5.20}$$

Eliminating the integral over D,

$$\dot{m} = \frac{2 \ \rho \ A \ v \ \kappa \ D_{32}}{3 \ < Qe >} = \frac{2 \ \rho \ A \ v \ \kappa}{3 \ \overline{Q}_e} \tag{5.21}$$

where $\overline{Q}_e$ is the mean specific extinction efficiency. Therefore, in the j^{th} annular region

$$\kappa_j = 3 \ \sigma_j \ \overline{Q}_j \ / \ 2 \ \rho \ v \tag{5.22}$$

where $\sigma_j = dm_j/dA$ and $\overline{Q}_j$ represents the mean specific extinction efficiency in region j. The beam attenuation along a path through a given annular region, therefore, must be described by

$$\tau_{ij} = 3 \ \sigma_j \ x_{ij} \ \overline{Q}_j \ / \ 2 \ \rho \ v = \kappa_j \ x_{ij} \tag{5.23}$$

where κ_j is determined as above from known path lengths and measured optical depths.

Particle size information is contained in the parameter $\overline{Q}_j$. Because κ_j is dependent on both σ_j and $\overline{Q}_j$, the functional form of $\sigma(r)$ must be known or estimated to obtain particle size estimates in any region of the cloud. For situations in which $\sigma(r)$ is unknown, multiple wavelength measurements must be employed, as mentioned previously.

Inversion of the average particle size distribution follows a procedure similar to that of ascertaining the $\kappa(r)$ profile. The results of the previous chapter indicate that the optical depth also can be expressed as a function of the flow geometry, the mean extinction efficiency, and the average particle size, for a homogeneous particle distribution, as

$$\tau = \frac{6\ \dot{m}\ < Q_e >}{\pi\ \rho\ L\ v\ D_{32}} \tag{5.24}$$

To simplify the notation, introduce the flow parameter, e, defined by

$$e = \frac{6\ \dot{m}}{\pi\ \rho\ L\ v} \tag{5.25}$$

and recall from Equation (4.11) the definition of the mean specific extinction efficiency

$$\overline{Q}_e = < Q_e > \ / \ D_{32} \tag{5.26}$$

Note that each of these parameters varies from region to region. The quantities $\dot{m}$ and L are determined from the radial attenuation coefficient. With this notation, the above linear system of equations for N regions are written and solved in terms

of the mean specific extinction efficiency

$$\begin{aligned}
\tau_1 &= \overline{Q}_{e1}\ e_{11} \\
\tau_2 &= \overline{Q}_{e1}\ e_{21} + \overline{Q}_{e2}\ e_{22} \\
\tau_3 &= \overline{Q}_{e1}\ e_{31} + \overline{Q}_{e2}\ e_{32} + \overline{Q}_{e3}\ e_{33} \\
&\vdots \\
\tau_N &= \sum\ \overline{Q}_{ei}\ e_{Ni}
\end{aligned} \tag{5.27}$$

Performing the inversion procedure as above, the mean specific extinction efficiency is solved in region 1 using the optical depth and the flow parameter

$$\overline{Q}_{e1} = \tau_1\ /\ e_{11} \tag{5.28}$$

The particle size then is determined by the relationship between the mean particle size and the mean specific extinction efficiency discussed in Chapter IV.

The general form for the mean specific extinction efficiency for N beams is

$$\overline{Q}_{ei} = \left[\tau_i - \sum\ \overline{Q}_{ej}\ e_{ij}\right]\ /\ (e_{ii}) \tag{5.29}$$

The average particle size is therefore determined for each of the N rings used in the inversion, provided that e_{ij} is known.

Potential errors in the particle size determined with this procedure occur because of uncertainties both in the measurement geometry and the calculation of the mean extinction efficiency. Discussion of the uncertainties associated with extinction measurements was presented earlier in Chapter IV, where it was shown that uncertainties in the mean extinction efficiency should be small if the wavelengths are appropriately chosen. The error in particle size is proportional to the uncertainty in the mean extinction efficiency. Uncertainties due to the measurement geometry are primarily due to the uncertainity in the overall cloud radius, which introduces

error in the inversion process through the calculation of κ in the outer annular region. The geometry of the inner regions is predefined for the inversion process, so additional errors of this nature are not propagated.

CHAPTER VI

PARTICLE SIZE OBTAINED FROM SCATTERING MEASUREMENTS

Many investigators have used light scattering measurements to obtain particle size information for both single and ensemble particle measurements[66-76]. Methods have been proposed for average size measurements and for determining the complete particle size distribution. Techniques include multiple wavelength, multiple angle, and polarization ratio measurements. Scattering measurements are used primarily in applications in which the particle sizes are on the order of the wavelength of light.

Detailed size distribution measurements require scattering information at many angles or wavelengths and result in difficult numerical inversion procedures. Angular scattering measurements that use the Mie theory are often difficult to implement experimentally in high density or large volume particle ensembles. In the former case, this is caused by attenuation of the scattered light; in the latter case one must integrate over a finite range of angles comprising the detector field of view. The measurement volume, which is defined by the overlap of the incident beam, the detector field of view, and the particle cloud, must be precisely determined. Moreover, angular scattering is highly dependent on the refractive index of the particle material, and thus is more susceptible to uncertainties in the optical properties. In view of these complexities, the ideal particle sizing experiment must be designed to be relatively insensitive to these parameters.

In this chapter, the feasibility of using forward and backscatter measurements is examined for determining the average size of a particle ensemble. The objective for this part of the work is to establish a simple independent measurement technique to backup, validate, and corroborate the average sizes that are determined by the extinction technique. Forward and backscatter measurements are of particular

interest for these measurements because of the easily implemented and interpreted scattering geometries, and because these techniques tend to be less sensitive than sidescatter to uncertainties in refractive index and distribution shape. Scattering measurements are best suited in optically thin particle clouds, suggesting the use of the forward and backscatter techniques on the outermost annular region in the multiple path extinction approach when applied to spatially extended particle clouds.

When a particle is illuminated by an unpolarized plane wave of irradiance E_o, the intensity per unit solid angle scattered in the direction θ, is[46]

$$I(\theta) = (i_1 + i_2) \; / \; 2k^2 \tag{6.1}$$

where i_1 and i_2 are the intensity functions for perpendicular and parallel polarized light, as defined in Chapter II, and k is the wave propagation constant. The intensity scattering functions for spherical particles are obtained from Mie theory, but also may be calculated numerically for non-spherical particles.

The intensity of the light scattered from a group of small particles into a given angle is proportional to the scattering cross section of each particle and to the total number of particles of each size within the field of view. The geometry for this case is illustrated in Figure 6.1. The intensity generally depends both on the state of polarization of the incident light and on the optical properties of the particles. The total intensity observed at the location of a detector centered at an angle θ_1 relative to the incident unpolarized radiation is then

$$I(\theta_1) = \int \left[(i_1 + i_2) \; / \; 2k^2\right] \; n(D,r) \; dD \; dr \tag{6.2}$$

This intensity is an experimentally determined quantity. Intensity measurements typically are made at several angles in a given experiment, providing J measurements, $I(\theta_1)$, $I(\theta_2)$, ... $I(\theta_J)$, each in the form of the above equation. The

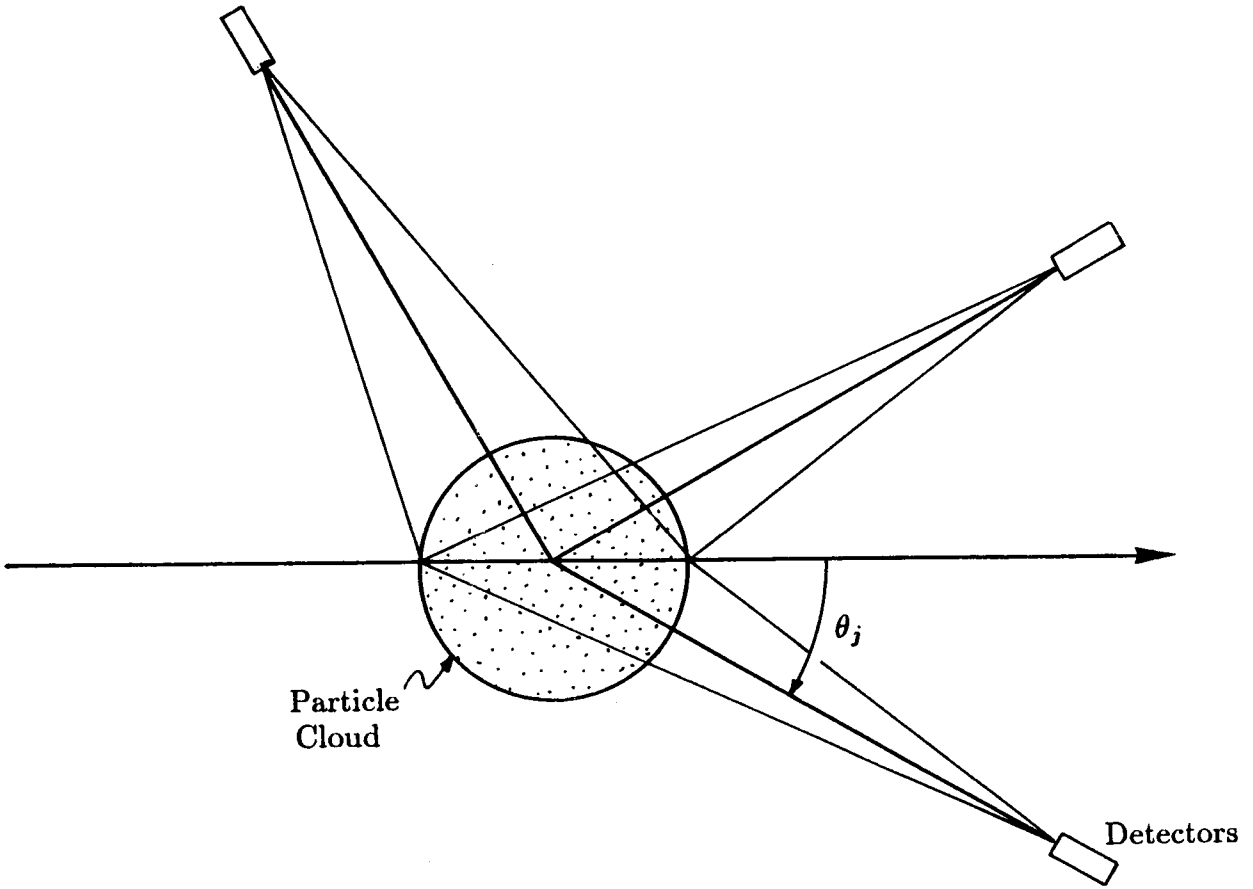


Figure 6.1. Measurement geometry for multiple angle scattering.

spherical particles are assumed to have a homogeneous spatial distribution and the detector angular field of view is small enough so that θ does not vary appreciably from one side of the distribution to the other. Under these conditions, the angular scattering data may, in principle, be inverted to obtain the complete particle size distribution function[33]. It is clearly desirable to make as many angular scattering measurements as possible, in order to obtain as much information as possible about the distribution. Practically, due to space and/or hardware limitations, these measurements may be limited to only a few angles. The following sections examine two alternate approaches to obtain average particle size from a distribution, one based on diffraction and the other utilizing backscattered light.

Diffraction Measurements of Mean Size

Light passing through an aperture or moving past an opaque object with dimension D and observed in the far field of the radiation, where the distance $z \gg D^2 \, / \, \lambda$, will exhibit Fraunhofer diffraction. The scattered light from a transparent particle results from interference between the internal and external electric fields near the particle and may be thought of as a combination of refracted and diffracted components. The angular distribution of scattered light in the forward direction yields particle size information even when the refractive index of the material is unknown. This is attributable to diffraction of light rays caused by the rays passing near the surface of, and not through, the particle.

Many investigators have studied the extraction of particle size information from diffraction or forward scatter measurements[66–76]. Hodkinson[77] has demonstrated that measurement of the forward scattering cone yields particle size information based on a diffraction analysis. Dobbins[78] has obtained estimates of D_{32} based on analysis of the diffractively scattered light. In this section, a new technique for

measuring the mean size of a distribution is presented.

The radiant intensity of the light scattered by a spherical particle into an angle measured from the forward direction is[78]

$$I(\theta) = E_o\ (D\alpha/4)^2 \left[2\ J_1\ (\alpha\ sin\ \theta)\ /\ (\alpha\ sin\ \theta)\right]^2 \tag{6.3}$$

where E_o is the irradiance of the incident plane wave illuminating the particle, and α is the size parameter. For a polydispersion of particles, this scattered intensity must be integrated over the entire size distribution. The normalized integrated intensity of the diffractively scattered light due to the particle distribution is[78]

$$I(\theta) = \frac{\int \left[2J_1\ (\alpha\ sin\ \theta)\ /\ (\alpha\ sin\ \theta)\right]^2\ D^4\ n(D)\ dD}{\int n(D)\ D^4\ dD} \tag{6.4}$$

where the denominator represents the radiant intensity of the light scattered into the angle $\theta = 0$. This expression describes the angular profile of the diffractively scattered light and is valid for optically thin particle distributions. High density distributions cause attenuation in the scattered radiation, which requires some modification to $I(\theta)$.

Dobbins[78] has noted that the measurement of the scattered light intensity profile alone is insufficient for uniquely determining the complete size distribution function. The scattered light intensity profile does provide, however, a good estimate of D_{32} when the sized distribution is described with the Upper Limit Distribution Function (ULDF) defined by[79]

$$n(D) = C\ exp\left(-\left\{dln\left[aD\ /\ (D_{max} - D)\right]\right\}^2\ /\ \left[D^4\ (D_{max} - D)\right]\right) \tag{6.5}$$

where a and d are shape parameters, C is a constant, and D_{max} is the maximum particle diameter in the distribution. This distribution is useful because it does not allow the existence of any particle greater than a specified D_{max} [78]. Roberts

and Webb[67] extended these results to the more general case of arbitrary size distributions and concluded that D_{32} may be accurately determined even if the form of the distribution function is unknown. Therefore, forward scattering measurements, when combined with extinction measurements, may yield both the particle concentration and Sauter mean diameter of the distribution.

An alternate way of obtaining an average particle size of a distribution through the analysis of the diffracted light signature was investigated in this work. Consider the normalized integrated intensity function described in Equation (6.4) above and recall that $\alpha = \kappa D$. Rewriting the integral in the numerator as

$$\int \left[2\ J_1\ (\alpha\ sin\ \theta)\ /\ (k\ sin\theta)\right]^2\ D^2\ n(D)\ dD \tag{6.6}$$

and defining the diffraction efficiency Q_d as

$$Q_d(D) = \left[2\ J_1\ (kD\ sin\ \theta)\ /\ (k\ sin\ \theta)\right]^2 \tag{6.7}$$

a mean diffraction efficiency, analogous to the mean extinction efficiency defined in Chapter IV, is written as

$$< Q_d > = \frac{\int \left[2\ J_1\ (\alpha\ sin\ \theta)\ /\ (k\ sin\ \theta)\right]^2\ D^2\ n(D)\ dD}{\int D^2\ n(D)\ dD} \tag{6.8}$$

Multiplying the numerator and denominator of the normalized integrated intensity equation by

$$\int D^2\ n(D)\ dD \tag{6.9}$$

and using the definition of D_{42} obtained from Equation (3.19), the normalized integrated intensity takes the simple form

$$I(\theta) = < Q_d > \ /\ D_{42}^2 \tag{6.10}$$

This remarkable result indicates that the normalized angular spectrum of the diffractively scattered light from an ensemble of particles depends only on the distribution

of particle sizes and is independent of particle concentration and velocity. In practice, measurement of the relative light intensity at two scattering angles is required to provide the mean particle diameter, D_{42}. The importance of this comparatively simple approach is that forward scattering measurements of D_{42} can, in principle, be combined with the extinction measurements of D_{32} to provide the particle size distribution function.

The usefulness of this result depends entirely on whether $I(\theta)$ is dependent on the type or shape of the PSDF. Parametric studies were performed to qualitatively evaluate the sensitivity of the technique to the details of the size distribution. In Figure 6.2, the effect of the type of particle size distribution function is shown by comparing the normalized angular scattered intensity profiles of log-normal, Gaussian, and rectangular distribution functions. The lower set of curves in this figure represents functions having a D_{42} of 4 microns, while the upper set of curves were calculated using $D_{42} = 2$ microns. The full width half maximum of each distribution shown is approximately 2 μm, and the wavelength of the incident beam used in the calculations was 1.06 μm. From the figure, it is evident that the type of PSDF has little effect on the shape of the normalized angular intensity profile for a given mean diameter, D_{42}. This method should therefore prove to be highly effective in determining the mean diameter of a distribution, even when the type of PSDF is unknown.

The effect of the width of the particle size distribution function was also studied, as demonstrated in Figure 6.3 for a log-normal distribution. For a monodisperse distribution, the angular spectrum of the diffractively scattered light will be identical to that of a single particle having the same diameter. Broadening the distribution reduces the total relative intensity measured at a particular angle because the angular divergence of the central diffraction lobe is dependent on particle size. Thus,

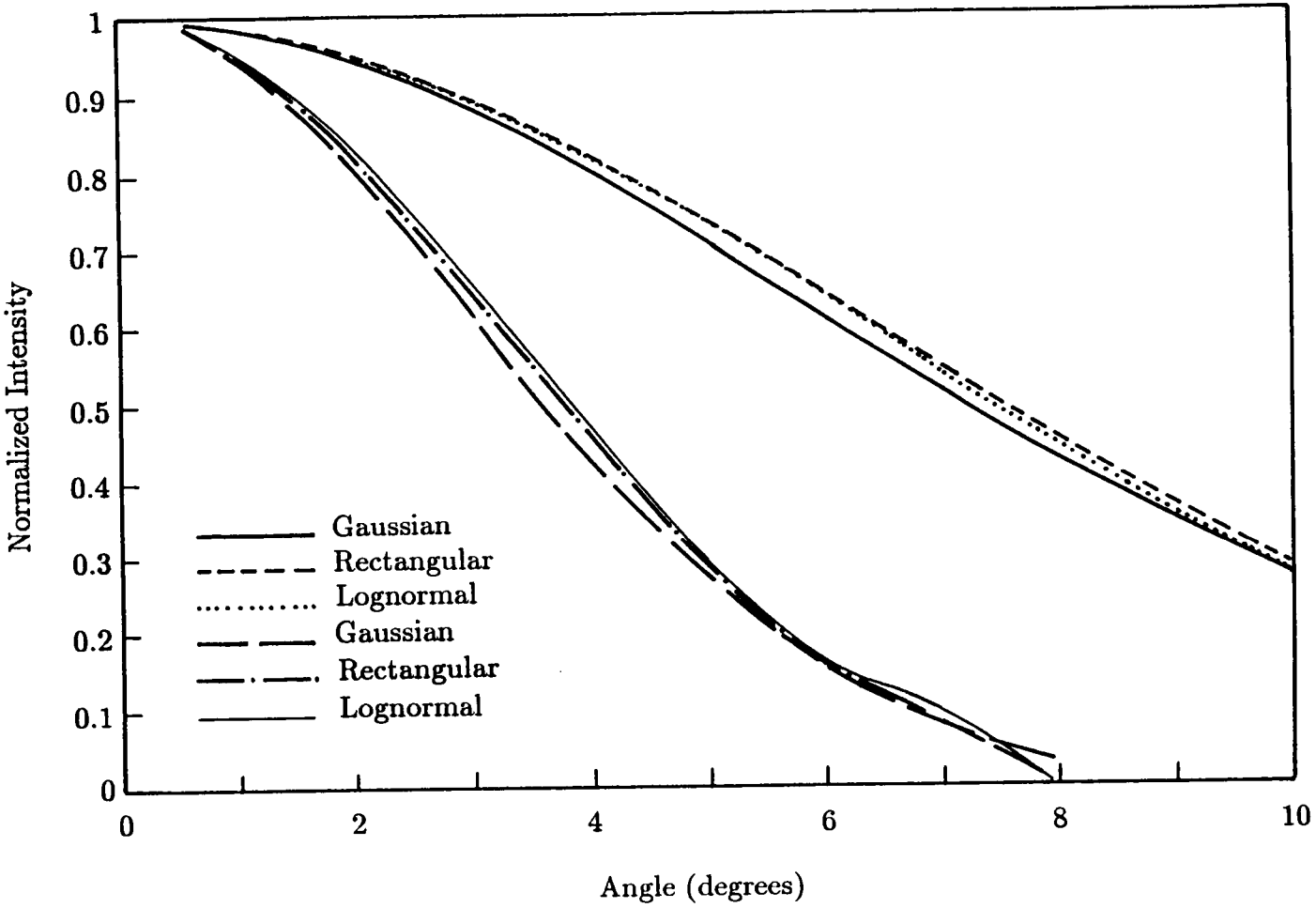


Figure 6.2. Effect of distribution type on angular diffraction profile.

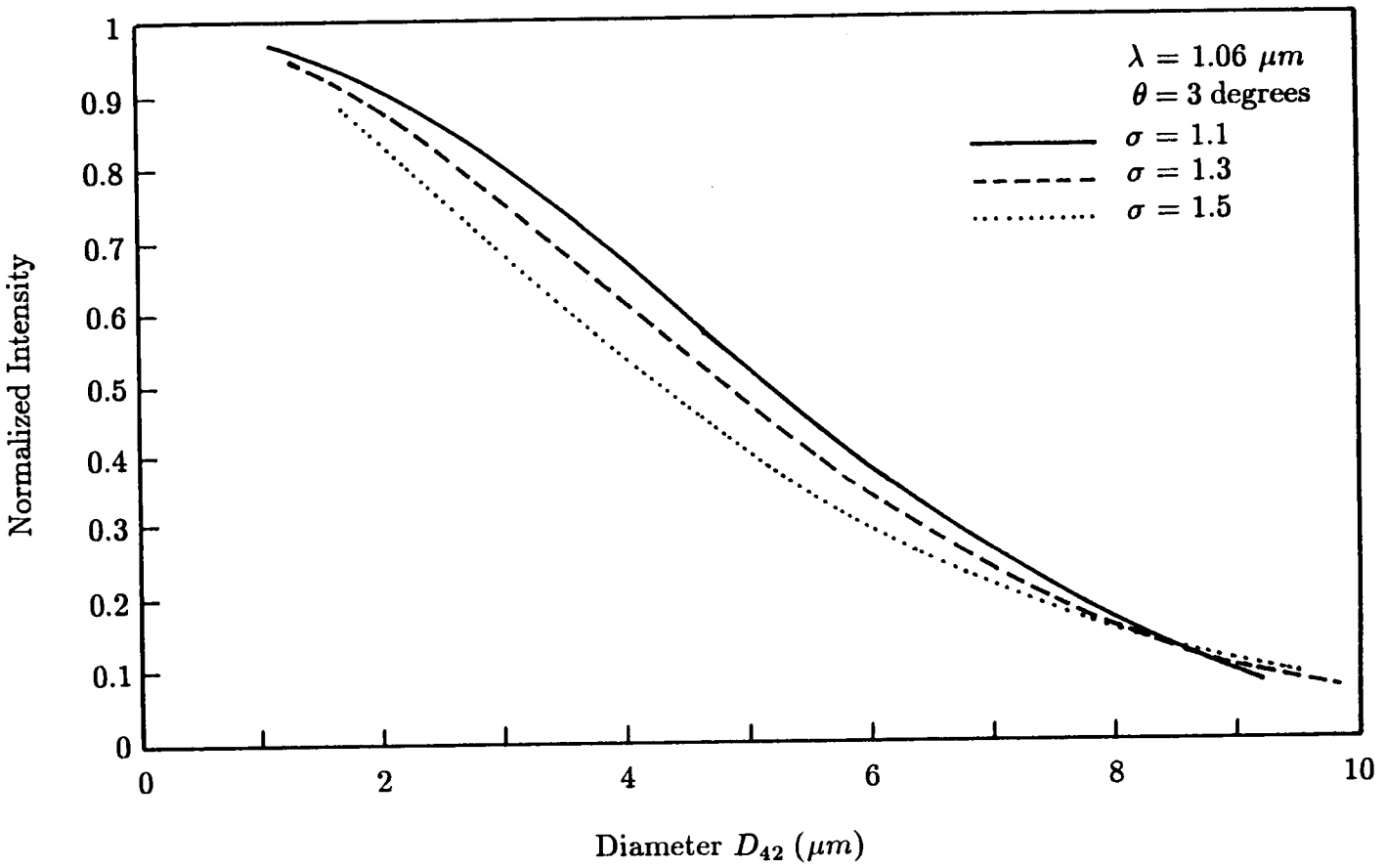


Figure 6.3. Effects of distribution width on angular diffraction profile.

as shown in Figure 6.3, uncertainty in the width of the size distribution results in an uncertainty in the mean particle diameter, D_{42}. The uncertainty in the measurement of D_{42} can be reduced with the use of multiple detectors at suitable chosen angles.

Implementation of this technique will generally require forward scatter measurements at two small angles, since calibration of an absolute scattering measurement would be impractical. Ideally, one of these detection angles will provide the normalization measurement, and should be chosen as close to zero degrees as possible. Figure 6.4 shows the normalized integrated intensity as a function of D_{42} for a log-normal particle size distribution function with a width $\sigma = 1.3$. The calculations were made at two viewing angles, 3 and 5 degrees, at a wavelength of 1.06 μm. For these angles, mean particle diameters up to approximately 10 μm can be resolved with two measurements.

Of particular interest is the relationship between the Fraunhofer theory and the Mie theory, as applied to the backscatter profile caused by an ensemble of spherical particles. Light backscattered by a spherical particle with diameter on the order of the wavelength of light will have an angular divergence similar in appearance to light that is forward diffracted from an equivalent circular aperture. Based upon Mie scattering calculations, the diameter of the equivalent circular aperture is expected to be close to, but not necessarily equal to, the physical diameter of the particle. The angular width of the principal backscatter lobe depends on the refractive index of the particle. It, however, can be approximated for a given size particle by the width of the principal lobe of the Fraunhofer diffraction pattern of a circular aperture, which thereby eliminates the need for the more complicated Mie theoretical calculations. The forward scattering approach presented in this section can therefore be applied to angular backscatter measurements if the proper scaling

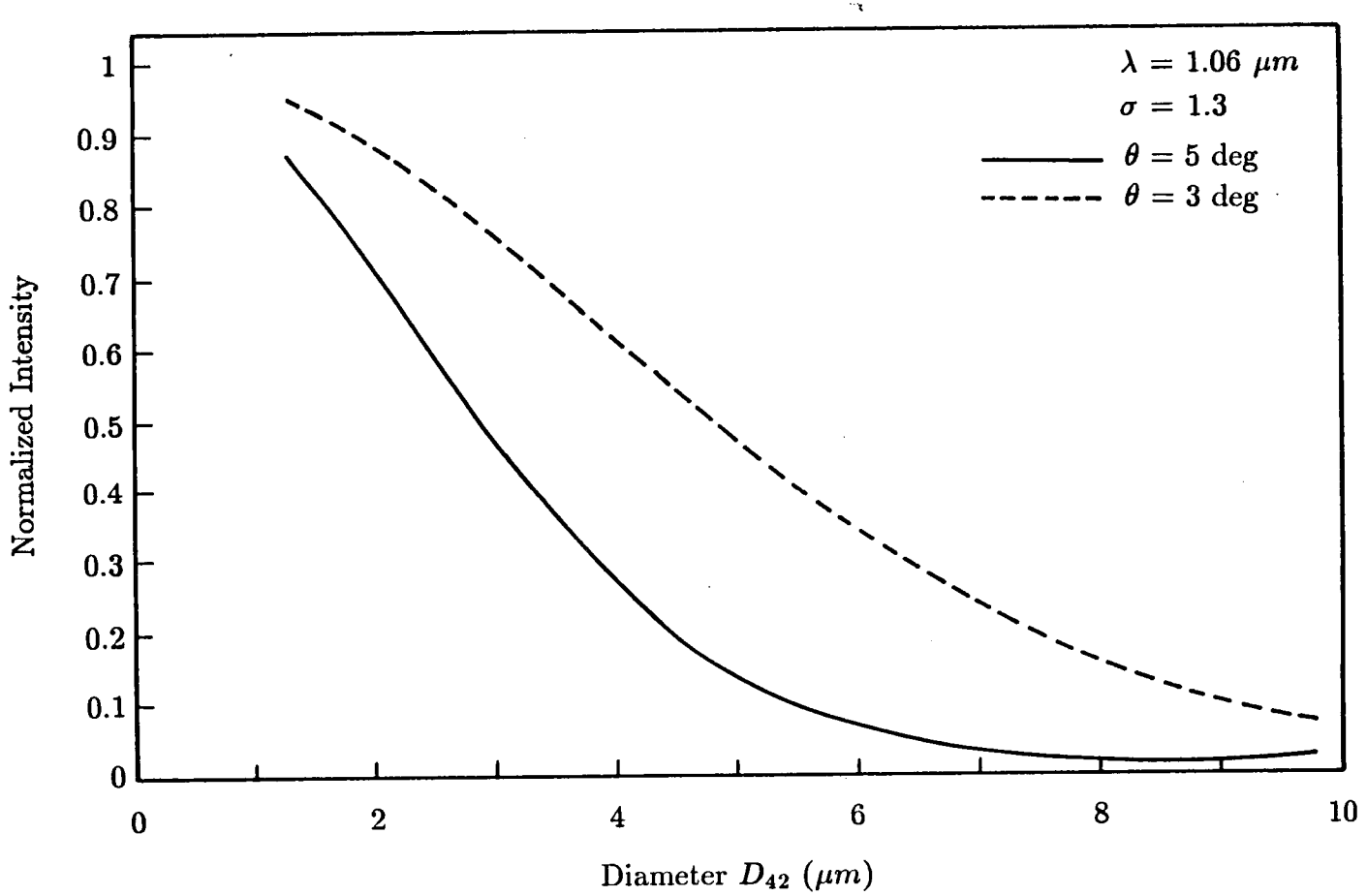


Figure 6.4. Normalized angular diffraction profile.

is incorporated for the refractive index of the particle.

A comparison was made of the angular intensity profiles of several different sized particles as predicted by the Mie theory and by Fraunhofer diffraction. Figure 6.5 illustrates that for a particle with refractive index of 1.75, the widths of the primary lobes predicted by the two theories are very similar and, in fact, are approximately related by a constant value of 3/4. In other words, the backscatter lobe of a 3/4 micron particle predicted by the Mie theory, has approximately the same angular width as a 1 micron particle predicted by Fraunhofer diffraction theory for the refractive index value used in this example. The average particle size thus can be approximated using the diffraction technique applied to the angular backscatter profile if proper account is taken of the particle refractive index.

Backscatter Measurements of Mean Size

Backscatter measurements are perhaps the easiest to obtain experimentally because of the measurement geometry, and also may provide supplemental information on the particle flow. The accessibility of the backscattered radiation usually is greater than that of extinction or forward scattering, especially in remote measurement applications. Interpretation of backscatter information, however, is more difficult to treat than extinction or diffraction, because the backscatter efficiency, Q_b, is highly wavelength dependent, as shown in Figure 6.6, and oscillates rapidly as a function of particle diameter[80]. The scattering function also is strongly polarization sensitive in the backscatter direction, in part caused by the size dependence. This indicates that backscatter measurements will be strongly influenced by particle shape. Particle shape effects are not examined here, but should be considered in measurements in which the particles are known to be non-spherical or irregularly shaped. This section establishes the feasibility of using the backscatter signal from

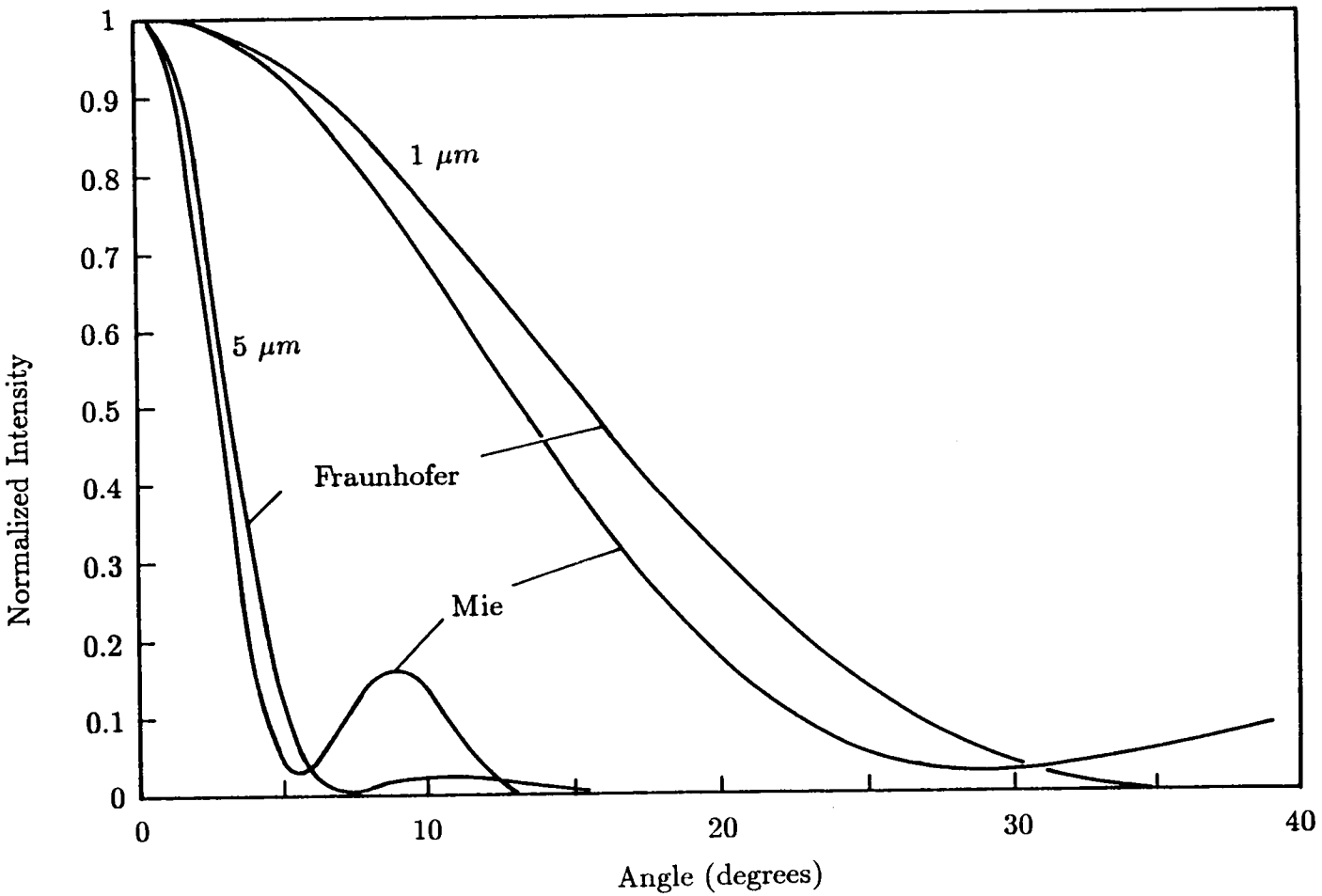


Figure 6.5. Comparison of backscatter profile predicted from Mie and Fraunhofer theories.

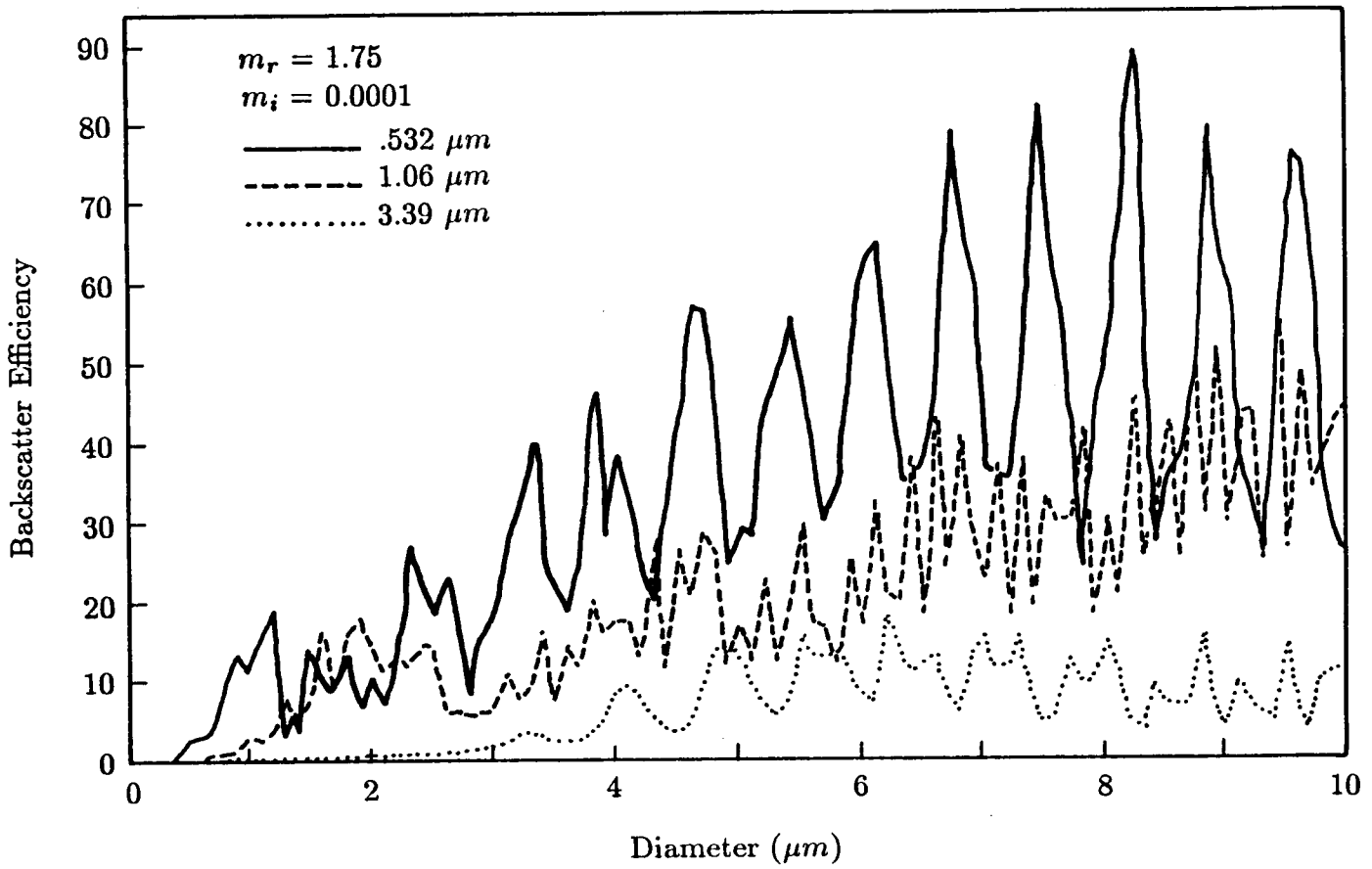


Figure 6.6. Backscatter efficiency as a function of particle size.

an ensemble of spherical particles to determine an average particle size.

Consider a small, optically thin volume element dV that contains particles with distribution $n(D)$ flowing through a cross sectional area A with velocity v. The geometry for this discussion is shown in Figure 6.7. In the time δt the total mass flux through the area per unit time is

$$\dot{m} = A\ v\ \rho\ \frac{\pi}{6} \int D^3\ n(D)\ dD \tag{6.11}$$

where ρ is the particle material density. The flow of particles through a laser beam of diameter W, and path length L, is expressed as a function of the Sauter mean diameter of the particle distribution

$$\dot{m} = W\ L\ v\ \rho\ D_{32}\ \frac{\pi}{6} \int D^3\ n(D)\ dD \tag{6.12}$$

The total backscatter signal, B_s, produced by the particles in this flow is found by adding the backscatter contribution from each particle in the distribution. This is given by integrating the product of the differential backscatter cross section, the number density, the detector solid angle, and the incident power, in the form

$$B_s = I_o\ \Omega\ A\ L \int \frac{dC_b(D)}{d\Omega}\ n(D)\ dD \tag{6.13}$$

The differential backscatter cross section is related to the Mie backscatter efficiency by[46]

$$\frac{dC_b}{d\Omega} = \frac{\pi D^2\ Q_b}{4\ (4\pi)} \tag{6.14}$$

The backscatter signal power can then be written as

$$B_s = \frac{I_o\ \Omega\ A\ L}{16}\ < Q_b(D) > \int D^2\ n(D)\ dD \tag{6.15}$$

where $< Q_b >$ is the mean backscatter efficiency defined by

$$< Q_b > = \frac{\int Q_b(D)\ D^2\ n(D)\ dD}{\int D^2\ n(D)\ dD} \tag{6.16}$$

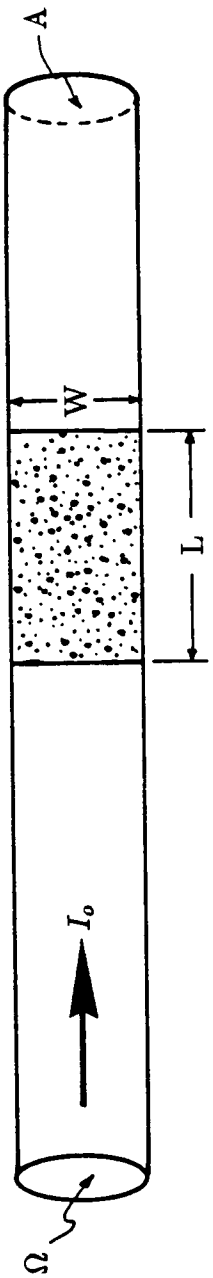


Figure 6.7. Backscatter measurement geometry.

Effective use of the mean backscatter efficiency to provide realistic size estimates of particle distributions depends on the functional dependence of this quantity on particle size. Figure 6.8 shows the mean backscatter efficiency, as calculated from Mie theory, as a function of particle mean diameter for log-normal distributions that have several widths. For narrow distributions, the backscatter efficiency varies considerably with particle size. However, for polydisperse size distributions, the oscillations in the backscatter efficiency are averaged out, resulting in a reasonably smooth dependence on particle size. In fact, calculations indicate that the mean backscatter efficiency is relatively independent of the details of the particle size distribution function when the mean particle diameter ranges from approximately 2 to 10 times the illumination wavelength. The variation of $< Q_b >$ as a function of D_{32} is within $\pm 10\%$ in this size range.

The backscatter signal is proportional to the incident intensity and solid angle of the backscatter detection optics. In a practical experiment it is desirable to use a calibration technique that does not require absolute calibration of these quantities. A useful calibration procedure consists of placing a Lambertian reflectance target of hemispherical reflectivity, R_h, at the center of the small volume through which the particles will flow. The depth of the particle field, L, is assumed to be small enough that the solid angle seen by the detector is constant throughout the volume, i.e., L is much less than the distance to the detector.

For an incident power P_o and illumination beam diameter A, the radiant exitance from the calibration target surface is

$$M = R_h \; P_o \; / \; A \tag{6.17}$$

The radiance reflected from the target surface is then M/π. The optical power collected from the calibration target by the backscatter detection optics, which are

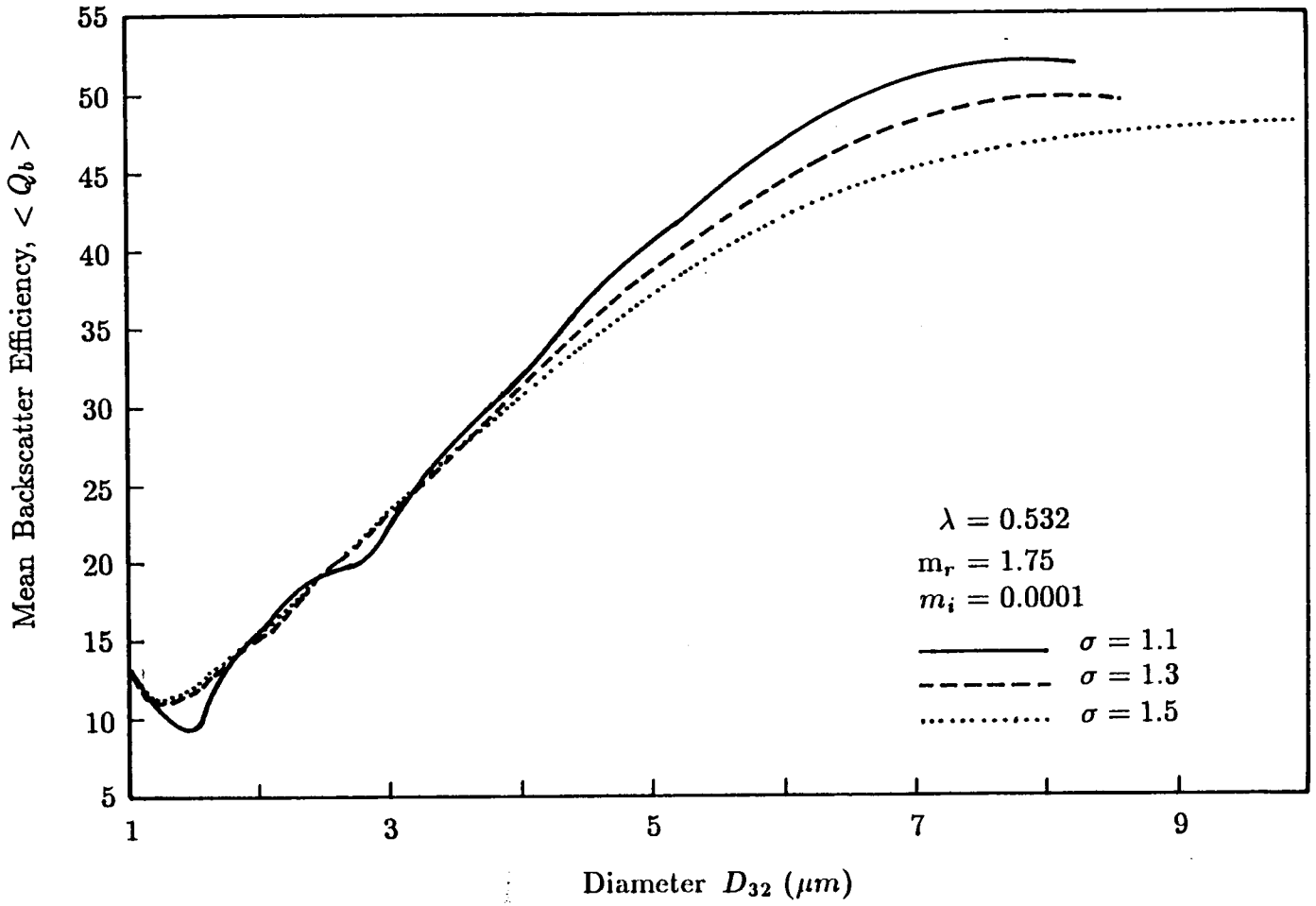


Figure 6.8. Mean backscatter efficiency as a function of mean particle diameter.

located at a large distance from the measurement volume, is then

$$B_c = R_h \; P_o \; \Omega \; / \; \pi \tag{6.18}$$

The backscatter signal from the particle ensemble can now be described in terms of the backscatter from an ideal Lambertian detector by defining the ensemble backscatter efficiency as

$$\begin{aligned} \beta &= B_s \; / \; B_c \\ &= \frac{L \; \pi \; < Q_b >}{16 \; R_h} \int D^2 \; n(D) \; dD \end{aligned} \tag{6.19}$$

Combining the equations for the ensemble backscatter efficiency and the mass flow rate, the backscatter signal should be proportional to the mass flow rate and inversely proportional to the average particle size:

$$\beta = \frac{3 \; \dot{m} \; < Q_b >}{8 \; R_h \; \rho \; W \; v \; D_{32}} \tag{6.20}$$

This result is similar in form to that obtained for the extinction of light through an ensemble of particles. The ensemble backscatter efficiency also can be related to the mean specific backscatter efficiency, $\overline{Q}_b$, defined in the same manner as the mean specific extinction efficiency as

$$\overline{Q}_b = < Q_b > \; / \; D_{32} \tag{6.21}$$

With this definition, the ensemble backscatter efficiency becomes

$$\beta = \frac{3 \; \dot{m} \; \overline{Q}_b}{8 \; R_h \; \rho \; W \; v} \tag{6.22}$$

Figure 6.9 demonstrates that the mean specific backscatter efficiency is a function of the mean particle diameter for log-normal distributions of various widths. For relatively broad distributions, $\overline{Q}_b$ is very weakly dependent on particle diameter for diameters ranging from approximately 2 to 10 wavelengths. The variation

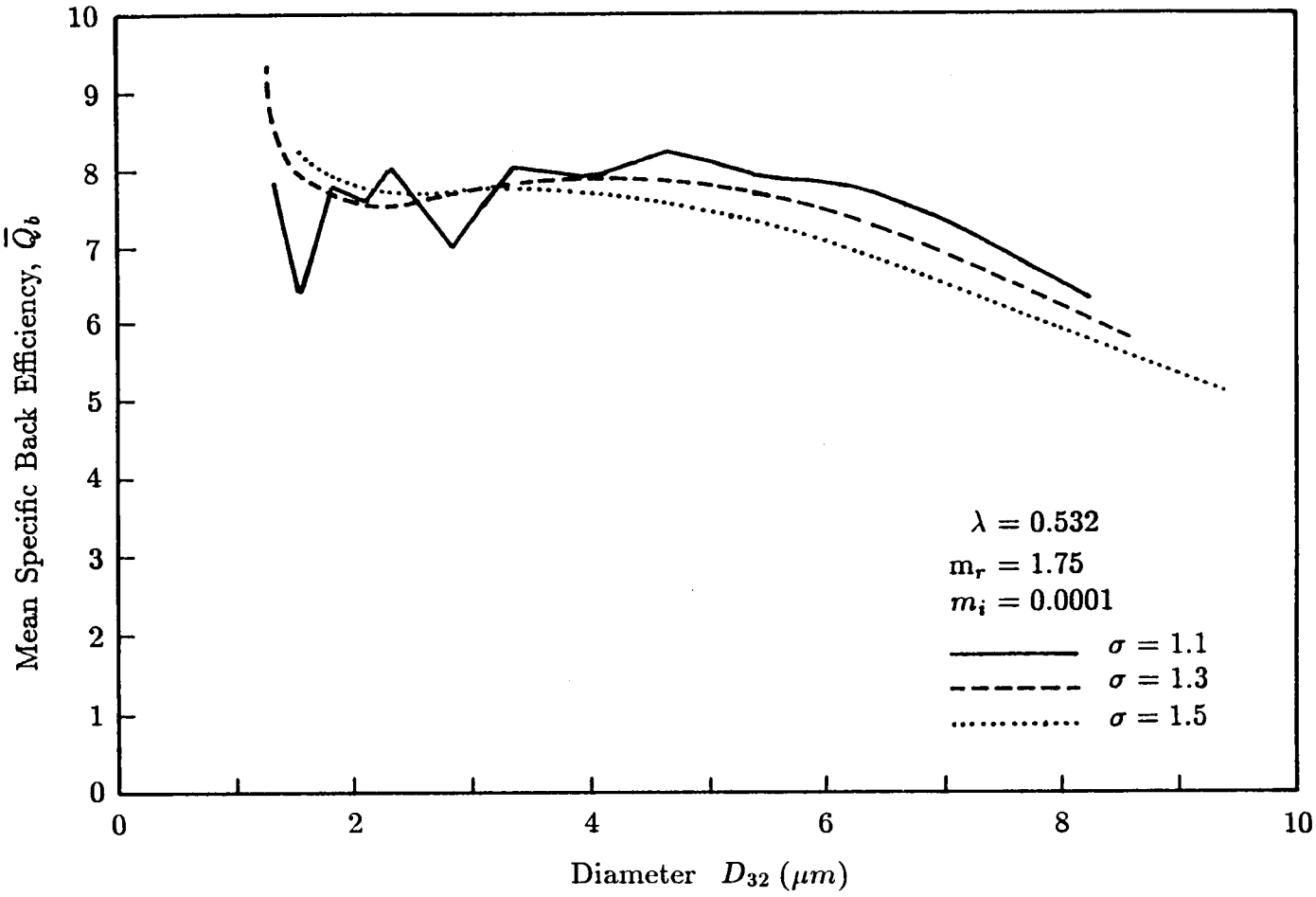


Figure 6.9. Mean specific backscatter efficiency as a function of mean particle diameter.

in $\overline{Q}_b$ is within $\pm 10\%$ over this size range. As an approximation, the ensemble backscatter efficiency is simply proportional to the mass flux through the laser beam. When used in conjunction with optical extinction measurements, backscatter measurements offer a secondary means of verifying the results of the extinction measurements described earlier.

This completes the discussion of procedures used to obtain the average size of a distribution and the spatial distribution of average particle sizes in a large particle ensemble. In the next chapter, the extinction and scattering techniques that have been discussed will be applied to a numerically simulated particle cloud in order to demonstrate the feasibility and validity of the approach developed here.

CHAPTER VII

DETERMINATION OF THE PARTICLE SIZE DISTRIBUTION

The general technical approach to the problem of obtaining complete size distributions from optical measurements is to use a combination of extinction and scattering measurements which can be solved approximately for the particle size distribution, $n(D)$ [33-34,81-82]. Tractable solutions exist when the size distribution function is well behaved, when the particle sample volume is relatively small, and when the particle cloud is optically thin. These conditions are typically not met in the case of a large axisymmetric particle cloud as discussed in previous chapters.

General solutions of the remote sensing problem have been adequately addressed in the literature[38,82-83]. However, for completeness, a brief review of the mathematical procedures required to obtain the particle size distribution function from a set of optical measurements will be presented. The approach outlined is based on that developed by Twomey[84] and later applied by Shaw[33].

Light traversing a small volume containing an optically thin distribution of particles, as shown in Figure 7.1, will experience scattering, resulting in attenuation of the incident beam. In Chapter IV, the extinction of this beam was expressed in terms of the optical depth as

$$\tau(\lambda) = \int C_e\ (D, \lambda)\ n(D)\ dD \tag{7.1}$$

Recovery of $n(D)$ is accomplished by obtaining extinction measurements at several wavelengths, and inverting the integral equation[85-89]. Care must be taken in the choice of wavelengths so that the added information will improve the accuracy of the results. Ben-David and Herman[80] have shown that measurement errors of up to 10% may yield acceptable solutions for $n(D)$.

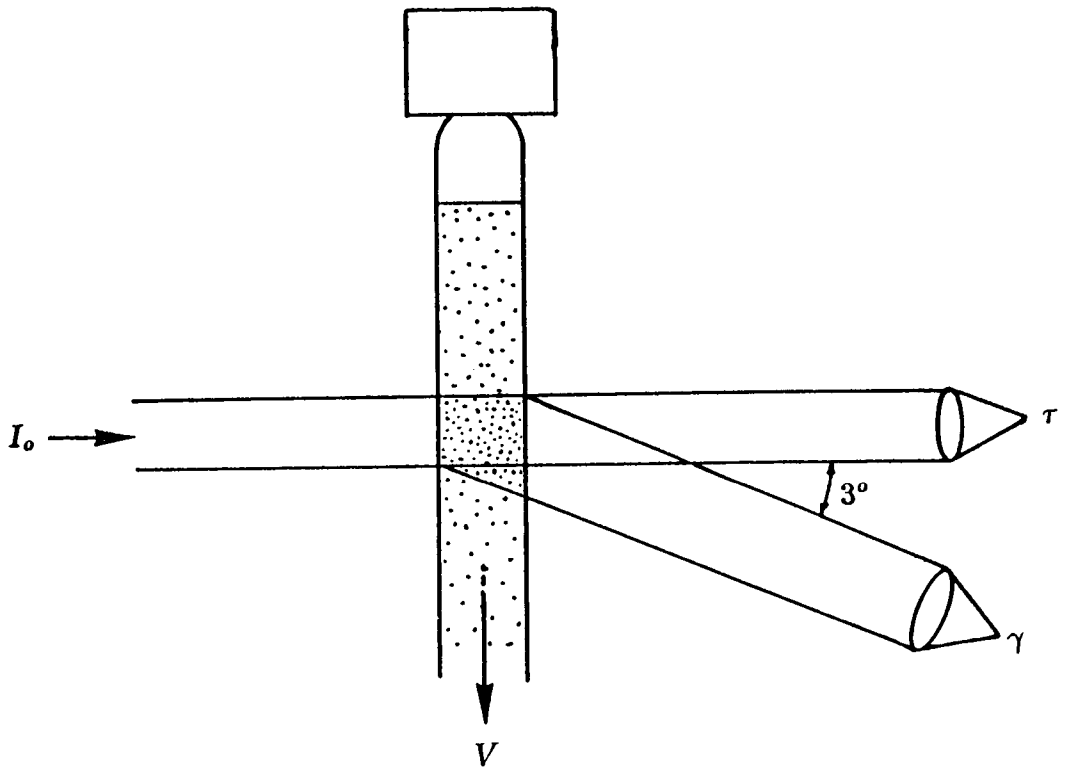


Figure 7.1. Measurement geomentry for combined scattering and extinction.

The backscattered light intensity from the particle cloud was given by the integral equation

$$\beta(\lambda) = \int C_b\ (D, \lambda)\ n(D)\ dD \tag{7.2}$$

where C_b is the backscatter cross section. As with the extinction measurements, in principle it is possible to invert the set of integral equations representing backscatter measurements at multiple wavelengths[80]. The mathematical inversion techniques are similar to those applied to the extinction problem, but the information content available from the backscatter is greater because of the oscillatory nature of the backscatter efficiency[38]. Ben-David[80] and Hutt[81] have employed a constrained nonlinear inversion technique using a second derivative smoothing matrix in conjunction with an iteration scheme to solve this problem. Backscatter inversion is generally more appropriate to distributions of small particles, since the backscatter cross section for large particles is only weakly dependent on the particle size.

Angular scattering measurements provide additional clues to the solution of $n(D)$ [90–95]. The light scattered at a specified wavelength and an angle θ is described by

$$\gamma(\lambda,\ \theta) = \int C_s\ (D, \lambda, \theta)\ n(D)\ dD \tag{7.3}$$

Inversion of the scattering problem is more difficult to interpret than extinction because of the sensitivity of the angular scattering measurements to refractive index uncertainties, effects of multiple scattering, finite detector field of view, etc. Measurements of angular scattering at several angles, multiple wavelengths, and both polarizations provide a potentially large set of equations to be inverted.

Another integral equation which contains $n(D)$ is available in many experimental configurations, yet apparently has not been addressed in the literature. The mass flow rate, which is a known or measurable quantity in many experiments, is a function of the particle size distribution function and is represented by the integral

equation

$$\dot{m} = \rho \, A \, v \, \frac{\pi}{6} \int D^3 \, n(D) \, dD \tag{7.4}$$

In the case of stationary particle ensembles, the equation for mass concentration could be used instead.

The amount of detail recoverable from the size distribution is increased by combining the different measurements described above. Shaw[33] and others[34,81] have described this process for combinations of extinction and backscattering, but little work has apparently been done to combine all of the available measurements in an effort to recover $n(D)$.

The equations describing remote measurements on a particle cloud, whether for extinction, scattering, or backscattering, represent a general class of problems known as Fredholm integral equations of the first kind. Extensively studied for remote sensing applications [83], these equations can be written in the general form

$$g(\lambda, \theta) = \int K(D, \lambda, \theta) \, n(D) \, dD \tag{7.5}$$

where $K(D, \lambda, \theta)$ is the kernel function provided by either the Mie theory or the known mass flow rate, and $g(\lambda, \theta)$ is the known or measurable quantity. In the case of extinction, $\theta = 0$ degrees, and one integral equation exists for each wavelength at which a measurement is made. Multiple angle scattering measurements will provide one equation for each angle and wavelength, and one for the special case of backscatter, an equation will exist for each wavelength with $\theta = 180$ degrees.

The kernel functions in the Fredholm equation relating the optical information to the particle size distribution are generally poorly conditioned and difficult to invert. Instabilities in the solution of $n(D)$ may be reduced by employing various smoothing constraints in the numerical solution procedure [33]. Numerical solutions to the Fredholm integral equation may be obtained by writing it as a first-order

linear system of equations having the form

$$g_i + \delta_i = w_{ij}\ K_{ij}\ n_j \tag{7.6}$$

where w_{ij} is the quadrature weighting function and δ_i is the error term resulting from experimental measurement uncertainty. Generally, the measured quantity is considered to be the sum of $g_i + \delta_i$, and g_i is the ideal, error-free measurement.

The expanded integral equation can be written in matrix form

$$M + E = S\ N \tag{7.7}$$

where M represents the measurement matrix with components g_i, E is the error matrix, S represents the kernel and associated weights, and N is the particle size distribution function. M, E, and N are column vectors having I components representing the total number of measurements plus the mass flow rate, if known. The measurement matrix M is defined by

$$M = \left| \begin{array}{c} \tau_i \\ \beta_j \\ \gamma_k \\ \vdots \\ \dot{m} \end{array} \right| \tag{7.8}$$

for i extinction measurements, j backscatter measurements, and k scattering measurements and knowledge of $\dot{m}$. The particle size distribution can be expressed as a matrix N, elements of which include the number density evaluated at discrete particle diameters

$$N = \left| \begin{array}{c} n(D_1) \\ n(D_2) \\ \vdots \\ n(D_K) \end{array} \right| \tag{7.9}$$

where K is the number of discrete size bins in the inverted particle size distribution function. The scattering matrix S is a $J \times K$ matrix, elements of which are the

scattering, backscatter, and extinction cross sections calculated from the Mie theory, along with elements associated with the mass loading

$$S = \begin{vmatrix} C_{e1}(D_1) & C_{e1}(D_2) & \dots & C_{e1}(D_K) \\ C_{b1}(D_1) & C_{b1}(D_2) & \dots & C_{b1}(D_K) \\ C_{s1}(D_1) & C_{s1}(D_2) & \dots & C_{s1}(D_K) \\ \vdots & \vdots & & \\ D_1^3 & D_2^3 & \dots & D_K^3 \end{vmatrix} \tag{7.10}$$

In the ideal case where error free measurements are made, the elements of $E = 0$, and the matrix equation can be solved by inverting the kernel matrix

$$N = S^{-1}\ M \tag{7.11}$$

Solutions exist only if $Det(S)$ is not equal to zero. If the kernel matrix is not a square matrix, a least squares solution is afforded by [33]

$$N = \left[S^t S\right]^{-1}\ S^t\ M \tag{7.12}$$

if $Det(S^t S)$ is non-zero. However, in practice, direct inversion using the least squares approach is generally unsuccessful because the components of S are not entirely linearly independent. Twomey [84] has shown that difficulties in the direct inversion approach are caused by the presence of small eigenvalues in $S^t S$.

In order to obtain the complete spatial and particle size distribution $n(D, r)$ for spatially extended particle clouds, the onion-peel inversion approach would, in principle, be employed using the solutions to the matrix inversion problem. When the size distribution has been determined in region 1, this procedure will then be continued in the traditional onion-peel inversion approach. A measurement through region 2 will contain information about both regions 1 and 2, with the result that

$$M_2 = 2cM_1 + S_2\ N_2 \tag{7.13}$$

or

$$N_2 = S_2^{-1} \left[M_2 - 2cM_1 \right] \tag{7.14}$$

where M_i, N_i, and S_i represent the measurement, number density, and scattering kernel matrices, respectively, in region i.

The number density distribution is now known in both outer regions of the cylindrical cloud. Number densities in the interior regions of the cloud are determined by continuing this process for as many annular regions as there are elements in the measurement matrix. Caution must be exercised in implementing this approach, however, since in practice assumptions of small measurement volumes and low optical density may no longer apply in cases of spatially extended particle ensembles.

CHAPTER VIII

NUMERICAL SIMULATION OF MEAN PARTICLE SIZE MEASUREMENT TECHNIQUES

Several measurement techniques have been described for the determination of the mean size of a particle distribution. Before these techniques can be used to obtain particle sizes on distributions of unknown size composition, each must be tested on hypothetical distributions in an effort to recover the known average sizes. Ideally, tests would be made on many types of size distributions, with a broad range of average sizes; many different wavelengths would be employed in order to examine the wavelengths best suited for a given technique and size range; particles with a wide range of real and imaginary refractive indices would be examined. Unfortunately, an extensive test matrix of this proportion would be a Herculean task, and would result in many volumes of data.

In this chapter, a simple numerical scattering problem will be presented in order to demonstrate the basic average size measurement techniques on a small optically thin volume element. Extinction, backscatter, and diffraction measurement techniques were employed to obtain average particle size information from a numerically generated particle ensemble. Several numerical problems were investigated in the course of this work; however, the simulation described here has been designed to illustrate the salient features of each of the optical techniques developed for measuring mean particle size. Several important "rules of thumb" arising from observations on the results of these simulated experiments should prove beneficial in designing similar physical experiments.

The numerically simulated experiment described here represents a two phase particle flow, consisting of solid particles entrained in a non-absorbing gas, ema-

nating from a free jet particle generator. The particles are defined to have uniform spatial distribution, with a known velocity, mass flow rate, and geometry. The spherical particles are assumed to be composed of aluminum oxide, Al_2O_3, and have known refractive index of $m_r = 1.75$. The particle size distribution is represented by a log-normal distribution with a standard deviation of $\sigma = 1.3$. Three cases, or numerically simulated experimental conditions, are considered with the mode of the size distribution function having a different value for each case. The simulated measurements are made at the wavelengths, 0.337 μm, 1.06 μm, and 3.39 μm, corresponding to three commonly available lasers: nitrogen, Nd:YAG, and Helium-Neon, respectively. Parameters associated with the simulation are summarized in Table 8.1. A schematic of the experimental setup is shown in Figure 8.1.

TABLE 8.1

EXPERIMENTAL SIMULATION PARAMETERS

PARAMETER	RUN #1	RUN #2	RUN #3
D_m	1 μm	3 μm	5 μm
σ	1.3 μm	1.3 μm	1.3 μm
N_o	4.67 e-6 μm^{-3}	1.73 e-7 μm^{-3}	3.74 e-8 μm^{-3}
m	.01875 kg/s	.01875 kg/s	.01875 kg/s
p	3 g/cm^3	3 g/cm^3	3 g/cm^3
L	0.025 m	0.025 m	0.025 m
W	0.025 m	0.025 m	0.025 m
v	3000 m/s	3000 m/s	3000 m/s

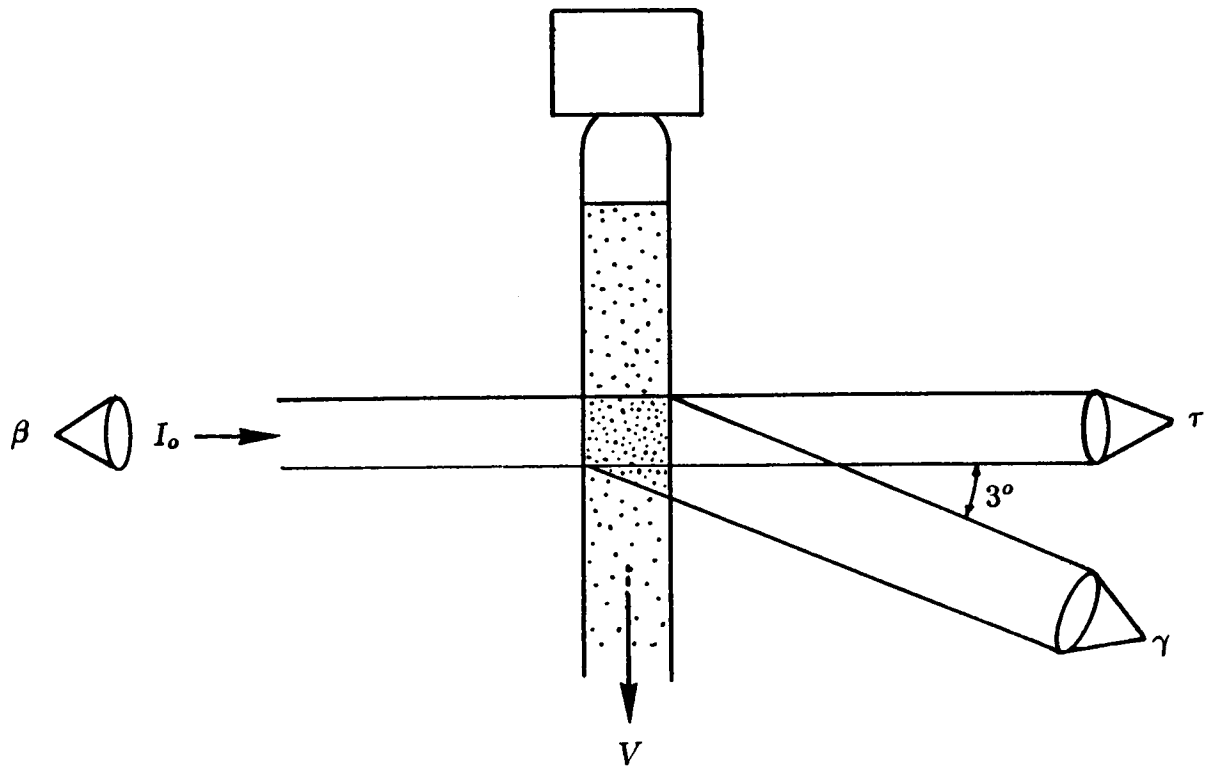


Figure 8.1. Measurement geometry for simulated extinction/backscatter/diffraction experiment.

In the simulated experiment, three laser beams of diameter 2.5 cm are passed through the flowing particle ensemble which has a 2.5 cm square cross section. The log-normal particle size distribution function used for this simulation has the form

$$n(D) = \frac{N_o}{\sqrt{2\,\pi}\; ln\,(\sigma)\; D}\; exp\;\left(-.5\left[ln(D/D_m)\;/\;ln\,(\sigma)\right]^2\right) \tag{8.1}$$

where the mode and the standard deviation have the values defined in Table 8.1. The number density was determined for each numerically simulated condition by the mass flow and the mode diameter of the distribution.

Theoretical values for the extinction of the laser beams were calculated directly from Equation (4.5)

$$\tau = \frac{L\,\pi}{4} \int Q_e(D)\; D^2\; n(D)\; dD \tag{8.2}$$

for each of the three conditions, with $D_m = 1,\ 3$, and 5 μm. These are defined to be the exact values of optical depth for the prescribed particle cloud and wavelength used. The values of extinction obtained from Equation (8.2) had $\pm$ 5% error superimposed and were used as the simulated measured parameter. In other words, in order to represent an actual extinction measurement, the true value of optical depth, τ, for each wavelength was replaced with a simulated experimental optical depth that has a value $\tau \pm 0.05\tau$. Plots of optical depth, proportional to $< Qe >\ /\ D_{32}$, as a function of D_{32}, were then obtained from the expression relating the mean diameter to the optical depth

$$\tau = \frac{6\;\dot{m} < Q_e >}{\pi\;\rho\;L\;v\;D_{32}} = .1592\;\frac{< Q_e >}{D_{32}} \tag{8.3}$$

where the units of D_{32} must be in microns. Figure 8.2 shows the plots of optical depth versus mean particle diameter for each wavelength. On each plot is superimposed the specified value of the optical depth for each wavelength, with a 5%

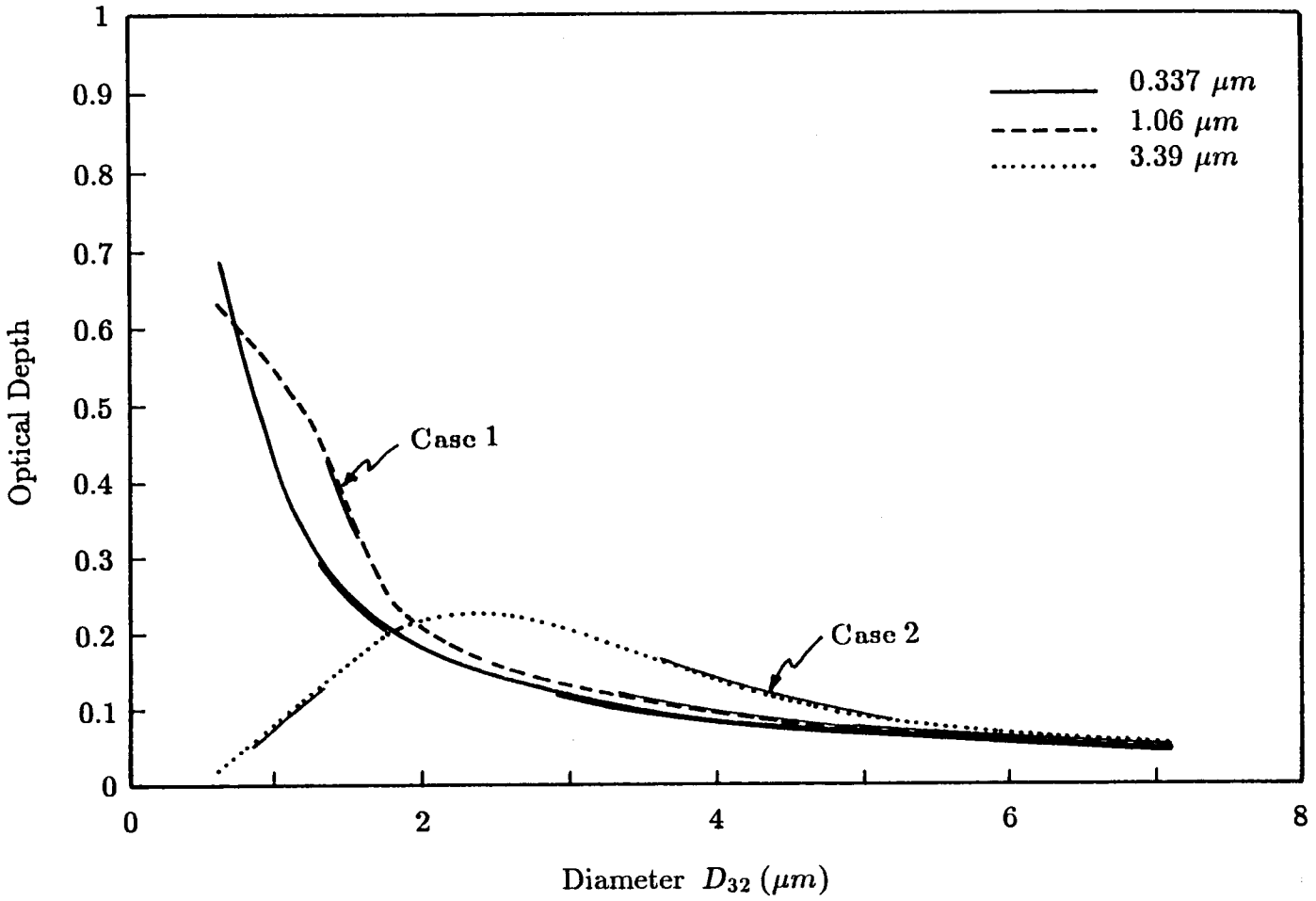


Figure 8.2. Theoretical optical depth as a function of D_{32}.

uncertainty added to simulate experimental error. The recovered values with uncertainties are listed in Table 8.2. The root-mean-square average diameters were calculated from the expression

$$D_{rms} = \left[\sum D_i^2 \; / \; N \right]^{1/2} \tag{8.4}$$

where N is the number of measurements yielding an average particle diameter.

Several conclusions can be drawn from the results of the simulated extinction measurements. The best accuracy is generally obtained when the illumination wavelength is approximately 2-3 times the mean particle diameter of the distribution.

TABLE 8.2

RECOVERED D_{32} USING SIMULATED OPTICAL EXTINCTION

CASE #	D_m (μm)	σ (μm)	ACTUAL D_{32} (μm)	λ (μm)	RECOVERED D_{32} (μm)
1	1	1.3	1.19	0.337	1.50 ± 0.25
				1.06	1.45 ± 0.15
				3.39	1.05 ± 0.35
					1.35 ± 0.26 (Average)
2	3	1.3	3.56	0.337	4.85 ± 2.15
				1.06	5.00 ± 1.80
				3.39	4.35 ± 0.85
					4.74 ± 1.69 (Average)
3	5	1.3	5.94	0.337	7.10 ± 2.90
				1.06	7.10 ± 2.90
				3.39	7.10 ± 2.90
					7.10 ± 2.90 (Average)

The recovered value of D_{32} using the true value of optical depth (no error superimposed) for mean particle diameters on the order of or greater than the illuminating wavelength is generally 20-30 percent too high. This bias error is probably due to the fact that the extinction efficiency is averaged with a D^2 weighting function as shown in Equation (4.6). For mean particle diameters much greater than the wavelengths, extinction at each wavelength will approach similar values, because of the fact that the extinction efficiency asymptotically approaches a value of two for large size parameters. Extinction measurements can be used to estimate the mass flow rate or mass concentration in this case. Sensitivity is reduced at all wavelengths when the measured optical depth is very small (approximately < 0.05). A final observation is that when the mean recovered size is greater than the wavelength, the bias error may be partially compensated for by choosing the smallest mean particle size within the error measurement.

Simulated forward scattering measurements were also made by calculating true values of the angular intensity profile from

$$I(\theta) = \frac{\int \left[2J_1\ (\alpha\ sin\ \theta)\ /\ (\alpha\ sin\ \theta)\right]^2\ D^4\ n(D)\ dD}{\int D^4\ n(D)\ dD} \tag{8.5}$$

for each of the distributions considered in cases 1-3. Three wavelengths were used in this analysis, including 0.337, 1.06, and 3.39 μm, and the detectors were located at a forward scattering angle of 3 degrees. Each simulated wavelength measurement was assumed to be normalized to a second detector at the same wavelength located within 0.5 degrees. The theoretical values calculated from this expression were combined in a manner similar to the extinction simulation, with a $\pm 5\%$ error superimposed in order to simulate experimental measurement uncertainty in the angular scattered intensity profile.

Figure 8.3 shows the results of the normalized angular scattered intensities for each wavelength, at an angle of three degrees, plotted as a function of D_{42}. This

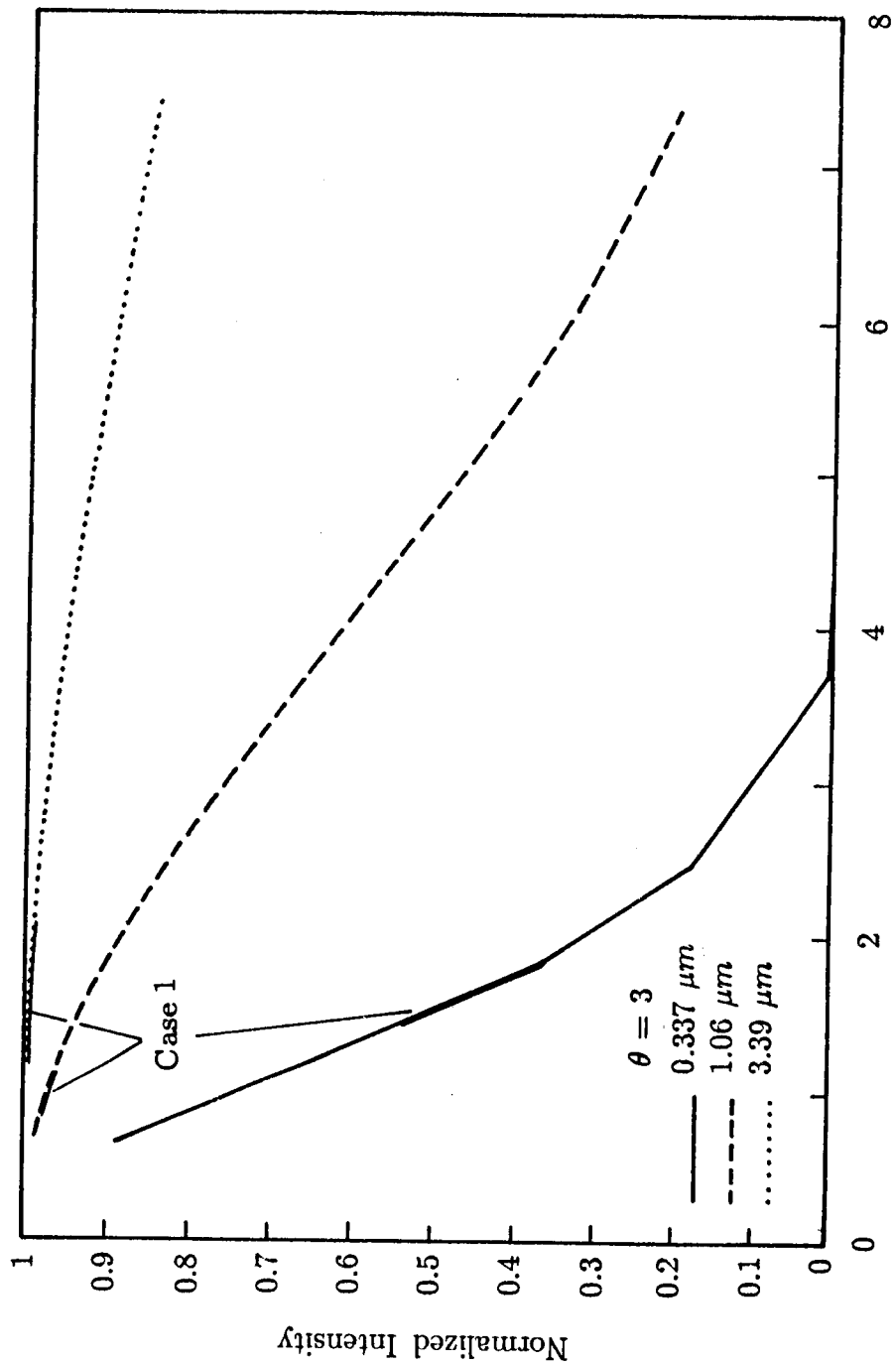


Figure 8.3. Theoretical normalized diffraction profiles.

plot shows the results of the simulated experimental data with uncertainty. The recovered mean particle diameters, D_{42}, for each wavelength and distribution are listed in Table 8.3.

TABLE 8.3

RECOVERED D_{42} FROM SIMULATED DIFFRACTION MEASUREMENTS

CASE #	D_m (μm)	σ (μm)	ACTUAL D_{42} (μm)	λ (μm)	RECOVERED D_{42} (μm)
1	1	1.3	1.23	0.337	1.25 ± 0.10
				1.06	1.15 ± 0.60
				3.39	2.05 ± 2.00
					1.54 ± 1.21 (Average)
2	3	1.3	3.69	0.337	—
				1.06	3.75 ± 0.35
				3.39	3.15 ± 2.65
					3.46 ± 1.89 (Average)
3	5	1.3	6.15	0.337	—
				1.06	6.15 ± 0.25
				3.39	6.20 ± 1.20
					6.18 ± 0.87 (Average)

Several noteworthy features are evident from these results for the scattering simulation. When the mean particle size is much greater than the wavelength of light the angular spread of the forward scattered lobe is too narrow to provide any useful information so the technique is not applicable for this range of particle diameter. This was the case for the 0.337 μm measurements for the 3 μm and 5 μm mode diameter distributions. Excellent size discrimination, however, is obtained when the mean diameter D_{42} is in the range of approximately 2-10 times the illumination wavelength. This range corresponds to the part of the diffraction profile plots that have the steepest slopes and, therefore, the highest sensitivity. Multiple wavelengths can be used to improve the confidence in the measurement and to cover a wider range in diameters if the wavelengths are carefully chosen for a particular experiment. However, as seen from the simulation results, attempting to apply a wavelength to a distribution with mean diameter less than approximately 2 wavelengths can actually increase the uncertainty in the measurement due to the fact that the slope of the angular scattering profile approaches 0 for this condition.

Simulated backscatter measurements were also made by calculating the true ensemble backscatter efficiency for each size distribution using the expression

$$\beta = \frac{\pi\ L}{16\ R_h} \int Q_b(D)\ D^2\ n(D)\ dD \tag{8.6}$$

A five percent measurement uncertainty was added to the exact backscatter values to represent simulated experimental error, as was done for the extinction and scattering measurements. Plots of the ensemble mean specific backscatter efficiency versus the mean particle diameter D_{32} were then made using the equation

$$\beta = \frac{3\ \dot{m} < Q_b >}{8\ R_h\ \rho\ W\ v\ D_{32}} = .03472\ \overline{Q}_b \tag{8.7}$$

The simulated measurements with added uncertainty are shown in Figure 8.4. The results of the recovery of D_{32} are shown in Table 8.4. Note that the recovered values of D_{32} using backscattering data were generally very good for the particle sizes and wavelengths chosen.

TABLE 8.4

RECOVERY OF D_{32} FROM SIMULATED BACKSCATTER MEASUREMENTS

CASE #	D_m (μm)	σ (μm)	ACTUAL D_{32} (μm)	λ (μm)	RECOVERED D_{32} (μm)
1	1	1.3	1.19	0.337	1.45 ± 0.35
				1.06	1.15 ± 0.05
				3.39	$\underline{1.40 \pm 0.40}$
					1.34 ± 0.31 (Average)
2	3	1.3	3.56	0.337	3.55 ± 0.35
				1.06	> 3
				3.39	$\underline{3.60 \pm 0.30}$
					3.58 ± 0.33 (Average)
3	5	1.3	5.94	0.337	6.00 ± 0.30
				1.06	> 3
				3.39	$\underline{5.90 \pm 1.30}$
					5.95 ± 0.94 (Average)

From the simulated data, the best size recovery occurs when the mean diameter D_{32} is on the order of the wavelength. For mean diameters in the range of approximately 2-10 times the wavelength, the ensemble backscatter efficiency is relatively independent of particle size. This fact may provide an excellent method for obtaining the mass flow rate, since in this case the backscatter is proportional to m.

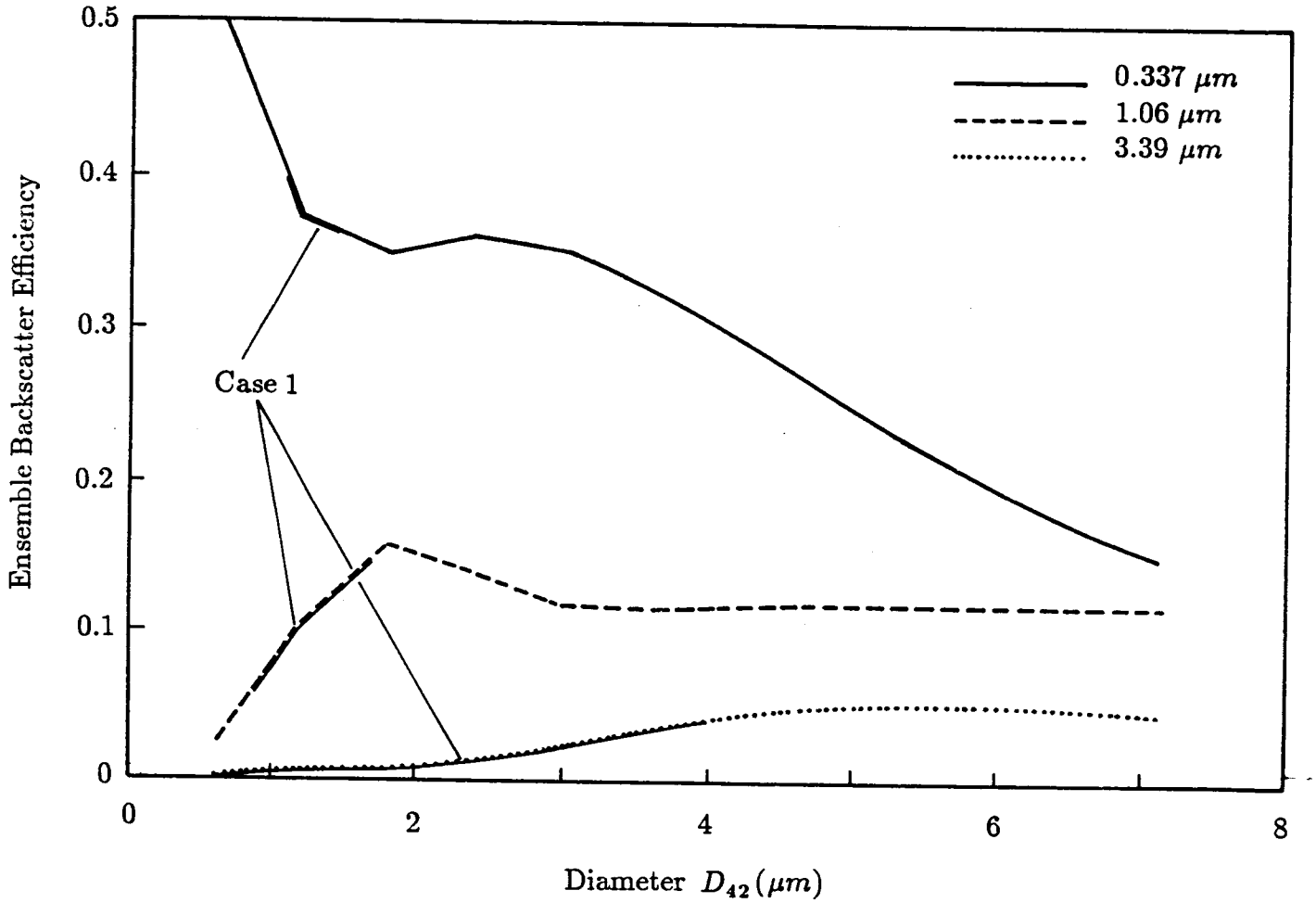


Figure 8.4. Theoretical ensemble backscatter efficiency.

When the mean diameter is greater than approximately 10 times the illuminating wavelength, the backscatter again becomes size dependent. This is most easily seen in Figure 8.4 from the backscatter plot for 0.337 μm wavelength.

Backscatter calculations are highly sensitive to refractive index uncertainty. Example calculations indicate that a $\pm 3\%$ variation in the real refractive index of the particle may result in as much as a $\pm 50\%$ variation in the backscatter efficiency because of the highly oscillatory nature of this function. However, broader distributions of particles will tend to be less sensitive to refractive index uncertainty because the oscillating values of the backscatter efficiency will tend to average out.

The results of the particle size recovery from the simulated measurements of the combined extinction, scatter, and backscatter are summarized in Table 8.5. The recovered values of D_{32} were obtained by taking the avreage values of the recovered extinction and backscattered data at all wavelengths, while the D_{42} values were simply the values recovered using the forward scattering approach.

TABLE 8.5

RESULTS OF DATA RECOVERY FROM COMBINED MEASUREMENTS

CASE #	$D_m(\mu m)$	ACTUAL	RECOVERED	PERCENT ERROR
1	1	$D_{32} = 1.19(\mu m)$	1.35 ± 0.29 (μm)	13.4 %
2	3	3.56	4.20 ± 1.22	18.0
3	5	5.94	6.55 ± 2.16	10.3
1	1	$D_{42} = 1.23(\mu m)$	1.54 ± 1.21	25.2 %
2	3	3.69	3.46 ± 1.89	06.3
3	5	6.15	6.18 ± 0.87	00.5

In Chapter IV a method for determining the mode and width of a log-normal distribution given any two mean diameters, D_{PQ} and D_{ST}, was presented. The mode diameter was given by the equation

$$D_m = D_{PQ}\ exp\ [-\{ln\ (D_{PQ}\ /\ D_{ST})\}\ \ \{(P+Q)\ /\ (P+Q-S-T)\}] \quad (8.8)$$

and the width σ was given by

$$\sigma = exp\ [(2\ ln\ (D_{PQ}\ /\ D_{ST})\ /\ (P+Q-S-T)] \quad (8.9)$$

Estimates of the size distribution parameters were obtained for case #1 of the simulation. Using the recovered average diameters listed in Table 8.5, the mode diameter for case #1 was estimated to be $D_m = 0.70\ \mu m$, and the width of the distribution $\sigma = 1.3$. In cases #2 and #3, the recovered values of D_{32} were larger than the recovered values of D_{42}. This is, of course, not possible for a log-normal distribution, so in this case, the distribution parameters can not be recovered using Equations (8.8) and (8.9) since the errors incurred were excessive for this approach. However, the results for Case # 1 indicate that D_m and σ may be obtained in certain measurements if the wavelenghts are appropriately chosen.

CHAPTER IX

EXPERIMENTAL RESULTS OF A MULTI-PATH EXTINCTION MEASUREMENT

Optical particle size measurements based on extinction, backscatter, and diffraction have been described for application to homogeneous particle fields, and an onion-peel inversion of extinction measurements has been presented to obtain the spatial distribution of average particle size in an axisymmetric cloud. Illustration of these techniques applied to homogeneous particle fields was presented in the last chapter. For the axisymmetric particle fields discussed in Chapter V, the flowfield mass distribution was tacitly considered to be a known experimental parameter. In many situations, however, the radial distribution of mass in a cloud of particles may be unknown. Extinction measurements can, in principle, provide information on both the mass flux distribution and the radial distribution of average particle sizes in some cases. In this chapter, the results of an experiment which illustrates this process are discussed.

Multiple path extinction measurements were made on an experimental two-phase free-jet particle source which provided an axisymmetric high velocity particle flowfield. The total mass flow rate was accurately known, but the radial mass flux distribution was unknown. The particles were assumed to be spherical and of known refractive index which was later verified by subsequent examination of particulate material collected during the experiment. Particle diameters were suspected to be within the range of $1 - 10\ \mu m$, based upon computer predictions of the flowfield parameters.

Extinction measurements were obtained with a Nd:YAG laser through three regions of the particle flow, as illustrated in Figure 9.1. One measurement was made

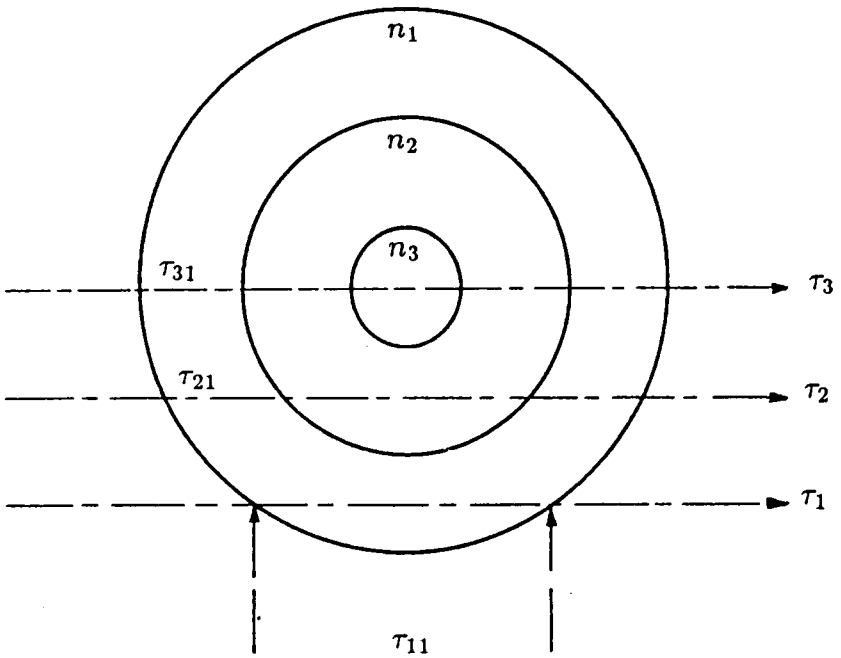


Figure 9.1. Multiple path extinction measurement geometry.

through the diameter of the plume, while the other measurements were obtained at radial locations of $0.2R$ and $0.875R$, where R is the radius of the flowfield. In addition, an extinction measurement was made at a second wavelength at the location $0.875R$ with an infrared helium-neon laser. The choice of the number of paths and wavelengths of the measurement made was dictated by the availability of equipment.

The Q-switched Nd:YAG laser had an output power of approximately 2000 Watts per pulse, with a 300 $nsec$ pulsewidth, and was operated at 1000 pps. The laser output had a wavelength of 1.06 μm, and was split into three separate illumination beams, as illustrated in Figure 9.2. One inch diameter F/4 receiving lenses coupled to 400 μm core diameter optical fibers were located 72 inches from the particle cloud and were used to collect the light transmitted by each beam. Light was transmitted via the optical fibers through 10 nm optical bandpass filters to high speed silicon photodiode detectors. Synchronous detection using boxcar integrating amplifiers with 10 KHz high pass electronic filtering was used to eliminate unwanted background radiation.

Operating at a wavelength of 3.39 μm, the infrared Helium-Neon laser provided approximately 7 mW of optical power in the continuous wave (CW) mode. A PbSe detector with active area of 9 mm^2 was used with a 110 nm optical bandpass filter centered at 3.4 μm. An F/3 CaF receiving lens with a 1 inch aperture was used to collect the transmitted radiation. The light source was chopped at a frequency of 1000 Hz and a lock-in amplifier was used to filter out background radiation. A schematic diagram of the Helium-Neon laser system is shown in Figure 9.3.

The resulting extinction measurements are summarized in Table 9.1 for each of the wavelengths and light paths used in the experiment. The attenuation of the 1.06 μm beam traversing the center of the cloud was relatively high with an optical depth

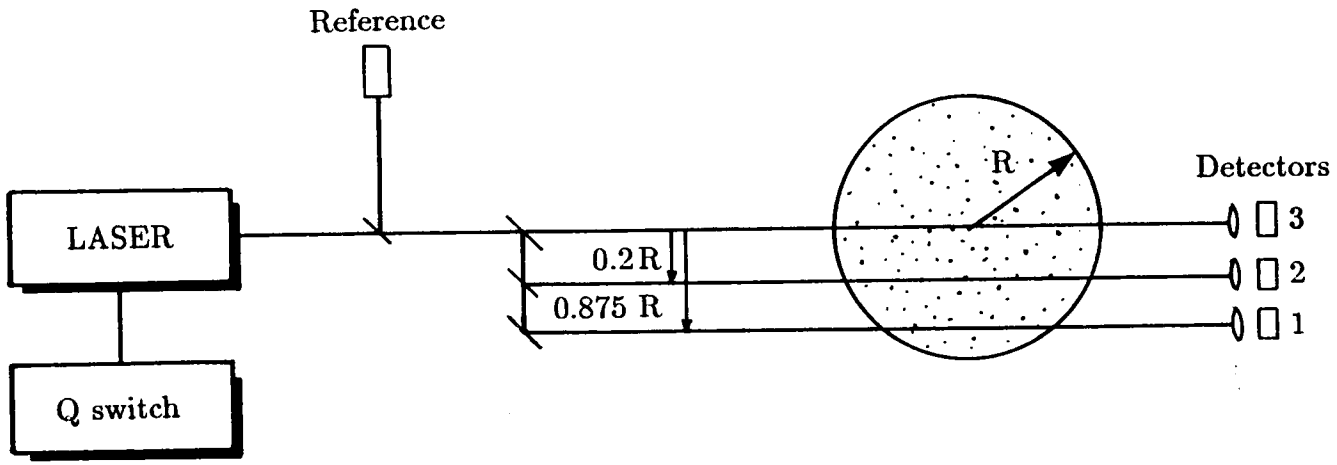


Figure 9.2. Nd:YAG laser system schematic diagram.

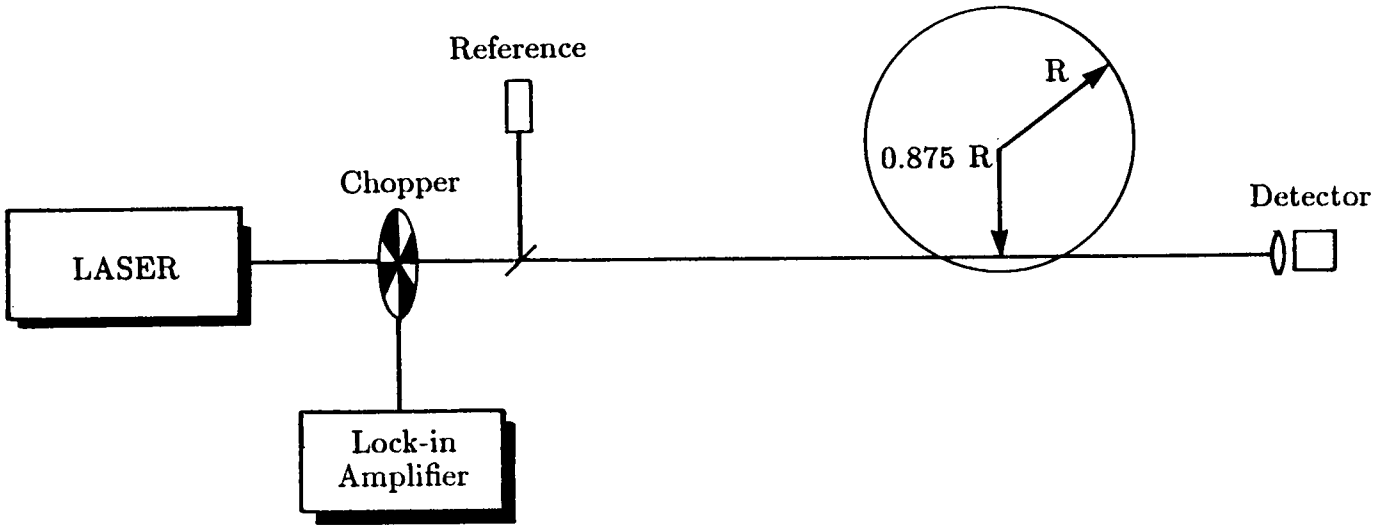


Figure 9.3. HeNe laser system schematic diagram.

$\tau_3(1.06) = 4.61$, while the edge of the cloud produced an optical depth of $\tau_1(1.06) = 0.48$. At the outermost beam path, the plume was more transparent at the 3.39 μm wavelength, with $\tau_1(3.39) = 0.34$. The measurement uncertainty for each of the laser systems was within $\pm 5\%$ and was due primarily to noise in the light source and detectors. Synchronous detection for each laser system guaranteed that background illuminations would not contribute to the measurement uncertainty. The cloud radius was known to within approximately $\pm 5\%$. According to Equation (5.17), the worst case uncertainty in the determination of κ, was approximately 7.07%. Additional calculations indicate that the attenuation coefficient uncertainties in regions 2 and 3 are, respectively, $U_2 = 5.9\%$ and $U_3 = 13.3\%$.

TABLE 9.1

RESULTS OF OPTICAL DEPTH EXPERIMENTAL MEASUREMENTS

RADIAL POSITION	$\lambda(\mu m)$	τ	κ (NORMALIZED)
0	1.06	4.61	5.31
0.2R	1.06	2.96	2.63
0.875R	1.06	0.48	0.46
0.875R	3.39	0.34	0.38

Although the radial mass flow density function was unknown, observations indicated a higher mass flow rate near the symmetry axis of the particle cloud due to the large attenuation in this region. From particle momentum considerations, larger particles are expected to have trajectories near the flow axis. In order to verify this and estimate the functional form of $\sigma(r)$, an Abel inversion of a fourth order curve fit of the Nd:YAG laser transmittance data[97] was used to obtain the radial profile of the attenuation coefficient $\kappa(r)$, shown in Figure 9.4. The decrease in $\kappa(r)$ exhibited near the cloud axis indicates that the particle field is locally more

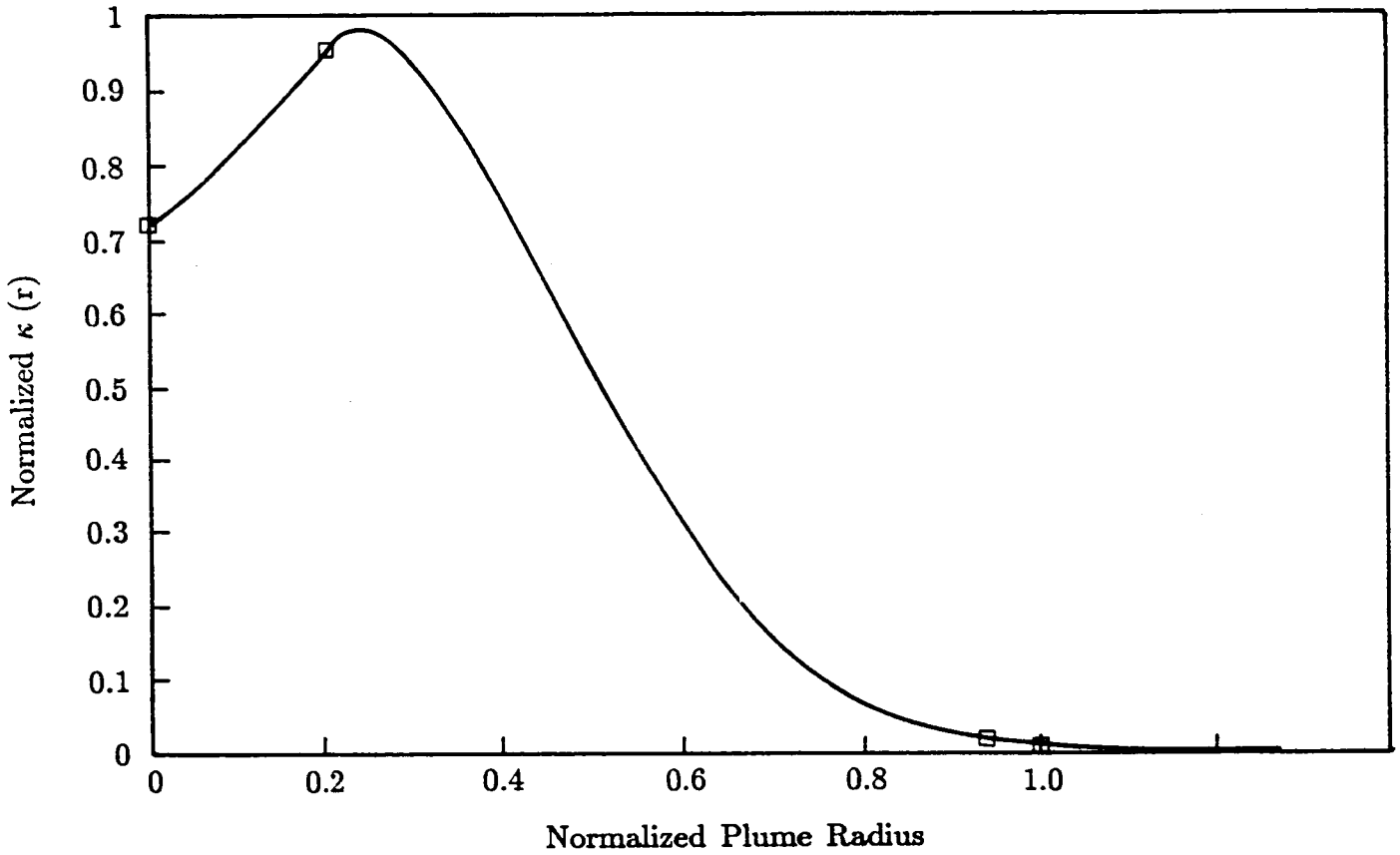


Figure 9.4. Inverted experimental attenuation coefficient.

transparent in this region, and has an annular region of higher optical density. This is not necessarily indicative of a lower mass flux density near the core, however, as will be demonstrated shortly.

The radial distribution of mass flux, $\sigma(r)$, was obtained by first directly inverting the optical extinction measurements to estimate $\kappa(r)$, and then trying different trial functions for the mass distribution assuming that $\sigma(r)$ is functionally similar to the annular function described by $\kappa(r)$. Approximations to the functional form of $\kappa(r)$ obtained with the inversion were normalized to the known total mass flow rate. Several of these normalized trial functions for $\sigma(r)$ are shown in Figure 9.5, including cosine, exponential, Gaussian, and uniform radial profiles. In addition, one profile was assumed to have a functional form similar to the annular $\kappa(r)$ function predicted by the inversion and shown in Figure 9.4. Each of these trial functions were used with the onion-peel inversion procedure of Chapter V to predict the average particle diameters near the axis of the particle cloud, and at the two radial locations $0.2R$ and $0.875R$. The results of the particle size calculations are shown in Figure 9.6, for each of the trial functions indicated. Note that, depending on the shape of the trial function, the predicted particle sizes vary considerably from the axis to the envelope of the particle cloud. For the cosine, $\kappa(r)$ annular, and uniform distributions, the predicted mean diameters, D_{32}, range from $1-2\ \mu m$ near the cloud centerline, and $4-8\ \mu m$ near the envelope, while the exponential and Gaussian $\sigma(r)$ profiles predict $3.5-4.5\ \mu m$ on axis and $1-2.5\ \mu m$ near the edge. The Gaussian $\sigma(r)$ profiles produce results which concur with the prediction that the more massive particles will concentrate near the symmetry axis. Calculated particle diameters are shown in Table 9.1.

It is important to note that without further information about the actual $\sigma(r)$ profile, more precise knowledge of the distribution of mean particle diameters is

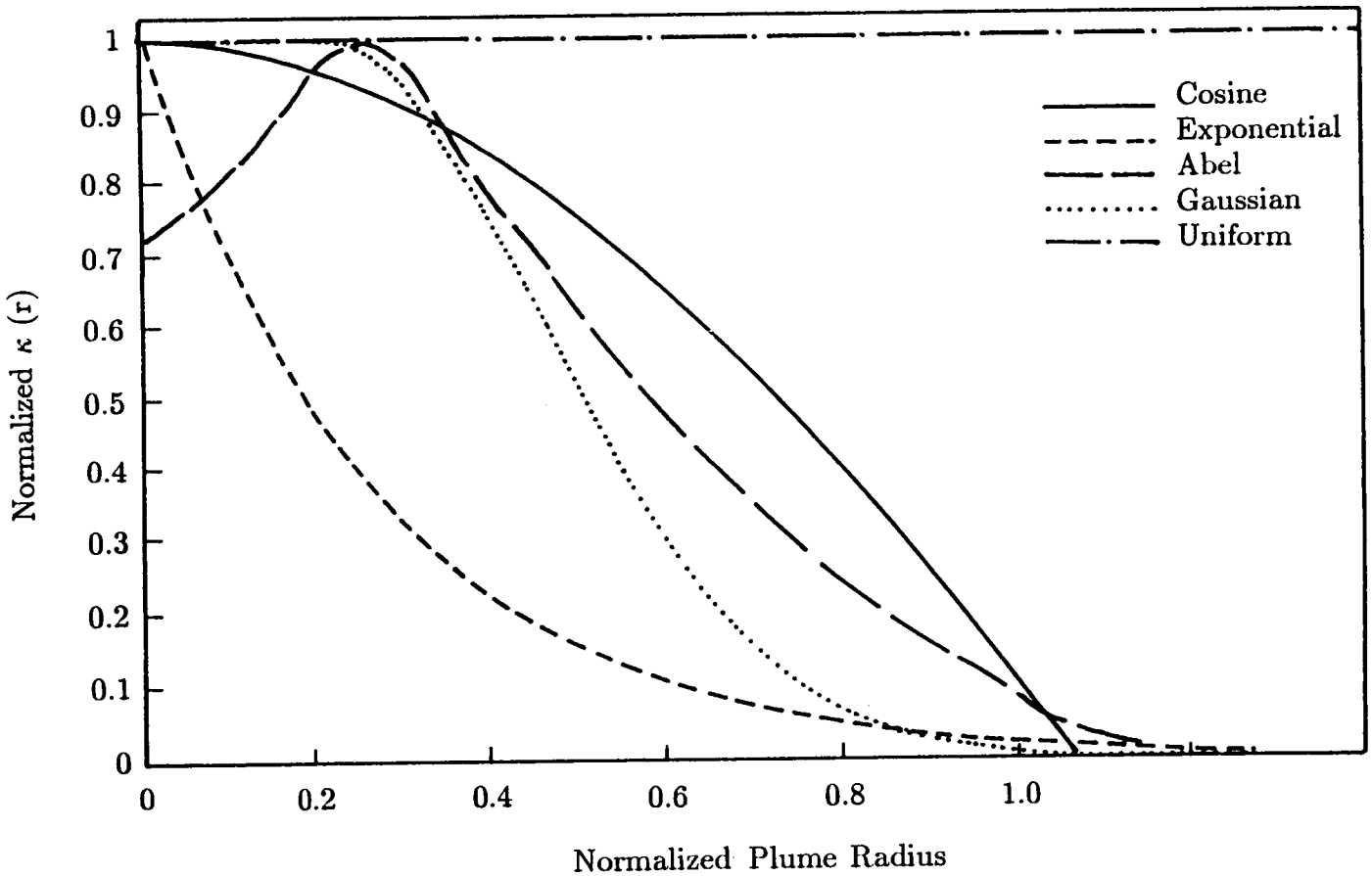


Figure 9.5. Trial functions for the experimental radial attenuation coefficient.

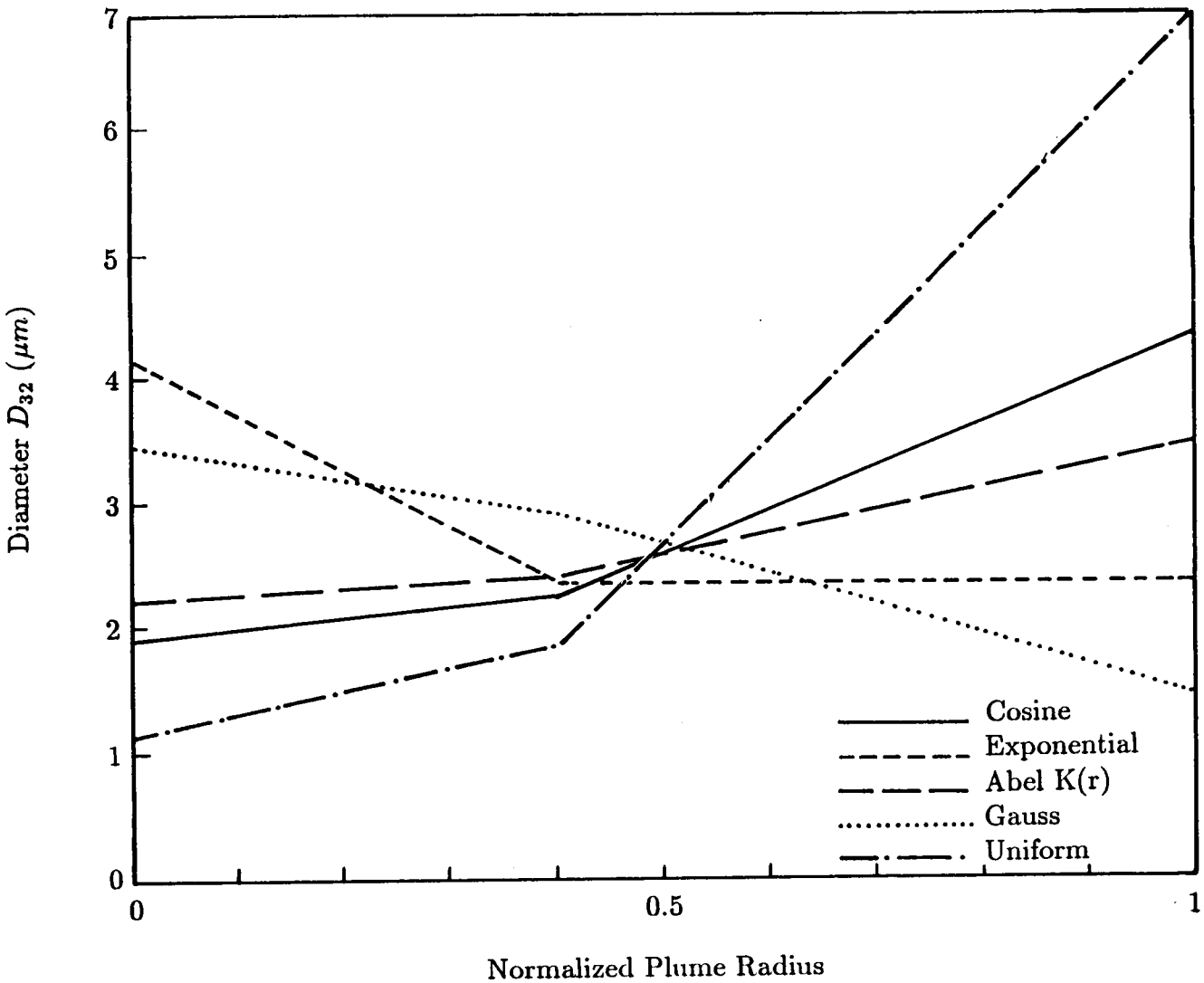


Figure 9.6. Calculated distribution of mean particle size based on trial functions.

impossible using single wavelength extinction measurements. In this experiment, however, transmittance data at a second wavelength was obtained through the outermost annular region of the particle cloud. The ratio of the optical depths measured at the same location with two wavelengths provides a determination of average particle size as discussed in Chapter IV.

The particulate material was known to have a real refractive index in the range of $1.6 - 1.8$ for both wavelengths. Mie calculations were made of the mean extinction efficiency using the extreme values of the refractive indices for each wavelength. The resulting optical depth ratios are presented in Figure 9.7. The experimentally obtained ratio of optical depths, τ_1/τ_2, was approximately $0.72 \pm .05$, which according to Figure 9.7, indicates a recovered mean particle size of $D_{32} = 1.65 \pm .2\ \mu m$ in the outermost annular region. This value of D_{32} corresponds to an uncertainty of approximately 12% in this region.

The prediction of an average particle diameter of approximately 1.65 in the outer region indicates that, semi-empirically, the $\sigma(r)$ profile must be very close to being Gaussian, according to the analysis of the trial functions performed. With the assumption that the $\sigma(r)$ profile is indeed Gaussian, the optical depth inversion produces the average particle size distribution listed in Table 9.2 under the Gaussian distribution.

In order to compare particle sizes obtained with the onion-peel inversion, Figure 9.8 shows the mean particle diameter obtained with a single path, single wavelength extinction measurement through the cloud diameter. In the figure, the measured optical depth is compared to the theoretical predictions of attenuation including upper and lower bounds on error sources. The mean particle size predicted based on the single path measurement is approximately $D_{32} = 2.40 \pm 0.7 \mu m$ which agrees well with the spatial distribution of sizes obtained with the inversion technique.

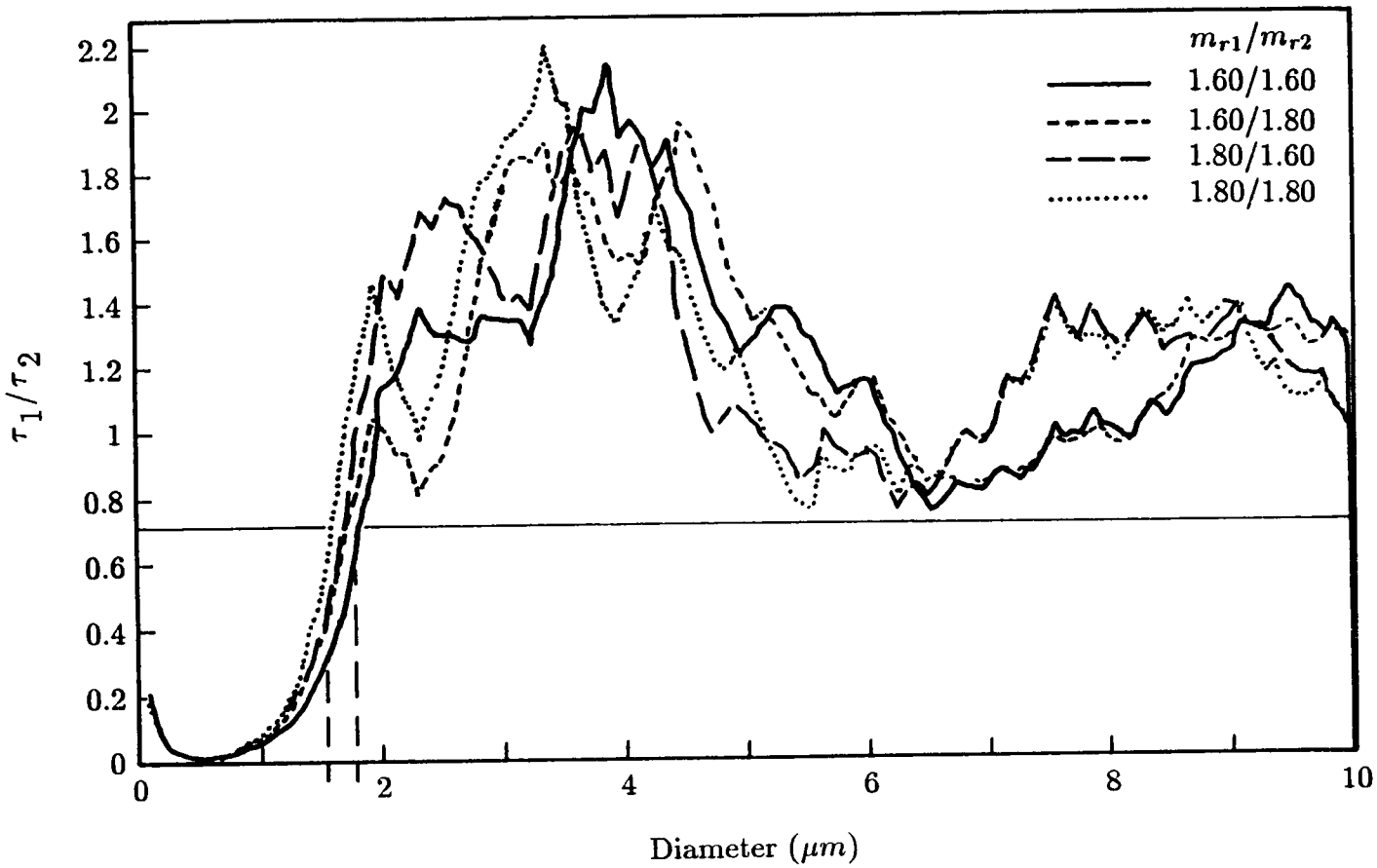


Figure 9.7. Optical depth ratios as function of mean particle diameter.

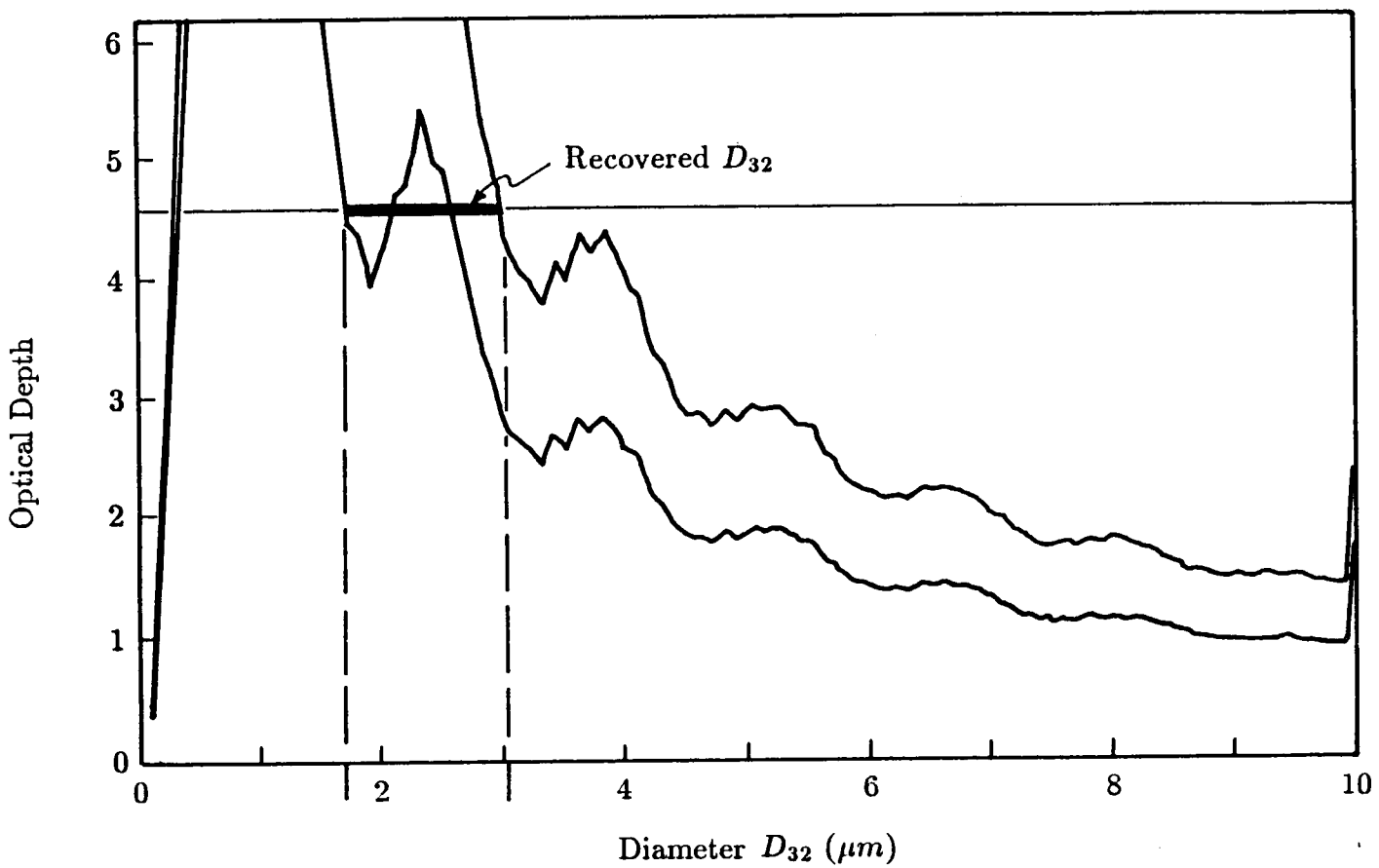


Figure 9.8. Optical depth for single path, single wavelength measurement.

TABLE 9.2

DISTRIBUTION OF MEAN PARTICLE SIZES, D_{32}

MASS PROFILE	LOCATION		
	0	0.2R	0.875R
Cosine	1.8 μm	2.2 μm	4.2 μm
Exponential	4.1	2.3	2.3
Abel	2.2	2.4	3.6
Gaussian	3.45	2.9	1.6
Uniform	1.1	1.8	7.1

CHAPTER X

SUMMARY AND CONCLUSIONS

The feasibility of obtaining average particle sizes in spatially large, cylindrically symmetric particle distributions using a variety of light scattering and extinction techniques has been presented. The optical measurement techniques described in this work are valid under the assumptions of Mie theory, i.e., that the particles are spherical and have known optical properties. Single particle scattering has also been assumed, which makes these techniques invalid for ensembles producing substantial attenuation.

The measurement techniques that were investigated were chosen because of their relative insensitivity to uncertainties in particle properties and to details of the particle size distribution function. Therefore, these techniques are especially useful when applied to distributions in which the optical properties, material composition, and type of size distribution function are poorly known.

Dobbins' method[35] for relating the mean particle size D_{32} to the mass concentration and optical extinction through a homogeneous slab of particles was discussed, and was modified for use with the general case of a cylindrically symmetric nonuniform mass distribution. This technique was shown to be highly useful for measurements on particle clouds in which the form of the PSDF is unknown. With appropriate choice of wavelengths, uncertainties of less than 20-30% can be expected for the recovery of D_{32}.

Using Dobbins' technique in conjunction with the onion-peel inversion method, a procedure was developed for using multiple path extinction measurements to obtain a spatial distribution of mean particle sizes in an axisymmetric cloud. Based on experimental measurements, it was shown that the propagated errors could be ex-

pected to be less than 10-20% with known geometry and with prior knowledge of the functional form of the radial mass flux distribution. Even in cases where the mass flux profile is unknown, it was shown that multiple path extinction measurements employing multiple wavelengths have the potential for simultaneously deducing the spatial distribution of mean particle size and the radial mass flux profile.

In order to obtain additional size information, a new method was proposed for obtaining the mean particle size D_{42} of a particle distribution using forward scattering techniques. Measurement of the shape of the angular profile of the forward scattered light was shown to be relatively insensitive to the shape of the particle size distribution function, and independent of the optical properties of the particles. This method can also be applied to the angular profile of the backscattered light if the particle optical properties are taken into account.

Ensemble backscatter measurement procedures were developed and shown to be directly related to the mass flow rate, or mass concentration, and to the Sauter mean diameter of the particle size distribution. Similarly to the extinction and backscatter efficiencies, the ensemble backscatter efficiency was shown to be relatively independent of the details of the size distribution for polydisperse particle ensembles, but is highly dependent on the particle optical properties. Nevertheless, this technique is useful in applications where the refractive index of the particles is known *a priori*. Numerical simulations have indicated that with appropriate choice of wavelengths uncertainties of less than 10-20% can reasonably be expected.

The optical techniques for measurement of the average size of a particle ensemble can be summarized in three simple formulae relating the optical measurements to the mean efficiencies for either extinction, backscatter, or diffraction:

$$\begin{aligned} \text{Extinction}: \ \tau(\lambda) &= 6\,\dot{m} < Q_e > \ / \ \pi\,\rho\,L\,v\,D_{32} \\ \text{Backscatter}: \ \beta(\lambda) &= 3\,\dot{m} < Q_b > \ / \ 8\,R_h\,\rho\,W\,v\,D_{32} \\ \text{Diffraction}: \ I(\lambda,\theta) &= < Q_d > \ / \ D_{42}^2 \end{aligned} \qquad (10.1)$$

The first equation for ensemble averaging is simply a restatement of a procedure that was introduced by Dobbins[35], while the remaining equations were developed in this work. A noteworthy feature of this set of equations is that extinction, backscatter and forward scattered signals are all proportional to a mean optical efficiency. The extinction equation is applicable to the Abel or "onion-peel" inversion technique, since it is geometry independent and can be used in optically dense particle flows. Backscatter was shown to be limited to farfield measurements, and to cases where the extinction of the beam through the particle cloud is negligible. Forward scattering, or diffraction, techniques have constraints similar to those of backscatter measurements and are somewhat geometry dependent.

Extensive numerical calculations were performed in order to simulate the proposed measurement techniques under a variety of conditions. Several resulting rules-of-thumb were developed in Chapter VIII based on empirical observations of the sensitivity of these techniques to the choice of appropriate wavelength and corresponding size range. It was noted that a 20-30% bias error in the recovered mean particle size can be expected, and that backscatter measurements can provide good estimates of particle size if the wavelength is chosen so that the expected range of particle diameters is approximately 2-10 λ. Forward scattering techniques can provide comparable accuracies if the scattering angles and illumination wavelengths are chosen for optimum sensitivity.

Mie scattering calculations require considerable computational effort, even with the availability of powerful, modern minicomputers. Although a large number of

numerical simulations were performed as part of this effort in an attempt to characterize parameters such as wavelength effects, refractive index uncertainties, and sensitivity to the shape of the PSDF, it would be virtually impossible to generalize these results to every possible measurement scenario. The intent has been, therefore, to develop a generalized approach which can be tailored to specific measurement applications. Selection of the optimum wavelengths and detector angles, and the total number of measurements required to achieve a given level of confidence in the results, will generally require substantial computational effort. This will, however, be facilitated by the availability of easy-to-use Mie scattering codes such as the one used in this work, developed by Bohren and Huffman[47].

Recommendations for Future Research

The study of particle size measurement using optical techniques is a continually expanding and progressing field of endeavor. Many complex issues relating to the measurement techniques explored in this work will require further research in order to understand more fully these phenomena. Specifically not addressed in this work were the effects that nonspherical particles, or those with inhomogeneous composition, have on the light scattering from the particle. Optically dense particle clouds, where multiple scattering becomes an important issue, were also not considered. In each of these cases, depolarization of the incident illumination occurs, and must be considered in a more detailed analysis.

Further research into the application of forward and backscatter measurement techniques to spatially large, optically thick particle clouds would be highly useful. This would require corrections for the attenuation of the light beam as it travels into and out of the particle cloud. Time resolved backscatter measurements, for example, have a simple measurement geometry and could provide valuable information about

the mass distribution and the distribution of average particle size along the beam path. Additional studies of methods for extracting more spatially resolved particle size information are also warranted. For example, the application of the extinction measurement technique could be combined with tomographic methods to obtain spatially resolved particle sizes in non-axisymmetric clouds. Determination of the optical constants of particles that have known size distributions should also be feasible using combined extinction and scattering measurements. This approach would be particularly useful for determining the optical properties of extremely high temperature particles which are not easily measured by conventional techniques.

BIBLIOGRAPHY

1. Bachalo, W.D., M.J. Houser, and J.N. Smith. "Behavior of Sprays Produced by Pressure Atomizers as Measured Using a Phase/Doppler Instrument." Atomisation and Spray Technology 3, pp. 53-72 (1987).

2. Ewan, B.C.R., J. Swithenbank, and C. Sorusbay. "Measurement of Transient Spray Size Distributions." Optical Engineering, 23(5), 620-625, September/October (1984).

3. Ootsuka, K., S. Tsuji, and Y. Arikawa. "A Stack Dust Monitor Based on Particle Counting and Sizing." Atmospheric Environment 13, 183-187, (1979).

4. Reisman, E. "Multiwavelength Transmissometer for Measuring Mass Concentration of Particulate Emissions." EPA Report No. EPA-600/ 2-79-022, February (1979).

5. Kadota, T. and H. Hiroyasu. "Soot Concentration Measurement in a Fuel Droplet Flame via Laser Light Scattering." Combustion and Flame, 55, 195-201 (1984).

6. Abubakar, K. "Particle Sizing in a Solid Rocket Motor Using the Measurement of Scattered Light." Master's Thesis, Naval Postgraduate School, Monterey, CA March (1985).

7. Cannon, Theodore W., and Robert Woltz. "A Camera for In-Situ Photography of Atmospheric Cloud Particles From an Armored T-28 Hail Research Aircraft." SPIE Proceedings Vol. 125. Advances in Laser Technology for the Atmospheric Sciences, 114-120 (1977).

8. Sadowski, J.W., and E. Byckling. "An On-line Device for Measurement of Particle Size Distribution." Proceedings of ICO-11, 391-394, Madrid, Spain (1978).

9. Houser, M.J. "Particle Field Diagnostics: Applications of Intensity Ratioing, Interferometry, and Holography." Optical Engineering, 19(6), 873-877, November/December (1980).

10. Prikryl, I. and C.M. Vest. "Holographic Imaging of Semitransparent Droplets or Particles." Applied Optics, 21(14), 2541-2547, July (1982).

11. Grabowski, W. "Measurement of the Size and Position of Aerosol Droplets Using Holography." Optics and Laser Technology, 199-205, August (1983).

12. Malyak, P.H. and B.J. Thompson. "Particle Displacement and Velocity Measurement Using Holography." Optical Engineering, 23(5), 567-575, September/October (1984).

13. Stanton, A.C., H.J. Caulfield, and G.W. Stewart. "An Approach for Automated Analysis of Particle Holograms." Optical Engineering, 23(5), 577-582, September/October (1984).

14. Knollenberg, R.G. "The Optical Array: An Alternative to Scattering or Extinction for Airborne Particle Size Determination." Journal of Applied Meteorology, 9(1),86-103, February (1970).

15. Knollenberg, R.G. "The Response of Optical Array Spectrometers to Ice and Snow: A Study of 2-D Probe Area-to-Mass Relationships." Final Report AFGL-TR-76-0273, November (1976).

16. Knollenberg, R.G. "The Response of Optical Array Spectrometers to Ice and Snow: A Study of Probe Size to Crystal Mass Relationships." Final Report AFCRL-TR-75-0494, September (1975).

17. Schleusener, Stuart A. "Automatic High Speed Particle Sizing Using a Gas Laser." Review of Scientific Instruments, 39(12), 1916-1919, December (1968).

18. Pinnick, R.G. and D.J. Hofmann. "Efficiency of Light-Scattering Aerosol Particle Counters." Applied Optics, 12(11), 2593-2597, November (1973).

19. Pinnick, R.G. and H.J. Auvermann. "Response Characteristics of Knollenberg Light-Scattering Aerosol Counters." Journal of Aerosol Science, 10, 55-74, (1979).

20. Hirleman, E. Dan. "Laser-Based Single Particle Counters for In-situ Particle Diagnostics." Optical Engineering, 19(6), 854-860, November/ December (1980).

21. Glantschnig, Werner J. and Sow-Hsin Chen. "Light Scattering from Water Droplets in the Geometrical Optics Approximation." Applied Optics, 20(14), 2499-2509, July (1981).

22. Wyatt, Philip J., et.al. "Aerosol Particle Analyzer." Applied Optics, 27(2), 217-221, January (1988).

23. Swithenbank, J., et.al. "A Laser Diagnostic Technique for the Measurement of Droplet and Particle Size Distribution." Progress in Astronautics and Aeronautics, 53, 421-447, (1977).

24. Jerkovic, A. and H.J. Fissan. "Monitor for Size Distribution Parameters and Number Concentration of Product Aerosols." Journal of Aerosol Science, 19(7), 1019-1022, (1988).

25. Roberds, D.W. "Particle Sizing Using Laser Interferometry." Applied Optics, 16(7), 1861-1868, July (1977).

26. Hirleman, E. Dan. "Laser Technique for Simultaneous Particle-Size and -Velocity Measurements." Optics Letters, 3(1), 19-21, July (1978).

27. Roberds, D.W., C.W. Brasier, and B.W. Bomar. "Use of a Particle Sizing Interferometer to Study Water Droplet Size Distribution." Optical Engineering, 18(3), 236-242, May/June (1979).

28. Saffman, M., P. Buchhave, H. Tanger. "Simultaneous Measurement of Size, Concentration, and Velocity of Spherical Particles by a Laser Doppler Method." Proceedings of The Second International Symposium on Applications of Laser Anemometry to Fluid Mechanics, Lisbon, July (1984).

29. Bachalo, W.D. and M.J. Houser. "Phase/Doppler Spray Analyzer for Simultaneous Measurments of Drop Size and Velocity Distributions." Optical Engineering, 23(5), 583-590, September/October (1984).

30. Laufer, Gabriel. "Instrument for Velocity and Size Measurement of Large Particles." Applied Optics, 23(8), 1284- 1288, April (1984).

31. Bachalo, W.D., R.C. Rudoff, and M.J. Houser. "Laser Velocimetry in Turbulent Flow Fields: Particle Response." AIAA 25th Aerospace Sciences Meeting, Reno, January (1987).

32. Mie, G. "Beitrage Żur Optik trüber Medien Speziell Kolloidaler Metallösungen." Ann.Phys. 25, 377-445 (1908).

33. Shaw, G. E. "Inversion of Optical Scattering and Spectral Extinction Measurements to Recover Aerosol Size Spectra" Applied Optics, 18(7), 988-993, April (1979).

34. Cheung, R.L. and A. Ishimaru. "Transmission, Backscattering, and Depolarization of Waves in Randomly Distributed Spherical Particles" Applied Optics, 21(20), 3792-98, October (1982).

35. Dobbins, R.A. "Measurement of Mean Particle Size in a Gas-Particle Flow" AIAA Journal, 1(8), 1940-1942, August (1963).

36. Wertheimer, A.L. and W.L. Wilcock. "Light Scattering Measurements of Particle Distributions." Applied Optics, 15(6), 1616-1620, June (1976).

37. Alger, T.W. "Polydisperse-Particle-Size-Distribution Function Determined from Intensity Profile of Angularly Scattered Light." Applied Optics, 18(20), 3494-3501, October (1979).

38. Capps, C.D., R.L. Henning, and G. M. Hess. "Analytic Inversion of Remote-Sensing Data." Applied Optics, 21(19), 3581- 3587, October (1982).

39. Holland, A.C. and G. Gagne. "The Scattering of Polarized Light by Polydisperse Systems of Irregular Particles." Applied Optics, 9(5), 1113-1121, May (1970).

40. Asano, Shoji. "Light Scattering Properties of Spheroidal Particles." Applied Optics, 18(5), 712-723, March (1979).

41. Wang, Dau-Sing and Peter W. Barber. "Scattering by Inhomogeneous Nonspherical Objects." Applied Optics, 18(8), 1190- 1197, April (1979).

42. Asano, Shoji and Makoto Sato. "Light Scattering by Randomly Oriented Spheroidal Particles." Applied Optics, 19(6), 962-974, March (1980).

43. Asano, Shoji. "Light Scattering by Horizontally Oriented Spheroidal Particles." Applied Optics, 22(9), 1390-1396, May (1983).

44. Purcell, E.M. and C.R. Pennypacker. "Scattering and Absorption of Light by Non-Spherical Dielectric Grains." Astrophysical Journal, 186, 705-714 (1973).

45. Van de Hulst, H. C. LIGHT SCATTERING BY SMALL PARTICLES. Dover Publications, Inc., New York (1981).

46. Kerker, M. THE SCATTERING OF LIGHT AND OTHER ELECTRO-MAGNETIC RADIATION. Academic Press, New York (1969).

47. Bohren, C.F. and D.R. Huffman. ABSORPTION AND SCATTERING OF LIGHT BY SMALL PARTICLES. John Wiley & Sons, Inc., New York, (1983).

48. Dave, J.V. "Effect of Coarseness of the Integration Increment on the Calculation of the Radiation Scattered by Polydispersed Aerosols." Applied Optics, 8(6), 1161-1167, June (1969).

49. Grehan, Gerard and Gerard Gouesbet. "Mie Theory Calculations: New Progress, With Emphasis on Particle Sizing." Applied Optics, 18(20), 3489-3493, October (1979).

50. Jackson, J.D. CLASSICAL ELECTRODYNAMICS. 2nd ed. John Wiley & Sons, Inc., New York (1975).

51. Leighton, Robert B. PRINCIPLES OF MODERN PHYSICS. McGraw-Hill Book Company, New York (1959).

52. Skolnick, Merrill I. INTRODUCTION TO RADAR SYSTEMS, 2nd ed. McGraw-Hill Book Company, New York (1984).

53. Dobbins, R.A. and L.D. Strand. "A Comparison of Two Methods of Measuring Particle Size of Al_2O_3 Produced by a Small Rocket Motor." JPL TR-32-1383. June (1969).

54. Salita, Mark. "Some Effects of Particle Size Averaging on Rocket Motor Performance Prediction." Minutes of the JANNAF PSS 17th Meeting, pp. 95-113, March (1984).

55. Dobbins, R.A. and G.S. Jizmagian. "Optical Scattering Cross Sections for Polydispersions of Dielectric Spheres." J.O.S.A. 56(10), 1345-1350, October (1966).

56. Uthe, Edward E. "Calibration and Performance Evaluation of a Single-Wavelength Transmissometer for Monitoring Particulate Mass Concentration of Emissions from Stationary Sources." Final Report, EPA Contract 68-01-4137 , July (1976).

57. Smith, T.J., et.al. "A Multi-Channel, Electro-Optical Turbidity Meter." Journal of Physics E: Scientific Instruments, 13, 488-493, (1980).

58. Holve, D. and S. Self. "Optical Measurements of Mean Particle Size in the Exhaust of a Coal-Fired MHD Generator." Presented at the Western States Section of the Combustion Institute, Univ. of California/ San Diego, October (1976).

59. Cashdollar, K.L., et.al. "Three-Wavelength Light Transmission Technique to Measure Smoke Particle Size and Concentration." Applied Optics, 18(11), 1763-69, June (1979).

60. Gougeon, P., et.al. "Optical Measurements of Particle Size and Concentration in Densely Laden Media Using a Visible/Infrared Double Extinction Technique," Journal of Physics E: Scientific Instruments, 20, 1235- 1241, November (1987).

61. Uthe, Edward E. "Particle Size Evaluations Using Multiwavelength Extinction Measurements." Applied Optics, 21(3), 454-459, February (1982).

62. Horvath, H. "Experimental Investigation on the Validity of the Lambert-Beer Law at High Particle Concentrations." Journal of Aerosol Science, 19(7), 837-840, (1988).

63. Hodkinson, J.R. AEROSOL SCIENCE. C.N. Davies, ed. Academic Press, New York (1966).

64. Reed, R. A. Personal communication. January (1988).

65. Limbaugh, C.C., and W.K. McGregor. Personal communication. March (1988).

66. Goodman, J.W. INTRODUCTION TO FOURIER OPTICS. McGraw-Hill Book Company, New York (1968).

67. Roberts, J.H. and M.J. Webb. "Measurement of Droplet Size for Wide Range Particle Distributions." AIAA Journal, 2, 583- 585, March (1964).

68. Belz, R.A. "Analysis of the Techniques for Measuring Particle Size and Distribution From Fraunhofer Diffraction Patterns." Final Report AEDC-TR-68-125, September (1968).

69. Gravatt, C.C. "Real Time Measurement of the Size Distribution of Particulate Matter by a Light Scattering Method." Journal of the Air Pollution Control Association, 23(12), 1035- 1038, December (1973).

70. Winstanley, J.V. and M.J. Adams. "Point Visibility Meter: A Forward Scatter Instrument for the Measurement of Aerosol Extinction Coefficient." Applied Optics, 14(9), 2151-2157, September (1975).

71. McSweeney, A. "A Diffraction Technique to Measure Size Distribution of Large Airborne Particles." Final Report EPA- 600/3-76-073, July (1976).

72. Weiner, Bruce B. "Particle and Spray Sizing Using Laser Diffraction." SPIE Vol. 170 - Optics in Quality Assurance II, 53-62, (1979).

73. Muly, E.C. and H.N. Frock. "Industrial Particle Size Measurement Using Light Scattering." Optical Engineering, 19(6), 861-869, November/ December (1980).

74. Nakadate, Suezou and Hiroyoshi Saito. "Particle-Size-Distribution Measurement Using a Hankel Transform of a Fraunhofer Diffraction Spectrum." Optics Letters, 8(11), 578-580, November (1980).

75. Fischbach, F.A. and J.S. Bond. "Fraunhofer Diffraction Patterns of Microparticles." American Journal of Physics, 52(6), 519-521, June (1984).

76. Hirleman, E. Dan, V. Oechsle, and N.A. Chigier. "Response Characteristics of Laser Diffraction Particle Size Analyzers: Optical Sample Volume Extent and Lens Effects." Optical Engineering, 23(5), 610-619, September/October (1984).

77. Hodkinson, J. Raymond. "Particle Sizing by Means of the Forward Scattering Lobe." Applied Optics, 5(5), 839-844, May (1966).

78. Dobbins, R.A., L. Crocco, and I. Glassman. "Measurement of Mean Particle Sizes of Sprays from Diffractively Scattered Light." AIAA Journal, 1(8), 1882-1886, August (1963).

79. Mugele, R.A. and H.D. Evans. "Droplet Size Distribution in Sprays." Ind. Eng. Chem. 43, 1317-1324 (1951).

80. Ben-David, A. and B.M. Herman. "Method for Determining Particle Size Distributions by Nonlinear Inversion of Backscattered Radiation," Applied Optics, 24(7), 1037-1042, April (1985).

81. Hutt, D.L. "Measurement of the Droplet Size Distribution of Fog Using Multi-Wavelength Lidar: A Feasibility Study." Journal of Aerosol Science, 19(7), 833-836, (1988).

82. Thomalla, Edith. and Heinrich Quenzel. "Information Content of Aerosol Optical Properties With Respect to Their Size Distribution." Applied Optics, 21(17), 3170-3177, September (1982).

83. Twomey, S. INTRODUCTION TO THE MATHEMATICS OF INVERSION IN REMOTE SENSING AND INDIRECT MEASUREMENTS. Elsevier Scientific Publishing Co., Amsterdam (1977).

84. Twomey, S. "Information Content in Remote Sensing." Applied Optics, 13(4), 942-945, April (1974).

85. Grassl, H. "Determination of Aerosol Size Distributions from Spectral Attenuation Measurements." Applied Optics, 10(11), 2534-2538, November (1971).

86. Fymat, A.L. "Analytical Inversions in Remote Sensing of Particle Size Distributions. 1: Multispectral Extinctions in the Anomalous Diffraction Approximation." Applied Optics, 17(11), 1675-1677, June (1978).

87. Fymat, A.L. "Analytical Inversions in Remote Sensing of Particle Size Distributions. 2: Angular and Spectral Scattering in Diffraction Approximations." Applied Optics, 17(11), 1678- 1680, June (1978).

88. Tao, Rong-jia. "Determination of the Size Distribution of Atmospheric Aerosols by Means of Optical Attenuation Measurements." Chinese Physics, 1(4), 817-827, October-December (1981).

89. Nicholls, R.W. "Wavelength-Dependent Spectral Extinction of Atmospheric Aerosols." Applied Optics, 23(8), 1142-1143, April (1984).

90. Klett, J.D. "Anomalous Diffraction Model for Inversion of Multispectral Extinction Data Including Absorption Effects." Applied Optics, 23(24), 4499-4508, December (1984).

91. Cooke, D.D. and M.Kerker. "Response Calculations for Light-Scattering Aerosol Particle Counters." Applied Optics, 14(3), 734-739, March (1975).

92. Lewis, J.W.L., B.P. Curry, and D.P. Weaver. "Determination of the Size Distribution Function for Particles in a Hypersonic Flow Field." Final Report AEDC-TR-77-101 , July (1978).

93. Shah, H.S., R.V. Mehta, and R.V. Desai. "Estimation of Particle Size Distribution Parameters With Forward-Scattering Techniques." Applied Optics, 18(24), 4173-4177, December (1979).

94. Fymat, A.L. and K.D. Mease. "Mie Forward Scattering: Improved Semiempirical Approximation With Application to Particle Size Distribution Inversion." Applied Optics, 20(2), 194-198, January (1981).

95. Curry, B.P. and E.L. Kiech. "Improved Methods to Invert the Particle Size Distribution Function from Mie Scattering Measurements." Final Report AEDC-TR-83-52, February (1984).

96. Curry, B.P. "Constrained Eigenfunction Method for the Inversion of Remote Sensing Data: Application to Particle Size Determination from Light Scattering Measurements." Applied Optics, 28(7), 1345-1355, April (1989).

97. Beale, K.S. Personal communications. March 1988.

APPENDICES

APPENDIX A

PARTICLE SIZE DISTRIBUTION FUNCTIONS

Several distribution functions commonly employed when performing particle size statistics include the normal, the log-normal, and the gamma distribution functions. In this work, reference has also been made to the uniform, or rectangular, distribution for comparison with the more physically realistic distribution functions. This appendix lists the mathematical forms of the functions used most extensively in this work.

NORMAL

The normal, or Gaussian, distribution is usually employed because of its nice mathematical properties, and not necessarily because it represents any physical distributions. The normal distribution has the form given by

$$f(D) = exp\left[-(D - D_m)^2/\sigma^2\right] \qquad (A.1)$$

where D_m represents the mean particle size, and σ is a measure of the width of the distribution.

LOG-NORMAL

The log-normal distribution function is commonly used in particle size applications, because its skewed profile closely resembles actual measured particle size distributions. The log-normal function can be expressed in several different forms, but one of the most common forms is given by

$$f(D) = \frac{1}{\sqrt{2\pi}\ D\ ln(\sigma)}\ exp\left[-\left(ln(D/D_m)\ /\ ln(\sigma)\right)^2\ /\ 2\right] \qquad (A.2)$$

where D_m represents the geometric mean diameter, and σ represents the geometric standard deviation. The most probable size, D_p, which is also the peak of the

distribution function is located by setting $df/dD = 0$, with the result

$$D_p = D_m \; exp\left[-\left(ln(\sigma)\right)^2 \; / \; D_m\right] \tag{A.3}$$

UNIFORM DISTRIBUTION

The simplest distribution function to deal with mathematically is perhaps the uniform, or rectangular, distribution, which is defined such that the probability of finding a particle of diameter D in the interval $D_{min} < D < D_{max}$ is equal everywhere within the interval. Although this is generally not a very realistic distribution, except perhaps in controlled spray applications, it provides some insight into the characteristics of distribution functions, and is useful for comparisons with other more physically realizable functions. The rectangular distribution function can be written as

$$n(D) = n_o \qquad D_{min} < D < D_{max} \tag{A.4}$$

where n_o is a constant.

Calculations indicate that the moments of the size distribution can be written as

$$< D_M >= \int D^M \; n_o \; dD = \frac{1}{M+1} \left\{ D_{max}^{M+1} - D_{min}^{M+1} \right\} \tag{A.5}$$

The mass median diameter, D_m, is found to be

$$D_m = 1 \; / \; (2 \; D_{max}) \tag{A.6}$$

Ratios of the moments of diameter are found from looking at

$$D_{MN} = \frac{N+1}{M+1}^{1/M-N} \left\{ \frac{D_{max}^{M+1} - D_{min}^{M+1}}{D_{max}^{N+1} - D_{min}^{N+1}} \right\} \tag{A.7}$$

With the equation for D_{32}, for example, having the form

$$D_{32} = 3/4 \left[\frac{D_{max}^4 - D_{min}^4}{D_{max}^3 - D_{min}^3} \right] \tag{A.8}$$

GAMMA

Another distribution function with a skewed profile is the gamma function. The mono-mode gamma distribution function is described by

$$f(r) = N \frac{b^{(a+1)}\, r^a\, exp\,(-br)}{\Gamma(a+1)} \tag{A.9}$$

where a and b are parameters of the distribution and r in this case is the particle radius. The most probable size for this distribution function is given by

$$D_p = 2\ a\ /\ b \tag{A.10}$$

The mean size, D_{32}, for the gamma distribution has the form

$$\begin{aligned} D_{32} &= 2\ (3+a)\ /\ b \\ &= 2\ <D^3>\ /\ <D^2> \end{aligned} \tag{A.11}$$

Similarly, other ratios of moments have simple forms such as

$$D_{IJ} = 2\ (I+a)\ /\ b \tag{A.12}$$

where $I = J + 1$. Also

$$D_{MN} = H\left[(a+I)\ /\ b\right]^{(1/(M-N))} \tag{A.13}$$

APPENDIX B

COMMENTS ON EXTINCTION MEASURMENT UNCERTAINTIES

The determination of mean particle size by the method of extinction has been shown to be dependent on both the flow geometry and the optical properties of the particulate material. Uncertainties in these parameters may be treated either statistically or in terms of absolute errors, depending on whether the errors are normally distributed or not. A brief discussion of the sensitivity of the measurement to uncertainties in the parameters used to calculate D_{32} based on extinction measurements is therefore appropriate.

Consider again the expression for mean particle diameter in the form

$$D_{32} = 6\ \dot{m} < Q_e > g\ /\ \pi\ \rho\ L\ v\ \tau \qquad (B.1)$$

The generalized form of this equation may be represented by

$$D_{32} = f(q_i) \qquad (B.2)$$

where q_i is one of the independent variables contributing to D_{32}. For normally distributed errors, the uncertainty in the quantity D_{32} can be written as

$$U = \sum \left[(\partial f/\partial q)^2\ dq^2\right]^{1/2} \qquad (B.3)$$

if the measurements of the variables are uncorrelated. The term dq represents the error in the quantity q, and the relative error for a specific parameter is dq/q. The uncertainty is the net result of the accumulated effect of the elemental errors. Uncertainties of the type exemplified in the measurement of the optical depth, τ, would typically be treated in this fashion.

When only a range of uncertainties is specified for the parameters q_i, the net uncertainty in D_{32} is determined by

$$U = \sum \left(\partial f/\partial q\right)\, dq \qquad (B.4)$$

Uncertainties in the quantities m, p, L, v, and $< Q_e >$ would typically be treated in this way by specifying their values within some range about a mean value.

The uncertainty in the particle size as determined by the previous equation is

$$dD = \frac{6}{\pi}\,\frac{< Q_e > gd\,\dot{m}}{\rho L v \tau} + \frac{< Q_e > \dot{m}\, dg}{\rho L v \tau} + \frac{\dot{m}\, gd < Q_e >}{\rho L v \tau} \qquad (B.5)$$

The relative error in particle diameter, as determined by the combined elemental errors described, is given by the expression

$$U = \frac{dD}{D} = \frac{dm}{m} + \frac{dg}{g} + \frac{d < Q_e >}{< Q_e >} - \frac{d\rho}{\rho} - \frac{dL}{L} - \frac{dv}{v} - \frac{d\tau}{\tau} \qquad (B.6)$$

In the case of unsymmetrical bias error, an upper and lower uncertainty will normally be specified, and are represented by D_+ and D_-, respectively where

$$D_+ = f(q_i + dq_i)$$

and

$$D_- = f(q_i - dq_i) \qquad (B.7)$$

The worst case uncertainty is determined by taking the largest possible range of error values for each parameter dq_i using the minimum and maximum extreme values of the parameters. First using maximum values of $\dot{m}$, $< Qe >$, and g, along with minimum values of ρ, L, v, gives the upper boundary on $\tau(D)$. Switching min/max roles of the parameters we obtain a lower boundary on $\tau(D)$. The upper and lower limit on the measurement of optical depth, τ, then determines the range of possible D_{32} values, since

$$dD = D_+ - D_- \qquad (B.8)$$

The most probable value of D_{32} occurs between the extreme values, with the best estimate of D_{32} occurring at the center of this range.

The worst case statistical uncertainty is obtained with the root-sum-square of the error of D_{32}

$$U = \left[\left(\frac{dm}{m}\right)^2 + \left(\frac{dg}{g}\right)^2 + \left(\frac{d < Q_e >}{< Q_e >}\right)^2 - \left(\frac{d\rho}{\rho}\right)^2 - \left(\frac{dL}{L}\right)^2 - \left(\frac{dv}{v}\right)^2 - \left(\frac{d\tau}{\tau}\right)^2\right] \tag{B.9}$$

The relative errors denoted above will typically be either precision or bias errors with known magnitude but unknown sign, i.e., $\pm\ h$ percent.

Error estimates of the parameters $\dot{m}$, ρ, L, are typically known a priori in typical experimental applications. The uncertainty in optical depth is associated with experimental error, and is usually limited by noise in the optical source or detector circuitry, and possibly by angular misalignment between the source and receiver optics.

Misalignment errors constitute bias effects, while noise contributions are random or precision errors. Both types of error must be treated separately.

Uncertainties may arise in the material density when there exists a strong temperature coefficient, or when the density value changes dramatically through a change of state. For example, liquid Al_2O_3 has a material density of approximately 3 g/cm^3, while solid Al_2O_3 has a density of approximately 4 g/cm^3.

The velocity uncertainty is affected by the fact that velocity may, in some flow situations, be size dependent. The worst case uncertainty could be argued to be the total range of expected velocities. However, a more realistic approach might require a statistically averaged particle velocity, which takes into account varying velocity with flow.

As previously discussed, the effects of the spatial distribution of mass flow within the particle ensemble can be large, depending on how the mass is actually

distributed. If the spatial distribution is initially assumed uniform ($g = 1$), but the real distribution is radially dependent, then g can take values as high as perhaps 2. Code predictions for certain spray nozzle applications may be available, and could reduce the distribution uncertainty considerably. Multiple path extinction measurements can also serve to significantly reduce this uncertainty.

The mean extinction efficiency has been shown to be relatively independent of the shape of the distribution, with a maximum uncertainty of approximately $\pm$ 5% of the mean particle size is approximately equal to the illumination wavelength. For larger and smaller particles, the uncertainty due to the shape of the distribution is even less. The mean extinction efficiency may also contain errors due to uncertainties in the Mie scattering calculations due to the effects of unknown optical properties, particle shape, and even the particle orientation if they are nonspherical. Since, in this work, the particles are assumed spherical, the major source of error may be attributed to unknown real and imaginary refractive indices. The extinction method tends to be relatively insensitive to the particle absorption, so only the effects of the real index need be considered.

The real refractive index, and hence the Mie calculated extinction efficiency for a given particle, is dependent on the wavelength of illumination because of frequency dispersion, the type of material, the temperature of the material for a specific phase, and the phase of the material itself.

Additional confidence in the measurement results may in some cases be gained by making simultaneous transmission measurements at several wavelengths. Each wavelength measurement will have a set of uncertainties associated with it. The quantities τ and $< Q_e >$ are functions of the wavelength, and will have different uncertainties associated with each of the transmission measurements. The quantities $\dot{m}$, L, v, and ρ are independent of wavelength, so uncertainties in these quantities

will be the same for each measurement.

The errors for this type of experiment will typically be specified in terms of absolute error bounds, and the resulting error for multiple wavelength measurements will be found by taking the smallest upper bound for the maximum uncertainty limit, and the largest lower bound for the minimum uncertainty limit. Since the two measurements have different ranges of uncertainty which overlap, the particle size uncertainty is actually determined by the smaller of the two individual uncertainty ranges. In this case, the addition of a second transmission measurement offers no improvement in the overall particle size uncertainty.

VITA

Patrick J. Murphy was born in Chicago, Illinois and subsequently moved to the Minneapolis, Minnesota area. He received a B.A. degree in Physics from St. Cloud State University in 1977, and a M.S. degree in Physics from the University of Tennessee in 1980. Since 1978, he has been employed full-time as a research engineer in the field of optical measurement instrumentation, having spent approximately four years with Rosemount, Inc. in Minneapolis, and over eight years with Sverdrup Technology, Inc., at the Arnold Engineering Development Center in Tennessee. Mr. Murphy currently resides in Tullahoma, Tennessee with his wife, Jeanne, and four children.